Abstract

Wind-induced forces can cause aeroelastic instability or so-called flutter of the long span bridges. The response prediction of such structures to wind loading is determined by the flutter derivatives. The determination of the flutter derivatives is mainly based on section model wind tunnel tests by using two types of experimental methods: free vibration method and forced vibration method. In the present work, free vibration test results are used to identify the flutter derivatives of a rectangular section with an aspect ratio of 1:8 under smooth flow with zero angle of attack. Different system identification methods are investigated and the most appropriate and efficient method is chosen to identify the flutter derivatives simultaneously out of the noise-corrupted displacement time histories of the section model extracted from the free vibration tests. The experimental set-up and the system parameters extraction method are described and their influence on the flutter derivatives are discussed in detail. The flutter derivatives extracted from the free vibration test results are compared with the ones calculated with respect to the forced vibration tests for the same rectangular section model. And also another comparison is carried out by calculating the critical wind speed with the results of both methods. The validity of the flutter derivatives determined from the free vibration test results is verified by the corresponding comparisons.

Acknowledgements

I would like to express my appreciation to Prof. Dr.-Ing. Uwe Starossek for giving me the opportunity to work on this subject. I also would like to thank to Prof. Dr.-Ing. Uwe Starossek and Prof. Dr.-Ing. Otto von Estorff for their supervision.

In addition, special thanks to Dipl.-Ing Lydia Thiesemann for her support and assistance in every step of this project work. I would like to thank her not only for her valuable advices but also for her kindness and patience that she has showed me during the project work.

I take this opportunity to thank Dr.-Ing Jurgen Priebe and the technicians Thomas Jessen and Uwe Stender for their hard work and assistance during the experimental work from the construction of the experimental set-up till the end of the wind tunnel tests.

I would also like to put on record my thanks to Dipl.-Ing Rüdiger Körlin for his comments and advises.

It is almost impossible to thank to my parents and my fiancée in a few words for everything they have done which motivated me a lot in achieving my goal.

Finally, I would like to express my gratefulness to my friends, colleagues, and beloved ones who have helped me in many ways, and put up with me while I devoted time and energy to this project.

Table of Contents

List of Figures

Notation

A_i^*	=	flutter derivatives for aeroelastic moment
a_0, a_1	=	coefficients of second order equation (Eqn. 2.23)
B	=	model width
b	=	half model width
C^*	=	amplitude of the motion
C_s	=	damping matrix
C(k)	=	Theodorsen circulation function
$\overline{C}$	=	system damping matrix
$\overline{C}^{mech}$, $\overline{C}^{eff}$	=	mechanical and effective system damping matrices, respectively
c	=	damping coefficient
c_c	=	critical damping coefficient
c_{hh}, $c_{h\alpha}$, $c_{\alpha h}$, $c_{\alpha\alpha}$	=	complex aerodynamic-derivative functions
D_p	=	aerodynamic drag force
d	=	half distance between the springs
F(k)	=	real part of the Theodorsen circulation function
$F_L(t)$,F(t)	=	force vector
f	=	natural cyclic frequency
G(k)	=	imaginary part of the Theodorsen circulation function
G	=	modal integral
g	=	overall damping coefficient
H_i^*	=	flutter derivatives for aeroelastic lift
h	=	vertical displacement
I	=	mass moment of inertia
K	=	reduced frequency, $B\omega/U$
k	=	reduced frequency, $b\omega/U$
kv	=	(wind speed acting on model / tunnel wind speed); U/U_t
K_s	=	stiffness matrix
K^d	=	stiffness-damping matrix
K_h	=	vertical stiffness
K_α	=	torsional stiffness
K_{sp}	=	spring stiffness
$\overline{K}$	=	system stiffness matrix
$\overline{K}^{mech}$, $\overline{K}^{eff}$	=	mechanical and effective system stiffness matrices, respectively
L_h	=	aerodynamic lift force
M_s	=	mass matrix
M_α	=	aerodynamic moment
m	=	mass
N	=	number of data points
N_1, N_2	=	time shifts
P_i^*	=	flutter derivatives for aeroelastic drag
P	=	eigenvector
p	=	lateral displacement
Q_i	=	generalized force in the *i*th mode
Re	=	Reynolds number
R_α	=	amplitude ratio
r	=	reduced mass radius of gyration

t	=	time
U	=	wind speed acting on model
U_t	=	tunnel wind speed
U_{red}	=	reduced wind speed
u_x,u_y,u_z	=	wind disturbance components
$X(t),x(t)$	=	displacement vector
x	=	along-span coordinate
y	=	across-span coordinate
z	=	vertical coordinate

α	=	torsional displacement
β	=	real part of the eigenvalue (Eqn. 3.11)
γ	=	imaginary part of the eigenvalue (Eqn. 3.11)
ε	=	frequency ratio
ζ	=	damping ratio-to-critical
μ	=	relative mass
ρ	=	air density
ν	=	kinematic viscosity
ξ_i	=	generalized coordinate of mode *i*
ω	=	natural circular frequency
λ	=	decay rate
λ^e	=	eigenvalue
δ	=	logarithmic decrement of damping
φ	=	phase shift
Δt	=	time interval
κ,κ_1,κ_2	=	coefficients for flutter calculation
Ψ	=	eigenvector
$\Phi, \hat{\Phi}$	=	instrumental variables
$\overline{\Phi}, \overline{\hat{\Phi}}$	=	modified instrumental variables
$\Re(z)$	=	real part of the complex number z
$\Im(z)$	=	imaginary part of the complex number z

1 INTRODUCTION

Long span bridges, either suspension or cable stayed bridges must be designed to withstand the forces induced by the wind effect. In addition, such bridges are susceptible to aeroelastic effects, such as torsional divergence, vortex-induced oscillation, flutter, galloping, and buffeting in the presence of self-excited forces. Flutter instability, which can cause catastrophic failures, is the main topic of the present work for the determination of aeroelastic behavior of the long span bridges under wind loading.

Flutter is the dynamic aeroelastic instability phenomenon, which can be caused by the motion-induced or self-induced forces. Flutter is one of the most important design criterions for long span bridges, because flutter can lead to excessive vibration amplitudes or even total collapse of the bridge deck. The accurate prediction of flutter stability becomes more important with the increasing span length due to the decreasing flutter resistance. The most dramatic example for the flutter instability is the collapse of the center span (854 m) of the Tacoma Narrows Bridge in 1940 at a moderate wind speed of 68 km/h.

In order to predict the response of long-span bridges to the wind loading, it is necessary to identify the aeroelastic parameters. The parameters required for examining whether a bridge deck section is prone to flutter under certain wind speeds, are called the flutter derivatives.

If a system is given an initial disturbance, it starts to oscillate either in decaying or diverging motion, in other words the motion will be damped or grow to infinity. It should be investigated that if the energy applied from the flow motion is greater or less than the energy dissipated through the system by its mechanical damping. The critical flutter condition occurs as a harmonic motion at the separation line between the decaying and diverging motion, and the corresponding wind speed at that condition is called critical wind speed. The bridge deck will be unstable under the wind loading whose velocity is greater than or equal to the critical wind velocity. Therefore, the information for the aerodynamic loads is necessary to examine the effects of self-induced vibrations.

There are some methods to determine the aerodynamic wind loading by means of the flutter derivatives. One possibility is the calculation of flutter derivatives by the numerical approach, which is based on the computational fluid dynamics. The second and the most widely used one is the wind tunnel testing. Especially section model wind tunnel tests are very common because of their reliability, simplicity of application and inexpensive experimental set-up compared to the other wind tunnel tests. Also there are two kinds of

experimental techniques to determine the system parameters through the section model wind tunnel testing: the free vibration technique and the forced vibration technique. In the present work, the first technique is applied for the calculation of flutter derivatives and the results of the flutter derivatives calculated by using the latter technique are used for comparison.

System identification (SID) methods have been employed to extract all flutter derivatives of the bridge deck simultaneously. A reliable and simple system identification method is selected among a variety of methods, to extract all flutter derivatives simultaneously from two degree of freedom coupled-motion displacement time histories of section model tests. Among all the available system identification methods Modified Ibrahim Time Domain (MITD) method, which is developed by Sarkar [3], is found to be the most appropriate method for the identification of flutter derivatives.

The quality of the data that will be used as an input for the system identification method is very important to obtain reliable results. The experimental set-up and the data acquisition system play a very important role in the quality of the data. Therefore, care should be given during the design and construction stages of the experimental set-up. Some suggestions are given for the future experiments to obtain better results.

There are some problems in the calculation of flutter derivatives, such as uniqueness problem. The number of unknown parameters, which are necessary to find out the flutter derivatives, are less than the number of system parameters that provide information about the system. Such kind of problems is discussed and the best solutions are investigated.

In the present work, a rectangular section model with an aspect ratio of 1:8 is investigated under smooth wind flow at zero angle of attack in the wind tunnel. The section is allowed to make two-degree of motion, vertical and rotational motion. The critical wind speed that is the stability point of the section is measured from the wind tunnel and comparison is made with the theoretically calculated critical wind speed by the flutter derivatives obtained from the system identification method.

2 GENERAL DESCRIPTION

2.1 Introduction

In the standard bridge design practice, flutter analysis is based on the flutter derivatives, which give information for the evaluation of flutter instability condition and the bridge deck aeroelastic behavior. The flutter analysis of the linear elastic structures is considered as a standard stability problem according to Simiu and Scanlan [2]. This consideration is based on two main reasons: First, the supporting structure is treated as linear elastic and its actions control the shape of the response. Second is the starting condition, which is considered to be occurring in small amplitudes that separate the stable and unstable regimes. When the wind acts on the bridge deck with the critical wind speed, the motion of the bridge deck is a sinusoidal motion with constant amplitude, which is the stability border of the bridge deck.

The cross section properties of the bridge deck affect the flutter stability considerably. Different bridge deck sections are investigated in the past to find out interaction between the flowing fluid and the section itself. One of the most important former researches was done on the theoretical expressions for the aerodynamic derivatives of a thin airfoil oscillating sinusoidally by Theodorsen [14]. Because of the similarity in the dynamic behavior of the streamlined bridge deck sections with the airfoil, the Theodorsen's theoretical evaluations can be used in such kind of bridge deck sections. Some studies were carried out on the flutter stability of the bluff body sections by Scanlan and Tomko [10], for which the Theodorsen's theoretical evaluations are no more valid.

In the present work only two degree of motion (vertical and torsional) is taken into account. Therefore, the section is subjected to aerodynamic wind forces associated with the corresponding degrees of freedom, self-excited aerodynamic lift L_h and self-excited aerodynamic moment M_α.

Wind acts on the section model in only one direction, but due to some uncertainties in the wind tunnel, wind flow can be expressed in three dimensional as $U+u_x$, u_y, u_z, which includes the random disturbances in the flow. However, in the present work the wind flow is assumed to be laminar, therefore the disturbance components of the wind flow (u_x, u_y, u_z), which make turbulent flow, are neglected.

2.2 Theory of the Flutter Derivatives

For a two-degree-of-freedom linear dynamic system as seen in the Fig. 2.1, the equation of motion can be defined as

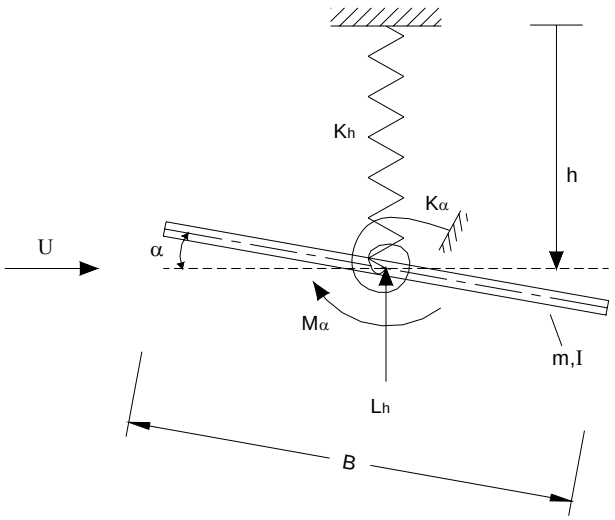

Figure 2.1: Two-dimensional aeroelastic system

$$M_s\,\ddot{x} + C_s\,\dot{x} + K_s\,x = F_L(t) \quad \text{with} \quad x(t) = \begin{bmatrix} h(t) \\ \alpha(t) \end{bmatrix} \quad \text{and} \quad F_L(t) = \begin{bmatrix} L_h \\ M_\alpha \end{bmatrix} \qquad (2.1)$$

The Eqn. 2.1 can be rewritten by inserting frequency and the damping parameters of the two-degree of freedom system as

$$\left.\begin{aligned} m\,(\ddot{h} + 2\zeta_h\omega_h\dot{h} + \omega_h^2 h\,) &= L_h \\ I\,(\ddot{\alpha} + 2\zeta_\alpha\omega_\alpha\dot{\alpha} + \omega_\alpha^2\alpha\,) &= M_\alpha \end{aligned}\right\} \qquad (2.2)$$

where m and I are the model mass and mass moment of inertia of the system, respectively; ζ_h and ζ_α are the mechanical damping ratios-to-critical in bending and torsion, respectively; ω_h and ω_α are the corresponding natural circular frequencies; L_h and M_α are the self-excited aerodynamic force and moment, respectively.

These equations are valid if the bridge deck section is symmetrical; which is the common case for most of the bridge deck sections. In other words, the elastic center of the section lies at the location of mass center, which is the case in Fig. 2.1.

The displacement vector x(t) is expressed with respect to the system parameters, which will be identified in the following chapters. Therefore they should be stated clearly.

$x(t) = C^{*} \cdot e^{\lambda \cdot t} \cdot \cos(\omega \cdot t + \varphi)$; where C^{*} is the amplitude, λ is the decay rate, ω is the natural circular frequency and φ is the phase shift of the oscillation.

$\lambda = \zeta \cdot \omega$; where ζ is the damping ratio-to-critical

$\zeta = c/c_c = c/(2m\omega)$; c = damping coefficient, c_c = critical damping coefficient

$\delta = 2\pi \cdot \zeta \;\Rightarrow\; \delta = 2\pi \cdot \lambda/\omega$, where δ is the logarithmic decrement of damping.

In order to calculate the self-excited aerodynamic forces that are set on the right of the equation of motion in Eqn. 2.2 for the airfoils or thin plate sections, Theodorsen [14] developed a theoretical formulation with respect to the basic principles of potential flow theory. These aerodynamic forces are defined in terms of the displacement, velocity, acceleration of the oscillation, the fluid density and flow speed, the half-chord of the section and the Theodorsen circulatory function C(k) = F(k) + iG(k). The aerodynamic forces defined as

$$\begin{aligned} L_h &= -\pi\rho b^2\left(\ddot{h} + U\dot{\alpha}\right) - 2\pi\pi\rho\, b\, C(k)\left(\dot{h} + U\alpha + \frac{b}{2}\dot{\alpha}\right) \\ &= -\pi\rho b^2\left[\frac{2U}{b}C(k)\,\dot{h} + \ddot{h} + \frac{2U^2}{b}C(k)\,\alpha + U\left(C(k)+1\right)\dot{\alpha}\right] \end{aligned} \qquad (2.3)$$

$$\begin{aligned} M_\alpha &= -\pi\rho b^2\left(\frac{Ub}{2}\dot{\alpha} + \frac{b^2}{8}\ddot{\alpha}\right) + \pi\rho U b^2 C(k)\left(\dot{h} + U\alpha + \frac{b}{2}\dot{\alpha}\right) \\ &= \pi\rho b^2\left[UC(k)\,\dot{h} + U^2 C(k)\,\alpha + \frac{Ub}{2}\left(C(k)-1\right)\dot{\alpha} - \frac{b^2}{8}\ddot{\alpha}\right] \end{aligned} \qquad (2.4)$$

where the approximate formulation for real and imaginary parts of C(k) are presented by Starossek [1] as

$$\left.\begin{aligned} F(k) &= \frac{0.500502\cdot k^3 + 0.512607\cdot k^2 + 0.210400\cdot k + 0.021573}{k^3 + 1.035378\cdot k^2 + 0.251239\cdot k + 0.021508} \\ G(k) &= -\frac{0.000146\cdot k^3 + 0.122397\cdot k^2 + 0.327214\cdot k + 0.001995}{k^3 + 2.481481\cdot k^2 + 0.934530\cdot k + 0.089318} \end{aligned}\right\} \qquad (2.5)$$

$k = b\cdot\omega\,/U$ is the reduced frequency, b=B/2 is the half-chord of the thin plate, ω is the natural circular frequency of the motion and U is the flow velocity, ρ is the fluid density.

The Theodorsen function only gives good results for the thin plates or streamlined sections, it is not applicable for bluff cross sections. Scanlan and Tomko [10] has shown that self-excited aerodynamic forces acting on bluff bodies under small oscillations can be taken as linear with respect to the displacement and the velocity of the motion of the system in the corresponding degrees of freedom. The latest linear form of self-excited aerodynamic forces are expressed by Scanlan as

$$L_h = \frac{1}{2}\rho U^2 B\left[KH_1^*(K)\frac{\dot{h}}{U} + KH_2^*(K)\frac{B\dot{\alpha}}{U} + K^2H_3^*(K)\alpha + K^2H_4^*(K)\frac{h}{B}\right] \qquad (2.6)$$

$$M_\alpha = \frac{1}{2}\rho U^2 B^2\left[KA_1^*(K)\frac{\dot{h}}{U} + KA_2^*(K)\frac{B\dot{\alpha}}{U} + K^2A_3^*(K)\alpha + K^2A_4^*(K)\frac{h}{B}\right] \qquad (2.7)$$

H_2^*, H_3^*, A_1^*, A_4^* are called cross-flutter derivatives, which are used to calculate the aerodynamic force of the corresponding degree of freedom for the coupled motion by using the effect of the motion of the other degree of freedom. And the rest of the flutter derivatives H_1^*, H_4^*, A_2^*, A_3^* are called direct-flutter derivatives, which can be also obtained by the single degree of freedom analysis.

$K = B\cdot\omega/U = 2\cdot k = 2\cdot b\cdot\omega/U$; K is the reduced frequency, B is the width of the section. If the reduced frequency formula is rearranged, it can be also concluded that the flutter derivatives depend on the reduced wind velocity, which is a different way of expressing the flutter derivatives.

$$K = B\cdot\omega/U = B\cdot 2\pi f/U = 2\pi/U_{red} \Rightarrow U_{red} = U/(B\cdot f) \qquad (2.8)$$

As mentioned earlier, the flutter derivatives depend on the geometry of the section and the non-dimensional reduced frequency K as seen the in the Eqns. 2.6 and 2.7. It is possible to determine the aerodynamic coefficients by means of special designed wind tunnel tests, which will be explained in detail in the oncoming sections.

The theoretical values of the flutter derivatives of a thin plate section are calculated in terms of Theodorsen function by matching the aerodynamic force terms in the Eqns. 2.3 and 2.4 with the ones in the Eqns. 2.6 and 2.7, Scanlan [2]. The theoretical flutter derivatives are calculated with respect to the following formulas to make comparison with the ones identified from the free vibration test results.

$$H_1^*(K) = -\frac{2\pi}{K} \cdot F(K) \qquad A_1^*(K) = \frac{\pi}{2K} \cdot F(K)$$

$$H_2^*(K) = -\frac{\pi}{2K}\left[1 + \frac{4 \cdot G(K)}{K} + F(K)\right] \qquad A_2^*(K) = -\frac{\pi}{2K^2}\left[\frac{K}{4} - G(K) - \frac{K \cdot F(K)}{4}\right]$$

$$H_3^*(K) = -\frac{\pi}{K^2}\left[2 \cdot F(K) - \frac{G(K) \cdot K}{2}\right] \qquad A_3^*(K) = \frac{\pi}{2K^2}\left[\frac{K^2}{32} + F(K) - \frac{K \cdot G(K)}{4}\right]$$

$$H_4^*(K) = \frac{\pi}{2}\left[1 + \frac{4 \cdot G(K)}{K}\right] \qquad A_4^*(K) = -\frac{\pi}{2K} \cdot G(K) \qquad (2.9)$$

where F(K) and G(K) are the real and the imaginary parts of the Theodorsen function C(K) given in the Eqn. 2.5.

Scanlan [2] made several comparisons between the flutter derivatives of an airfoil and some streamlined cross sections. Furthermore, Sarkar [3] compared the theoretically calculated flutter derivatives of an airfoil with the ones calculated experimentally by using free vibration method, which will be explained in the next section. Both derived flutter derivatives show good agreement in between, which proves the reliability of theoretical derivation of flutter derivatives for airfoils or thin plate sections.

2.3 Flutter Response of a Full-Span Bridge

The main reason for the calculation of flutter derivatives from different types of methods is that, to investigate the response of the full-span bridge deck to the wind loading and to calculate the critical wind speed for the deck section under the conditions of small displacements and linear structural behavior of the system. In the present work the results of the section model test are used to calculate the system parameters and the non-dimensional flutter derivatives, which can be applied in the dynamic analysis of a full-span bridge. Section model cannot be taken as a dynamic analog of the corresponding full-span bridge.

A state-of-the-art analysis procedure is described by Scanlan and Jones [15]. The deformation of the full-span bridge deck with respect to any mode can be defined by the functions of position along the span. Therefore, the deflection components of the bridge deck can be represented in terms of the generalized coordinate of the mode $\xi_i(t)$, the width of the deck B and the dimensionless normalized mode shapes $h_i(x)$, $\alpha_i(x)$ and $p_i(x)$, along the deck. The vertical, twist and sway deflections of a reference spanwise point x of the deck of a full bridge with three degree of freedom is represented by $h_i(x)$, $\alpha_i(x)$ and $p_i(x)$, respectively.

$$\left.\begin{aligned} &\text{vertical}: \quad h(x,t) = \sum_i h_i(x)\cdot B\cdot \xi_i(t), \\ &\text{twist}: \quad \alpha(x,t) = \sum_i \alpha_i(x)\cdot \xi_i(t), \\ &\text{lateral}: \quad p(x,t) = \sum_i p_i(x)\cdot B\cdot \xi_i(t), \end{aligned}\right\} \qquad (2.10)$$

With the governing equation of motion:

$$I_i\left(\ddot{\xi}_i + 2\zeta_i\omega_i\dot{\xi}_i + \omega_i^2\xi_i\right) = Q_i(t) \qquad (2.11)$$

where i=1,…N for N modes; I_i is the generalized inertia of the i^{th} mode; ω_i is the i^{th} mode circular natural frequency; ζ_i is the damping ratio-to-critical, $\xi_i(t)$ is the generalized coordinate of the i^{th} mode, and $Q_i(t)$ is the generalized force defined as

$$Q_i(t) = \int_{Deck}\left[L_h h_i(x)B + M_\alpha \alpha_i(x) + D_p p_i(x)B\right]dx \qquad (2.12)$$

Although a two-degree of freedom system is considered in the present work, in this section the bridge deck section supposed to have a three degree-of-freedom motion for the general explanation of the flutter response of the bridge deck. Since flow condition is assumed to be laminar in the present work only self-excited aeroelastic dynamic forces are considered, no buffeting forces are taken into account.

Three degree of freedom self-excited aerodynamic forces are defined as:

$$L_h = \frac{1}{2}\rho U^2 B\left[KH_1^*\frac{\dot{h}}{U} + KH_2^*\frac{B\dot{\alpha}}{U} + K^2H_3^*\alpha + K^2H_4^*\frac{h}{B} + KH_5^*\frac{\dot{p}}{U} + K^2H_6^*\frac{p}{B}\right]$$

$$M_\alpha = \frac{1}{2}\rho U^2 B^2\left[KA_1^*\frac{\dot{h}}{U} + KA_2^*\frac{B\dot{\alpha}}{U} + K^2A_3^*\alpha + K^2A_4^*\frac{h}{B} + KA_5^*\frac{\dot{p}}{U} + K^2A_6^*\frac{p}{B}\right]$$

$$D_p = \frac{1}{2}\rho U^2 B\left[KP_1^*\frac{\dot{p}}{U} + KP_2^*\frac{B\dot{\alpha}}{U} + K^2P_3^*\alpha + K^2P_4^*\frac{p}{B} + KP_5^*\frac{\dot{h}}{U} + K^2P_6^*\frac{h}{B}\right] \qquad (2.13)$$

Flutter criterion is described by some authors in the literature, i.e. Scanlan and Jones [15], Sarkar [3] in the same way, but with different number of flutter derivatives. The flutter criterion is fulfilled when the imaginary coefficients of ξ_i or namely the generalized damping of the i^{th} mode is equal to zero. By transforming the equation of motion in Eqn. 2.11 into the frequency domain, the flutter criterion is obtained as

$$
\begin{aligned}
&H_1^*(K)\cdot G(h_i,h_i)+H_2^*(K)\cdot G(\alpha_i,h_i)+H_5^*(K)\cdot G(p_i,h_i)\\
&+A_1^*(K)\cdot G(h_i,\alpha_i)+A_2^*(K)\cdot G(\alpha_i,\alpha_i)+A_5^*(K)\cdot G(p_i,\alpha_i)\\
&+P_1^*(K)\cdot G(p_i,p_i)+P_2^*(K)\cdot G(\alpha_i,p_i)+P_5^*(K)\cdot G(h_i,p_i)\geq \frac{4\zeta_i I_i}{\rho B^4}\frac{\omega_i}{\omega},
\end{aligned}
\qquad (2.14)
$$

where

$$
\begin{aligned}
\frac{\omega_i}{\omega}=1+\frac{\rho B^4}{2I_i}\Big[&H_3^*(K)\cdot G(\alpha_i,h_i)+H_4^*(K)\cdot G(h_i,h_i)+H_6^*(K)\cdot G(p_i,h_i)\\
&+A_3^*(K)\cdot G(\alpha_i,\alpha_i)+A_4^*(K)\cdot G(h_i,\alpha_i)+A_6^*(K)\cdot G(p_i,\alpha_i)\\
&+P_3^*(K)\cdot G(\alpha_i,p_i)+P_4^*(K)\cdot G(p_i,p_i)+P_6^*(K)\cdot G(h_i,p_i)\Big]
\end{aligned}
\qquad (2.15)
$$

where

$$
G(r_i,s_i)=\int_{\text{Deck}} r_i(x)\cdot s_i(x)\,dx\ ;\ \ r_i,s_i=h_i,\ \alpha_i \text{ or } p_i \qquad (2.16)
$$

By the application of above formula, it can be understood that which modes are flutter prone or have contribution to the flutter. For the bluff deck sections (e.g., in the original Tacoma Narrows case), flutter criterion can be obtained only checking the aerodynamic damping coefficient A_2^*, which exhibits a sign change from negative to positive with the increasing reduced wind velocity indicating the possibility of single degree torsional flutter. Such bluff bodies exhibit almost pure rotational response and their flutter stability criterion can be controlled simply with respect to one degree of freedom.

2.3.1 Calculation of Critical Wind Speed

Flutter criterion is specified by the damping of the system, where the total damping is equal to zero. The section model oscillates with a harmonic motion at the flutter limit under the so-called critical wind speed. There are some algorithms available in the literature to calculate the critical wind speed, e.g. Starossek [1], Scanlan [2]. In the present work, the critical wind speed is calculated with respect to the formulation developed by Starossek [1].

The equation of motion is simplified by transforming damping and stiffness terms into only one term at the Starossek [1] formulation.

$$
M_s\ddot{x}+K^d x=F_L \qquad (2.17)
$$

where, $M_s=\begin{pmatrix} m & 0\\ 0 & I\end{pmatrix}$; Mass matrix

$$K^d = \begin{pmatrix} (1+ig_h)k_h & 0 \\ 0 & (1+ig_\alpha)k_\alpha \end{pmatrix} \quad ; \text{Stiffness-damping matrix}$$

$$x = \tilde{x}e^{i\omega t} \quad \text{with} \quad \tilde{x} := \begin{pmatrix} \tilde{h}/b \\ \tilde{\alpha} \end{pmatrix} ; \text{Displacement vector}$$

$$F_L = \begin{pmatrix} -L_h/b \\ M_\alpha \end{pmatrix} = \omega^2 L x \quad ; \text{Force vector}$$

The components of the force vector are defined as

$$L = \pi\rho b^2 \begin{pmatrix} c_{hh} & c_{h\alpha} \\ b^2 c_{\alpha h} & b^2 c_{\alpha\alpha} \end{pmatrix} \qquad (2.18)$$

$$\begin{aligned} L_h &= \pi\rho k^2 U^2 (c_{hh} h + b c_{h\alpha} \alpha) \\ M_\alpha &= \pi\rho k^2 U^2 (b c_{\alpha h} h + b^2 c_{\alpha\alpha} \alpha) \end{aligned} \qquad (2.19)$$

K^d is the two-degree of freedom stiffness-damping matrix, where the stiffness and damping properties of the system are represented. The aerodynamic forces are expressed with respect to the complex number approach according to the Starossek [1] formulation. The dimensionless coefficients of flutter derivatives, $c_{mn} = c'_{mn} + i \cdot c''_{mn}$ are the functions of reduced frequency $k = b \cdot \omega / U$, where c'_{mn} and c''_{mn} are the real and imaginary parts of the flutter derivative functions, respectively. The indices of the flutter derivative c_{mn} indicate the force occurred in the degree of freedom 'm' due to the application of motion in the degree of freedom 'n'.

Both the notations (H_i^*, A_i^* ; i=1,..4) and (c_{mn} ; m,n = h or α), which are used to define the flutter derivatives, have the same theoretical background. The relation between the two notations is given in the Table 2.1 for both previous and current Scanlan notations. The following conversion formulas will be used in order to compare results of flutter derivatives in the next chapters.

Starossek Notation	c'_{hh}	c''_{hh}	$c'_{\alpha h}$	$c''_{\alpha h}$	$c'_{h\alpha}$	$c''_{h\alpha}$	$c'_{\alpha\alpha}$	$c''_{\alpha\alpha}$
Current Scanlan Notation	$\frac{2}{\pi} H_4^*$	$\frac{2}{\pi} H_1^*$	$\frac{4}{\pi} A_4^*$	$\frac{4}{\pi} A_1^*$	$\frac{4}{\pi} H_3^*$	$\frac{4}{\pi} H_2^*$	$\frac{8}{\pi} A_3^*$	$\frac{8}{\pi} A_2^*$
Previous Scanlan Notation	$\frac{4}{\pi} H_4^*$	$\frac{4}{\pi} H_1^*$	$\frac{8}{\pi} A_4^*$	$\frac{8}{\pi} A_1^*$	$\frac{8}{\pi} H_3^*$	$\frac{8}{\pi} H_2^*$	$\frac{16}{\pi} A_3^*$	$\frac{16}{\pi} A_2^*$

Table 2.1: Conversion between the notations of the flutter derivatives

The equation of motion in Eqn. 2.17 is rearranged by applying displacement and force vectors in the Eqn. 2.18 and $e^{i\omega t}$ term is eliminated, finally the following homogenous linear equilibrium system is obtained:

$$\left[K^{d} - \omega^{2}(M_{s} + L(k))\right]\tilde{x} = 0 \qquad (2.20)$$

Eqn. 2.20 represents an eigenvalue problem for a system with two degree of freedom. Non-trivial solution is possible only when the determinant of the terms in brackets vanishes. Both ω and the Eqn. 2.20 depend on the reduced frequency k. After fixing the k value, the solution of the eigenvalue problem results in two eigenvalues ω_j^2 and their corresponding eigenvector x_j. The eigenvalues ω_j^2 are generally complex, but just at the critical point where simple harmonic motion takes place, the eigenvalue ω_j^2 at that point is real and positive. The eigenvalue ω and the reduced frequency are separated in the Eqn. 2.20 by multiplying both sides of the equation by $(-(K^d)^{-1}/\omega^2)$. So that the Eqn. 2.20 is transformed to a simple linear eigenvalue problem:

$$(A(k) - \lambda^{e} E)\tilde{x} = 0 \qquad (2.21)$$

where $$A(k) = K^{d^{-1}}(M_s + L(k)) = \frac{1}{\mu}\begin{pmatrix} \dfrac{\mu + c_{hh}}{\omega_h^2(1+ig_h)} & \dfrac{c_{h\alpha}}{\omega_h^2(1+ig_h)} \\ \dfrac{c_{\alpha h}}{r^2\omega_\alpha^2(1+ig_\alpha)} & \dfrac{\mu r^2 + c_{\alpha\alpha}}{r^2\omega_\alpha^2(1+ig_\alpha)} \end{pmatrix}$$

$$\lambda^{e} = \frac{1}{\omega^2} \; ; \; E = \begin{bmatrix} 1 & 0 \\ 0 & 1 \end{bmatrix}$$

Provided that K^d is not singular. The complex system matrix A(k) is composed of the following system parameters:

$$\left.\begin{aligned}
&\varepsilon = \frac{\omega_\alpha}{\omega_h} \quad \rightarrow \text{frequency ratio} \\
&\mu = \frac{m}{\pi\rho b^2} \quad \rightarrow \text{relative mass} \\
&r = \frac{1}{b}\sqrt{\frac{I}{m}} \quad \rightarrow \text{reduced mass radius of gyration} \\
&g_i = 2\cdot\xi_i \;;\; i = h \text{ or } \alpha \quad \rightarrow \text{damping coefficient} \\
&\gamma = (1+ig_h)(1+ig_\alpha)
\end{aligned}\right\} \qquad (2.22)$$

The solution for the eigenvalues λ^e can be obtained by making the determinant of the expression $[A(k)-\lambda^e E]$ equal to zero. So that a second order equation system can be obtained.

$$\left|A-\lambda E\right| = \lambda^{e^2} + a_1\lambda^e + a_0 = 0 \qquad (2.23)$$

The coefficients of the Eqn. 2.23 are calculated with the application of simple calculus by using the system parameters defined in the Eqn. 2.22 as

$$\left.\begin{aligned}
a_0 &= \frac{(\mu + c_{hh})(\mu\cdot r^2 + c_{\alpha\alpha}) - c_{h\alpha}c_{\alpha h}}{\mu^2\varepsilon^2 r^2 \omega_h^4 \gamma} \\
a_1 &= \frac{\varepsilon^2 r^2(\mu + c_{hh})(1+ig_\alpha) + (\mu\cdot r^2 + c_{\alpha\alpha})(1+ig_h)}{\mu\varepsilon^2 r^2 \omega_h^2 \gamma}
\end{aligned}\right\} \qquad (2.24)$$

When the flutter derivatives and the system parameters are applied in the Eqn. 2.24, the coefficients of the second order equation system can be obtained for any k values. If the second order equation, Eqn. 2.23 is solved with respect to the calculated coefficients, eigenvalues λ^e_1 and λ^e_2, which are functions of reduced frequency, are simply calculated as

$$\lambda^e_{1,2}(k) = -\frac{a_1}{2} \pm \sqrt{\left(\frac{a_1}{2}\right)^2 - a_0} \qquad (2.25)$$

The complex circular frequency $\omega = \omega' + i\omega''$ is calculated from the relevant λ^e value in the Eqn. 2.26. The real part of the complex circular frequency corresponds to the natural circular frequency and the imaginary part corresponds to the damping value of the system.

$$\lambda^e = \frac{1}{\omega^2} \rightarrow \omega = \sqrt{\frac{1}{\lambda^e}} = \frac{\sqrt{\bar{\lambda}^e}}{\left|\lambda^e\right|} = \frac{\Re(\sqrt{\lambda^e})}{\left|\lambda^e\right|} - \frac{\Im(\sqrt{\lambda^e})}{\left|\lambda^e\right|}i \qquad (2.26)$$

By using the real and imaginary parts of the complex circular frequency, the logarithmic decrement that represents the damping of the system can be calculated as

$$\delta = 2\pi \frac{\omega''}{|\omega'|} = -2\pi \frac{\Im\left(\sqrt{\lambda}\right)}{\left|\Re\left(\sqrt{\lambda}\right)\right|} \qquad (2.27)$$

The damping curves of the system are drawn with respect to the corresponding reduced frequency values k. The torsion branch of the damping curve crosses the zero line at one of the specific k axis, which corresponds to the critical k value. That point is the flutter stability point, at which the system shows harmonic motion. The circular frequency of the torsion branch at the critical reduced frequency is obtained as calculated in the Eqn. 2.26. Finally, the critical wind speed can be simply calculated as

$$k_{critical} = \frac{b\omega}{U_{critical}} \quad \Rightarrow \quad U_{critical} = \frac{b\omega}{k_{critical}} \qquad (2.28)$$

After the calculation of the flutter derivatives and the system parameters, critical wind speed of any cross section can be determined by using the explained algorithm. During the predesign stage of a long span bridge, which has a streamlined deck section, it is reasonable to estimate the critical wind speed of the streamlined section by using thin plate flutter theory. So that, an approximate idea can be obtained before the final calculation of the critical wind speed.

2.3.2 Calculation of Phase Shift and Amplitude Ratio

After the calculation of system parameters and flutter derivatives, the phase shift and the amplitude ratio between the two motions can be calculated for any particular wind speed. Starossek [1] has developed the following formulation for the calculation of φ_α and R_α values by normalizing the displacement vector with respect to the h/b given in Eqn. 2.17.

$$R_\alpha = \frac{|\tilde{\alpha}|}{|\tilde{h}/b|} \quad \text{and} \quad \varphi_\alpha = \arg\left(\frac{\tilde{\alpha}}{\tilde{h}/b}\right) \qquad (2.29)$$

Since the displacement vector is normalized; h/b=1 and the α is obtained as

$$\tilde{\alpha} = \frac{(c''^2_{h\alpha}\kappa_1 + c'^2_{h\alpha}\kappa_2) + i\,(c'^2_{h\alpha}\kappa_1 + c''^2_{h\alpha}\kappa_2)}{c'^2_{h\alpha} + c''^2_{h\alpha}} \qquad (2.30)$$

where, $\kappa = \lambda\mu\omega_h^2 = -\frac{a_0''}{a_1''}\mu\omega_h^2$; $\kappa_1 = \kappa g_h - c''_{hh}$ and $\kappa_2 = \kappa - (\mu + c'_{hh})$

The system parameters and the imaginary part of the coefficients a_0 and a_1 are obtained from the Eqn. 2.22 and Eqn 2.24, respectively. By using the κ values and the flutter derivatives, φ_α and R_α are calculated as

$$R_\alpha^2 = |\tilde{\alpha}| = \frac{\kappa_1^2 + \kappa_2^2}{c_{h\alpha}'^2 + c_{h\alpha}''^2} \quad \Rightarrow \quad R_\alpha \tag{2.31}$$

$$\tan\varphi_\alpha = \frac{\Im(\tilde{\alpha})}{\Re(\tilde{\alpha})} = \frac{c_{h\alpha}'\kappa_1 - c_{h\alpha}''\kappa_2}{c_{h\alpha}''\kappa_1 - c_{h\alpha}'\kappa_2} \quad \Rightarrow \quad \varphi_\alpha \tag{2.32}$$

2.4 Extraction Techniques

Contrary to streamlined sections, a reliable theoretical calculation of flutter derivatives for the bluff cross sections or non-streamlined sections is not possible. There are some numerical approaches using Computational Fluid Dynamics (CFD) for the determination of aerodynamic derivative functions for arbitrary bridge deck sections, but their reliability depends on many factors. Before replacing wind tunnel testing, the reliability and the robustness of the CFD approach should be proved. Therefore, the final step for the determination of flutter derivatives should be done through wind tunnel testing on sectional models.

There are two kinds of experimental methods to obtain the system parameters by using a sectional model of the bridge deck through wind tunnel tests: the forced vibration method and the free vibration method. The free vibration section model test, which has a simple experimental set-up, is the easiest measurement method to obtain the flutter derivatives. However, contrary to its simplicity of experimental set-up, the identification method used for the calculation of flutter derivatives from the free vibration results is more complicated compared to the other methods. In the present work, free vibration section model tests are used to obtain the flutter derivatives and forced vibration section model test results are used for comparison.

2.4.1 Free Vibration Method

By the free vibration test, the bridge deck section model is supported with the help of springs, and when necessary additional damping elements can be added to the system. Then the system is given an initial displacement in the corresponding degrees of freedom. The system parameters such as the frequency and the damping of the vibration for the wind-on conditions are determined from the system response with the help of system identification methods. The same procedure is repeated for the vacuum case in order to calculate the

mechanical system parameters. After then, the aeroelastic derivatives are obtained through the difference of system parameters calculated according to the wind-on and wind-off cases either for a coupled or uncoupled system. The free vibration method is adopted widely because of its simplicity. The disadvantage of the free vibration method compared to the forced vibration method is, that the flutter derivatives cannot be obtained directly. A suitable system identification technique should be applied for the calculation of both system parameters and flutter derivatives. The measured free vibration displacement data of the section model is formulated as $x(t) = C^{*} \cdot e^{\lambda \cdot t} \cdot \cos(\omega \cdot t + \varphi)$ for both vertical and rotational displacement with the corresponding system parameters by using the appropriate system identification method. Therefore, the quality of the calculated flutter derivatives is highly depended on the performance of the system identification method and the quality of the experimental set-up, which affects the data quality severely. As a result, care should be given in every stage for the calculation of flutter derivatives.

2.4.2 Forced Vibration Method

Forced vibration method is one of the experimental techniques to determine the flutter derivatives. In the present work, this method is not explained in detail. The bridge deck section is forced to undergo a sinusoidal motion with constant amplitude either vertically or rotationally. Generally a balance system is used to measure and analyze the aerodynamic forces acting on the section model as explained in Bergmann [22]. Therefore, the experimental set-up of the forced vibration method is more complex and expensive compared to the experimental set-up of the free vibration method. The aeroelastic derivatives can be calculated with respect to the measured aerodynamic forces. On contrary to the free vibration method, it is not necessary to couple the degree of freedoms of the motion. Besides, it is only possible to extract the flutter derivatives, whose corresponding degree of freedom is forced to go under motion. The flutter derivatives H_1^{*}, H_4^{*}, A_1^{*}, A_4^{*} are extracted from the aerodynamic forces caused by the forced vertical motion, and the flutter derivatives H_2^{*}, H_3^{*}, A_2^{*}, A_3^{*} are extracted from the aerodynamic forces caused by the forced rotational motion.

Two different forced vibration test results are used to make comparison with the free vibration test results. Forced vibration test results of Bergmann [22] and Hortmanns [23] for the rectangular section model having the same aspect ratio of 1:8 are used for comparison.

3 SYSTEM IDENTIFICATION METHODS

3.1 Introduction

System identification methods are very useful tools to identify unknown parameters of a real system according to its output that are obtained usually from experiments. In order to apply system identification methods on the systems that are investigated, the mathematical model and the experimental model from the dynamic testing are necessary. Not all the system identification methods are suitable or applicable for structural dynamic problems involving such as wind or earthquake loading. Because the measurement output data can contain high noise level or the system cannot be modeled mathematically due to its nonlinear or complex behavior.

There are some system identification methods used in the field of structural dynamic problems. However, most of them are not always so efficient to identify the parameters of every type of system due to some reasons, which will be discussed in the section 3.2. On the other hand, each method has some advantages and disadvantages compared to the other methods. The time domain system identification methods will be discussed as applied to the linear structural dynamic problems, which is one of the main prerequisite for the identification of flutter derivatives from the system identification methods in the present work.

The purpose of this chapter is to compare the available system identification methods and select the most efficient and the easiest method among the investigated system identification methods in the literature. The selected method should be able to identify the flutter derivatives of the bridge deck sections with the data obtained from section model tests under smooth flow even for a relatively noisy time history data, which can be either displacement, velocity, acceleration or any combination of these time histories.

3.2 System Identification Methods

Some of the system identification methods are presented here to give brief information and make the comparison in between. The flutter derivatives can be extracted by using the following methods that are used in the time domain.

- Ordinary Least Square (OLS) Method
- Maximum Likelihood (ML)
- Limited Information Maximum Likelihood (LIML)

- Instrumental Variable (IV) Method
- Logarithmic Decrement Method
- Nonlinear Least Squares Method
- Extended Kalman Filtering with Weighted Global Iteration (EKF-WGI)
- Ibrahim Time Domain Method (ITD)
- Modified Ibrahim Time Domain Method (MITD)

In the calculation algorithm of these methods, an initial estimation of the parameters is necessary in order to start the identification procedure. Initial estimation is done mostly by OLS method, which minimizes the distance between the experimental transfer functions and the analytical ones calculated as a first approximation using the section model parameters.

The identification results of a two-degree of freedom system, whose estimations are based on simulated data, with different identification methods, are given by Shinozuka et al. [17] in order to compare the results of the methods OLS, IV, LIML and ML with the known exact parameter values. The results show that, except for the OLS method, other methods show good results in the estimation of parameters. Furthermore, the time duration of the final estimation for the IV and LIML methods are approximately five times shorter than for the ML method. A second set of comparison is made by Shinozuka et al. [17] between the results of LIML and IV methods for the estimation of aerodynamic coefficients of a suspension bridge by using field measurement data of a bridge deck model. It is shown that, the results of LIML method yield better estimates than the IV method. Even in the presence of local instability of the system under greater wind speeds, LIML method estimates reasonable results, whereas the IV method yields no longer consistent estimates. It is interpreted from these sets of comparisons that the LIML method is more reliable and more efficient than the other three methods (IV, ML, OLS). However, Sarkar [3] has indicated that all these methods do not work properly under the input disturbances, which were assumed to be always present as a measurable non-zero value. Therefore, these methods are evaluated as unstable for the identification of flutter derivatives.

In the logarithmic decrement method, the best estimate for the damping ratio is calculated through the peak amplitudes of the observed time histories, whose curve is fitted by OLS method. And the natural frequency of the system is calculated by taking the average of the time intervals between these peak points or simply by using standard fast fourier-transformation (fft) method. After the identification of the damping ratio and the frequency, direct flutter derivatives can be calculated. Since logarithmic decrement does not use all the

measured data point, it does not work properly with relatively noisy data, which makes the reliability of this method poor.

Non-linear least square method is also available for the system identification, which is based on the Taylor series expansion of the parameters with the initial estimates. The final estimates of the system parameters depend on the initial estimates, so that the reliability of the method is affected by the quality of initial value estimation of the parameters. And the second disadvantage of the non-linear least square method is that, the identified flutter derivatives at higher reduced wind velocities exhibit great discrepancies compared to the results of other system identification methods.

The extended kalman filter algorithm updates an extended space representation recursively as new observations starting from an initial estimate. Indeed the final estimation of algorithm is similar to the predictor-corrector algorithm used for solving numerical problems. In fact the concept is a form of sequential least square estimation adapted to the problem of parameter estimation for systems with measured input data. As explained in the previous methods the initial estimates play a very important role for the reliability of the identification method. Using weighted global iteration to the extended kalman filter algorithm eliminates the effect of initial estimate considerably. Application of weighted global iteration also provides to estimate the parameters with faster convergence.

Yamada et al. [18] discussed the feasibility and the problems of the extended kalman filtering method applied on the flat plate wing for coupled aerodynamic force using wind tunnel test results as:

(i) The extended kalman filter algorithm can estimate very accurate coefficients, even if the original signal includes considerable white noise.

(ii) When the analyzed signal includes very narrow band noise, such as beating signal, it is difficult to eliminate the effect of noise from the measurement data.

(iii) Sampling interval and its length play very important role in the stability of parameter estimation and the stability of convergence.

(iv) In order to get stable and nontrivial solutions it is important to check whether the assumed system description and the observed real system are identical. For example when the aerodynamic force is not coupled, the system identification as coupled model will not give any reasonable results. This is the case at low wind speeds, where the coupling between bending and torsion is hardly observed.

Both ITD and MITD methods use the free vibration system output data. MITD is a recursive method that uses the ITD method for the initial estimates. MITD can extract all the direct and cross derivatives from the coupled free vibration data of 2-DOF sectional model. The method simplifies the identification procedure and also works well even under high noise level. However, the selection of time shifts (N_1 and N_2) is very important for the sake of quality of the parameters to be identified. Sarkar [3] suggested an empirical formula to calculate the time shifts. The numerical simulations proved the robustness and reliability of the results of the MITD method by different researchers, such as Chen [13], Sarkar [3], Sarkar and Scanlan [12], etc. Also, MITD method does not have any restriction such as the need for the knowledge of process or measurement noise or the need for the velocity or acceleration time histories in addition to the displacement time history.

The type of the problem that is taken into account is very important for selecting the type of the system identification method. Therefore, it is not possible to apply each method to our main problem of the extraction of flutter derivatives. After examining the advantages and disadvantages of the methods mentioned above, MITD is selected to be the most suitable method for the identification of system parameters in the present work. A detailed explanation of the MITD method will be presented in the following sections.

3.3 Modified Ibrahim Time Domain (MITD) Method

A linear dynamic system can be represented with the following equation of motion as:

$$M_s\ddot{X}(t) + C_s\dot{X}(t) + K_sX(t) = F(t) \qquad (3.1)$$

F(t) is the externally acting force vector. M_s, C_s, K_s are the mass, damping, stiffness matrices of the system, respectively where X(t) represents the displacement vector of the system in the corresponding degrees of freedom. In the present work, since the system is considered in two degrees of freedom, which are vertical and torsional, the system parameters M, C, K are composed of (2×2) matrix and the displacement vector X(t) is (2×1) vector.

The calculations can be carried out according to the acceleration or velocity or displacement time histories. In the present work displacement time histories, which are easier and simpler to measure, are used as the input data for the identification process.

The measured time histories Y(t) (h(t) for vertical degree of freedom and $\alpha(t)$ for torsional degree of freedom) are represented as:

$$Y(t) = X(t) + \eta(t) \qquad (3.2)$$

where $\eta(t)$ is the total noise vector.

The total noise vector composed of the noise occurred during the experiment, such as measurement or randomness of input and output turbulences. Main task in the present work is the identification of flutter derivatives from the free vibration test results under smooth flow. However it is not possible to obtain a 100 % smooth flow condition, most probably some inevitable turbulences will occur, which are due to both wind turbulence and local induced turbulence. The turbulences are treated as additional noise to the system. Since MITD method is very effective to remove the noise from the measurement data. The turbulence effect is therefore can be eliminated from the measurement data with the application of MITD method. Therefore MITD method can be applied to all deck section types including bluff bodies, which are affected by significant amounts of turbulence making the displacement time history data noisy. That is the one of the reason that MITD is selected as the most appropriate method among the discussed system identification methods.

Before starting to explain MITD, it is better to start with the ITD method, which provides initial parameter estimation used in the first step of MITD method.

3.3.1 Ibrahim Time Domain (ITD) Method

A detailed description of ITD method is presented by Ibrahim, S.R., Mikulcik E.C. Both ITD and MITD methods are based on the free oscillating output vector X(t). That means external force in the Eqn. 3.1 is taken as zero (F(t)=0). In the case of turbulent flow condition, F(t) cannot be zero. However, as mentioned earlier the inevitable small turbulences are taken as additional noise to the system and therefore, ITD and MITD methods can be carried out for the free vibration test results even for noisy sets of data. Since the right side of the Eqn. 3.1 is turned out to be zero, the external force appears in the matrices C and K in the mathematical model.

The basic idea of the ITD method is explained in detail, because the MITD method is the modification of this method explained in Sarkar [3]. Displacement vector X(t) in the Eqn. 3.1 is represented as in the following form:

$$X_{2\times 1} = P_{2\times 1} \cdot e^{\lambda t} \qquad (3.3)$$

If the Eqn. 3.3 is substituted in the Eqn. 3.1, two complex conjugate pairs of λ_j, (j = 1-4) are obtained as eigenvalues and two complex conjugate pairs of P_j, (j = 1-4) are obtained as eigenvectors. Then the Eqn. 3.3 can be written in terms of the solutions obtained as

$$X_i = X(t_i) = \sum_{j=1}^{4} P_j \cdot e^{\lambda_j t_i} \qquad (3.4)$$

where t_i is the time sampling at i^{th} time step. The Eqn. 3.4 can be written for six discrete time steps.

$$X = P\Lambda, \quad Y = Q\Lambda, \quad Z = R\Lambda \qquad (3.5)$$

where $X = [X_i, i = 1\text{-}4]$, $P = [P_j, j = 1\text{-}4]$

$Y = [Y_i, i = 1\text{-}4] = X_{i+1} = X(t_i+\Delta t)$, $Q = [Q_j, j = 1\text{-}4]$; $Q_j = P_j \cdot e^{\lambda_j \Delta t}$

$Z = [Z_i, i = 1\text{-}4] = X_{i+2} = X(t_i+2\cdot\Delta t)$, $R = [R_j, j = 1\text{-}4]$; $R_j = P_j \cdot e^{2\cdot\lambda_j \Delta t}$

P_j, Q_j, R_j being the elements of vectors P, Q, R, respectively,

$\Lambda_{ij} = e^{\lambda_j t_i}$ is the element of Λ and Δt = 1/Sampling Rate; If the Eqn. 3.5 is rewritten:

$$\Phi = \Psi\Lambda; \quad \hat{\Phi} = \hat{\Psi}\Lambda \qquad (3.6)$$

where the matrices in the Eqn. 3.6 defined as

$$\Phi = [X\ Y]^T; \quad \hat{\Phi} = [Y\ Z]^T; \quad \Psi = [P\ Q]^T; \quad \hat{\Psi} = [Q\ R]^T \qquad (3.7)$$

The following general formula is obtained by eliminating Λ in the Eqn. 3.6 as

$$\hat{\Phi}\,\Phi^{-1}\Psi_j = e^{\lambda_j \Delta t}\Psi_j \qquad (3.8)$$

There are N data points of X_i, (i = 1-N). In order to make the formulations more practical, time shift coefficients N_1 and N_2 are introduced instead of Δt. The shift between the time histories X and Y is $(N_2\cdot\Delta t)$ instead of Δt while constructing the matrix Φ. Similarly, the time shift between the matrices in the Eqn. 3.6 is $(N_1\cdot\Delta t)$ instead of Δt. N_1 and N_2 are the integer numbers much less than the number of data points N.

By using the time histories of measured data, the matrices Φ and $\hat{\Phi}$ are formed with respect to time interval Δt and time shifts N_1 and N_2. Sarkar [3] suggested an empirical formula to select the time shifts close to optimal values. $N_2 = N_1 \pm (1 \text{ or } 2)$ where N_1 is calculated as the nearest integer below the ratio $1/(4\cdot\Delta t\cdot f_d)$ (f_d is the highest modal frequency of the time histories in [Hz]).

Φ and $\hat{\Phi}$ have the dimension of $(4\times N\text{-}N_1\text{-}N_2)$ for a two-degree of freedom system.

$$\Phi = \begin{bmatrix} Y(0) & Y(\Delta t) & \dots Y((N - N_1 - N_2 - 1)\Delta t) \\ Y((N_2)\Delta t) & Y((N_2 + 1)\Delta t) & \dots Y((N - N_1 - 1)\Delta t) \end{bmatrix} \quad (3.9)$$

$$\hat{\Phi} = \begin{bmatrix} Y((N_1)\Delta t) & Y((N_1 + 1)\Delta t) & \dots Y((N - N_2 - 1)\Delta t) \\ Y((N_1 + N_2)\Delta t) & Y((N_1 + N_2 + 1)\Delta t) & \dots Y((N - 1)\Delta t) \end{bmatrix} \quad (3.10)$$

N is the number of data points in the measurement vector Y(t). The selection of the time interval Δt and time shifts N_1 and N_2 has a great influence on the identification quality of the method MITD, which will be discussed later.

The least squares equivalent of the Eqn. 3.8 can be written as

$$[\hat{\Phi}\,\Phi^T][\Phi\,\Phi^T]^{-1}\,\Psi_j = e^{\lambda_j N_1 \Delta t}\Psi_j \quad (3.11)$$

Modal frequencies and modal damping ratios of the system can be identified by calculating the complex eigenvalues of the matrix $A_{4\times4} = [\hat{\Phi}\Phi^T][\Phi\Phi^T]^{-1}$. Matrix $A_{4\times4}$ has 4 eigenvalues, which are in the form of two complex conjugate pairs, such as $(\beta_1 \pm i\gamma_1)$ and $(\beta_2 \pm i\gamma_2)$.

The decay rate, λ for each motion calculated as:

$$\lambda_1 = \ln(\beta_1^2+\gamma_1^2)/2N_1\Delta t \qquad \lambda_2 = \ln(\beta_2^2+\gamma_2^2)/2N_1\Delta t \quad (3.12)$$

The natural circular frequency, ω for each motion calculated as:

$$\omega_1 = \tan^{-1}(\gamma_1 / \beta_1)/N_1\Delta t \qquad \omega_2 = \tan^{-1}(\gamma_2 / \beta_2)/N_1\Delta t \quad (3.13)$$

In order to prevent positive bias in the estimated values of λ, a negative time shift (N_1) should be introduced by changing the places of Φ and $\hat{\Phi}$ in the Eqn. 3.11. So that the matrix $B_{4\times4} = [\Phi\hat{\Phi}^T][\hat{\Phi}\hat{\Phi}^T]^{-1}$ can be formed and the modal damping ratios and the modal frequencies of the two degree freedom system is calculated with the same formulation as explained for the matrix $A_{4\times4}$ by using negative time shift N_1. Finally the modal damping ratios and the modal frequencies of the two-degree freedom system is calculated by taking the average

values of λ and ω calculated from the positive and negative time shifts of N_1. These calculated parameters will be used for the initial estimates of the MITD method.

3.3.2 Iterative Process of the MITD Method

After the initial estimates are calculated by ITD method, MITD method removes noisy signals from the measured data during the iterative process and identifies the system parameters accurately.

System response for a two-degree freedom system is represented with the vector $X(t)=\{h(t)\ \alpha(t)\}^T$, where h(t) and $\alpha(t)$ are the displacement time histories for vertical and torsional degree of freedoms, respectively. According to the structural dynamics, see Clough and Penzien [8], the free vibration response of a two-degree of freedom system can be written in the form:

$$h(t) = C_{11}^{*} \cdot e^{\lambda_1 t} \cdot \cos(\omega_1 t + \varphi_{11}) + C_{12}^{*} \cdot e^{\lambda_2 t} \cdot \cos(\omega_2 t + \varphi_{12}) \qquad (3.14)$$

$$\alpha(t) = C_{21}^{*} \cdot e^{\lambda_1 t} \cdot \cos(\omega_1 t + \varphi_{21}) + C_{22}^{*} \cdot e^{\lambda_2 t} \cdot \cos(\omega_2 t + \varphi_{22}) \qquad (3.15)$$

The system parameters in the Eqns. 3.14 and 3.15 are identified by the MITD method from the time histories h(t) and $\alpha(t)$. By using these parameters, $\overline{K} = M_s^{-1} \cdot K_s$ and $\overline{C} = M_s^{-1} \cdot C_s$ matrices are calculated under the wind-on and wind-off conditions. Finally these identified matrices will be used for the calculation of flutter derivatives, which are the final aim of this work.

Sarkar [3] presented a detailed description of the MITD method, which is used in the following calculations.

3.3.2.1 Identification Process

Parameters are identified according to the following steps.

step (1) The initial estimates of the system parameters ω and λ are obtained from the Eqns. 3.12 and 3.13 by the application of ITD method from the N data points of displacement time history data.

step (2) By using the initial estimated parameters, N data points of system response vector $X_g(t)$ are generated according to the Eqns. 3.14 and 3.15 where $X_g(t)$ is the pseudo representation of the response vector X(t). The noise in the measurement data Y(t) and the errors in the generated $X_g(t)$ are uncorrelated. The modified instrumental variables $\overline{\Phi}$ and $\overline{\hat{\Phi}}$ are generated just like Φ and $\hat{\Phi}$ in the Eqns. 3.9 and 3.10 except

that $X_g(t)$ is used instead of Y(t). $\overline{\Phi}$ and $\overline{\hat{\Phi}}$ matrices having the order of $4\times(N-N_1-N_2)$. Eqn. 3.11 is modified with respect to the new instrumental variables $\overline{\Phi}$ and $\overline{\hat{\Phi}}$ as

$$[\overline{\hat{\Phi}}\,\overline{\Phi}^{T}][\overline{\Phi}\,\overline{\Phi}^{T}]^{-1}\,\Psi_j = e^{\lambda_j N_1 \Delta t}\Psi_j \qquad (3.16)$$

The calculation of the complex eigenvalues and eigenvectors of $[\overline{\hat{\Phi}}\,\overline{\Phi}^{T}][\overline{\Phi}\,\overline{\Phi}^{T}]^{-1}$ yield a revised set of system parameters as done in Eqns. 3.12 and 3.13. As explained in the ITD method, to prevent positive bias in the estimated values of λ, the roles of $\overline{\Phi}$ and $\overline{\hat{\Phi}}$ are interchanged and with the application of same procedure explained above, the average values of the system parameters can be calculated as done in step 1. By using these parameters new time history $X_g(t)$ is generated, which is used to update the matrices $\overline{\Phi}$ and $\overline{\hat{\Phi}}$.

step (3) Step (2) is repeated with the revised set of parameters until all the values of the parameters of Eqns. 3.14 and 3.15 converge. Finally, $\overline{K} = M_s^{-1}\cdot K_s$ and $\overline{C} = M_s^{-1}\cdot C_s$ matrices can be estimated by using the converged values of these parameters.

The amplitude C_{ij}^{*} and the phase φ_{ij} of the motions in the Eqns. 3.14 and 3.15 need to be calculated for the iterative process in the *step(1)* and *step(2)*. The complex eigenvectors are usually normalized with respect to their amplitudes as well as phase. Hence, the amplitude ratios C_{11}^{*} / C_{21}^{*}, C_{12}^{*} / C_{22}^{*} and the phase difference $\varphi_{11}-\varphi_{21}$, $\varphi_{12}-\varphi_{22}$ can be identified from the first two rows of the eigenvector $\Psi_{4\times4}$,which correspond to $P_{2\times4}$, calculated from the positive time shift cycle. C_{ij}^{*} and φ_{ij} parameters can be calculated with the vector $P_{2\times4}$ and the knowledge of the initial displacements $h(0)$, $\alpha(0)$ and the initial velocities $\dot{h}(0)$, $\dot{\alpha}(0)$.

Initial values of the displacement and velocity have no effect on the calculation of system parameters λ_1, λ_2, ω_1, ω_2. Also, after making some trial calculations, the same system matrices $\overline{K}$ and $\overline{C}$ are calculated for both the exact and any arbitrary initial condition values. Therefore, it is not important to determine the exact initial condition values for the identification of flutter derivatives, which are calculated from the difference of the effective and the mechanical system matrices calculated in the wind-on and wind-off cases, respectively.

3.3.2.2 Calculation of System Matrices $\overline{K}$ and $\overline{C}$

The displacement time histories for vertical and torsional degree of freedoms are calculated in Eqns. 3.14 and 3.15 with the identified system parameters. The velocity and the acceleration time histories for the corresponding degrees of freedom can simply be derived from the displacement time histories. A discrete time state space representation of a two-degree of freedom free vibrating system is given as:

$$\dot{X} = \Theta X \qquad (3.17)$$

where

$$X = \begin{bmatrix} h \\ \alpha \\ \dot{h} \\ \dot{\alpha} \end{bmatrix} = A\,Y \quad ; \quad \dot{X} = \begin{bmatrix} \dot{h} \\ \dot{\alpha} \\ \ddot{h} \\ \ddot{\alpha} \end{bmatrix} = B\,Y \qquad (3.18)$$

and

$$\Theta_{4\times4} = \begin{bmatrix} 0 & I \\ -M_s^{-1}K_s & -M_s^{-1}C_s \end{bmatrix} \; ; \quad I = \begin{bmatrix} 1 & 0 \\ 0 & 1 \end{bmatrix} \qquad (3.19)$$

The matrices A and B are the functions of estimated parameters in Eqns. 3.14 and 3.15. And the column vector Y defined as

$$Y = \{\, e^{\lambda_1 t}\cdot\cos(\omega_1 t) \;\; e^{\lambda_1 t}\cdot\sin(\omega_1 t) \;\; e^{\lambda_2 t}\cdot\cos(\omega_2 t) \;\; e^{\lambda_2 t}\cdot\sin(\omega_2 t) \,\}^T \qquad (3.20)$$

After the calculation of system parameters, the column vectors $X_{4\times1}$ and $Y_{4\times1}$ are formed according to the Eqns 3.18 and 3.20, respectively. And then the matrices $A_{4\times4}$ and $B_{4\times4}$ are calculated by substituting the vectors $X_{4\times1}$ and $Y_{4\times1}$ in the Eqn. 3.18.

The necessary arrangements are made for the elements of the Eqn. 3.18 as follows

$$Y = A^{-1}X \;\rightarrow\; \dot{X} = (BA^{-1})X \qquad (3.21)$$

If the Eqns 3.17 and 3.21 are compared, it is obvious that $\Theta = B\cdot A^{-1}$. Finally the system matrices are calculated as

$$\overline{K} = M_s^{-1}\cdot K_s = -\Theta_{2,1} \quad \text{and} \quad \overline{C} = M_s^{-1}\cdot C_s = -\Theta_{2,2} \qquad (3.22)$$

3.3.3 Numerical Example

A numerical example is carried out in order to investigate the reliability of the MITD method. The measurement data (ow_20_01.dat) having the sampling rate of 100 Hz is used as an example, which is obtained in the wind-off condition with the section model whose four sides are simultaneously lifted 20 mm upwards. The effects of the number of measurement data N, the time shifts N_1 and N_2 and the initial condition values will be examined on the identified parameters.

After the sampling rate is fixed, the number of data points only depends on the length of the time history, which is now more important than the number of data points. The time history is recorded up to the minimum acceptable motion amplitude. Because, after a certain data point, the quality of the measured data decrease due to the increasing noise level.

3.3.3.1 Effect of the Time Shifts N_1 and N_2

As mentioned earlier, Sarkar [3] suggested an empirical formulation to calculate the time shifts. Time shifts not only affect the accuracy of the estimations but also influence the number of iterations required for the convergence of the MITD method to identify the parameters. Besides, in case of an irrelevant selection of the time shift values, MITD method cannot converge to a certain value. Therefore, the following formulation needs to be proved before the application of the MITD method.

$$N_2 = N_1 \pm (1 \text{ or } 2) \text{ or } N_2 = N_1, \text{ where } N_1 = 1/(4 \cdot \Delta t \cdot f_d) \qquad (3.23)$$

where, f_d is the highest modal frequency of the time histories in [Hz].

The second important task is to decide which N_2 value is used in the MITD method given in the Eqn. 3.22. Therefore, five different N_2 values are compared between each other. And the modal frequencies estimated by MITD for each different N_2 values are compared with the ones calculated by using the standard fast fourier transformation method. So that, the reliability of the time shift formulas can be investigated and the optimal formulation for the N_2 can be find out.

From the fft analysis $\omega_h = 16.5608$ [1/s] and $\omega_\alpha = 28.9814$ [1/s] for the measurement data ow_20_01. In order to calculate the N_1 from the Eqn. 3.22, f_d is calculated as

$$f_d = \max(f_h, f_\alpha) = \omega_\alpha/(2\pi) \rightarrow f_d = 4.6125 \text{ Hz}$$

$$N_1 = 1/(4 \cdot 0.01 \cdot 4.6125) = 5.42,$$

The time shift shifts should be integer numbers in order to form the instrumental variables in the Eqns. 3.9 and 3.10. Therefore, N_1 is taken as the nearest integer below the ratio $1/(4\cdot\Delta t\cdot f_d)$, $N_1 = 5$.

	N_1=5				
	$N_2=N_1-2=3$	$N_2=N_1-1=4$	$N_2=N_1=5$	$N_2=N_1+1=6$	$N_2=N_1+2=7$
ω_α [1/s]	28.8795	28.8829	28.8817	28.8841	28.8863
% Diff. btw. fft.	0.352	0.340	0.344	0.336	0.328
ω_h [1/s]	16.5509	16.5509	16.5509	16.5508	16.5507
% Diff. btw. fft.	0.060	0.060	0.060	0.060	0.061
λ_α	-0.3979	-0.3981	-0.3993	-0.3946	-0.3967
λ_h	-0.0958	-0.0959	-0.096	-0.0961	-0.0963

Table 3.1: Effect of the time shifts

In the Table 3.1, the identified system parameters λ_h, λ_α, ω_h, ω_α are presented with respect to the different N_2 values by using the MITD method. Also the difference between the circular frequency values calculated by standard fft method and by the MITD method is presented. As seen in the Table 3.1 the difference between the system parameters is very small for different N_2 values. Therefore, any suggested N_2 value can be used in the MITD method. However, to be consistent for the identification of the rest of the data, a fixed N_2 formula is selected; $N_2 = N_1+1$. And the small difference between the circular frequency values calculated by different methods shows not only the reliability of the empirical formula suggested for the time shifts, but also the reliability of the MITD method.

Although the measurement data has a noisy time history, especially torsional motion data, the curve obtained by the MITD method for the present example fits the measured data curve very well as seen in the Fig. 3.1.

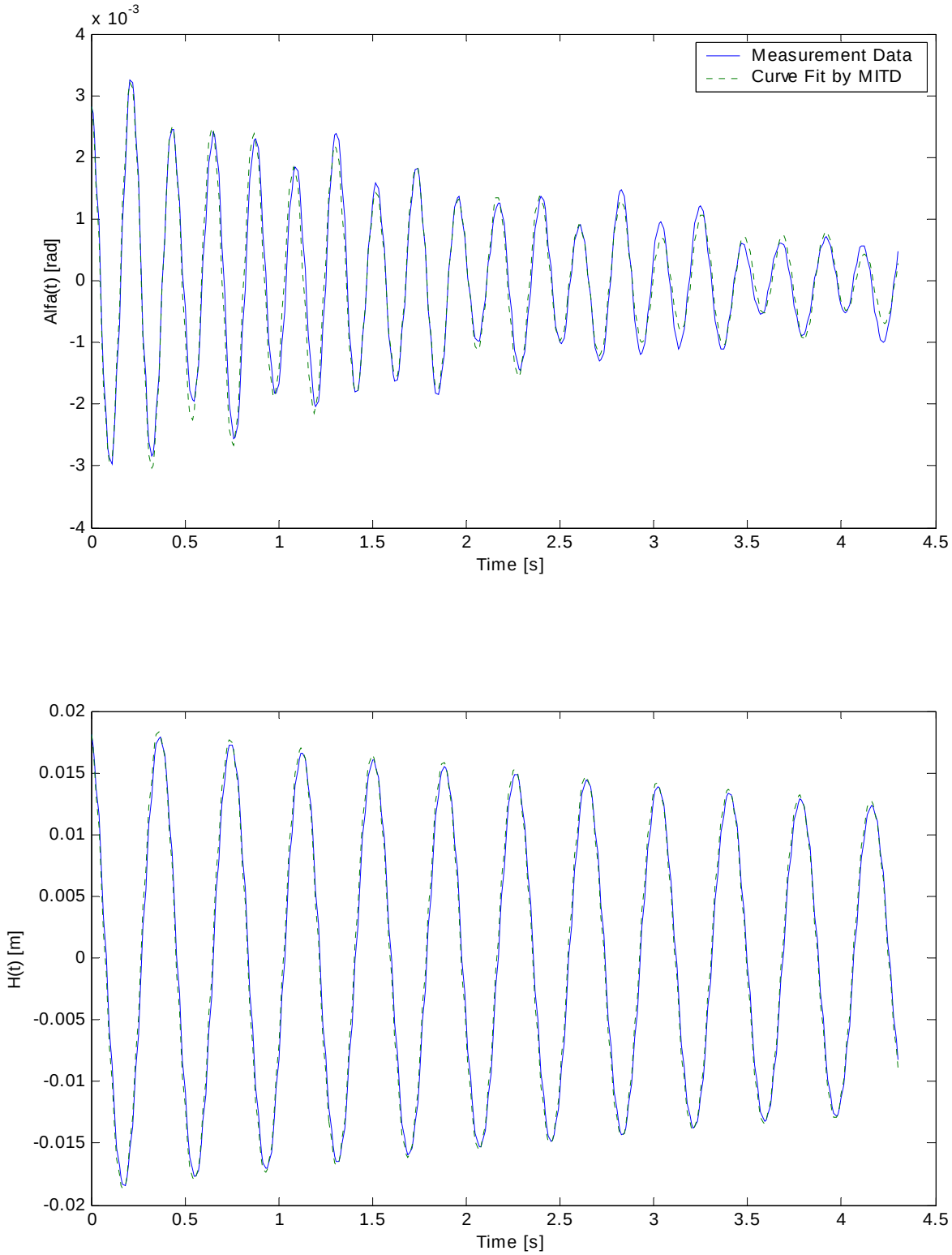

Figure 3.1: Curve fit by the MITD method to the noisy time histories

3.3.3.2 Effect of the Initial Condition Values

Initial displacement and velocity values are required to calculate the amplitude and phase of the motion. However, as mentioned previously, their values do not affect the identified system matrices and consequently the flutter derivatives. This is also checked by the application of MITD method on the same example.

Initial condition values are calculated from the first two elements of the time history data as follows:

$$\text{Initial Displacement} = \begin{Bmatrix} h(t_0) \\ \alpha(t_0) \end{Bmatrix}$$

$$\text{Initial Velocity} = \begin{Bmatrix} (h(t_1) - h(t_0))/\Delta t \\ (\alpha(t_1) - \alpha(t_0))/\Delta t \end{Bmatrix} \qquad (3.24)$$

The comparison is made between the different initial condition values. First the exact values are used and then two different arbitrary values are used in the MITD method. The same values are calculated for the system parameters λ_α, λ_h, ω_α, ω_h and the system matrices $\overline{K}$ and $\overline{C}$ through three different cases. However, the identified time history curve does not fit the curve obtained from measurement time history because of the different amplitude and phase shift for the arbitrary selected initial condition cases. It is concluded that MITD method does not need any information for the initial condition values to identify the flutter derivatives, which is an additional advantage over the other methods.

4 DESCRIPTION OF THE EXPERIMENTAL SET-UP

Aerodynamic parameters required for the analysis and the design of the bridge deck are extracted from the wind tunnel test results. Free vibration motion test results are obtained from the wind tunnel tests for a two-degree of freedom-coupled motion. These results are used in the system identification method to calculate all the flutter derivatives simultaneously. The experimental set-up for the section model needs to be properly designed to decrease the noise to a minimum level in order to extract more reliable and accurate values of flutter derivatives. If the details of the experimental set-up, such as springs, position encouders, data processing devices, etc., are designed and mounted accurately, the system response signals contain less noise for the input motion data to the system identification method, which can therefore calculate better results.

4.1 Types of Wind Tunnel Tests for Long Span Bridges

The aeroelastic effects of the wind on the bridge deck section, such as flutter, are investigated on the basis of information provided by wind tunnel tests. The proof of flutter stability of bridge decks is usually based on section model wind tunnel tests, which are proved to be a comparatively inexpensive experimental tool. Wind tunnel tests are not only carried out for the bridge deck, but they are also done for other parts of the bridge. Because aeroelastic phenomena may also affect the other parts of the bridge, i.e. cables, bridge pylons, hangers. Therefore different types of wind tunnel tests are developed to investigate aerodynamic behavior of the long span bridges. The need for the type of the wind tunnel test mostly depends on the economical aspects of the project and the time limitation for the construction of the wind tunnel test. Therefore, a brief information is given on the different types of wind tunnel tests explained by Simiu and Scanlan [2].

i) The Full Bridge Tests on Models: This type of models should satisfy the similarity requirements in terms of mass, mass moment of inertia, reduced frequency, mechanical damping, shapes of vibration modes and also the geometric similarity to the full scale bridge. Construction of full-bridge models is very detailed and therefore their costs are relatively high compared to other types of the wind tunnel tests. The usual scale of full bridge test models is in the order of around 1/300.

ii) Three Dimensional Partial Bridge Models: This type of wind tunnel tests is developed to reduce the high cost of full bridge tests. With this model, only the main span of the bridge or mostly half of it is modeled in an economical approximation.

iii) Section Model Tests: Section models represent a part of the bridge deck that is suspended to a supporting system, which allows the model to oscillate in the required degrees of freedom. The supporting system can be either a spring arrangement or a balance system depending on the type of the technique used, which were explained in section 2.4. Since section models are relatively inexpensive compared to the other types of wind tunnel tests, they can be constructed with the scale of 1/50 to 1/25, which reduces the discrepancies in the results calculated by section model and full bridge test models. Also section model tests provide quite reliable initial assessments such as the aeroelastic stability of the bridge deck. Another advantage of the section model test is calculating the aerodynamic properties of the bridge deck on the basis of comprehensive analytical studies, which can then be carried out.

4.2 Design and Construction of the Experimental Setup

All parts of the experimental set up were designed and constructed at the Structural Mechanics and Steel Structures Department and its laboratory of the Technical University of Hamburg-Harburg. After that the experimental set up was brought to the Ship Design and Construction Institute Laboratory of Technical University of Hamburg-Harburg, which has a sufficient wind tunnel with the cross section dimensions of 1.75 m × 1.00 m, to perform all the experiments.

4.2.1 Pre-dimensioning

First step before the construction of a wind tunnel experiment set-up was to decide some necessary dimensions and parameters roughly such as the distance between the springs, spring constants, etc. The width of the section model, B was selected as 0.3 m. The frequency ratio, mass and mass moment of inertia parameters were initially estimated from the literature, Iwamoto [9]; $\varepsilon = \omega_\alpha/\omega_h = 1.9$, m = 5.0 kg, I = 0.06 kg·m^2.

The system was supported by eight identical springs at the corners of the section model and the only upper four springs were under tension with the application of the own weight of the system. The relation between the torsional stiffness K_α and the vertical stiffness K_h of the system should be determined with respect to the distance between the springs. The vertical stiffness K_h of the system only depends on the stiffness of the upper four springs where $K_h=4\cdot K_{sp}$.

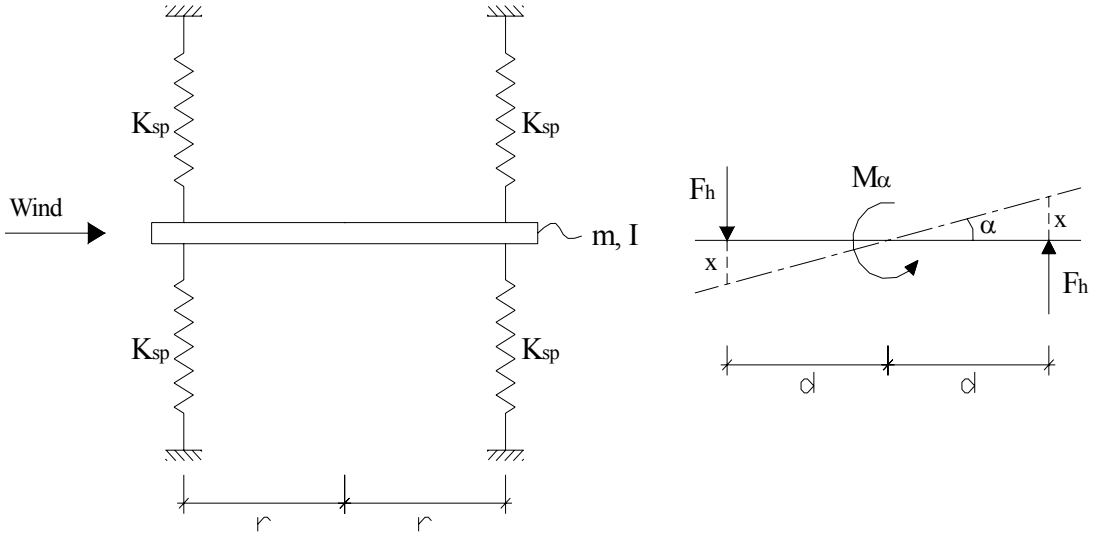

Figure 4.1: Section model supporting system

Forces M_α and F_h were calculated according to Fig. 4.1

$x = d \cdot \tan\alpha \approx d \cdot \alpha$ (provided that α is very small)

$F_h = K_{sp} \cdot x = K_{sp} \cdot d \cdot \alpha$

$M_\alpha = 2 \cdot 2F_h \cdot d = 4 \cdot K_{sp} \cdot \alpha \cdot d^2$ (both sides are taken into consideration)

$M_\alpha = K_\alpha \cdot \alpha = 4 \cdot K_{sp} \cdot \alpha \cdot d^2 \rightarrow K_\alpha = 4 \cdot K_{sp} \cdot d^2$ and $K_h = 4 \cdot K_{sp}$.

$$K_\alpha = d^2 \cdot K_h \qquad (4.1)$$

The distance between the springs was calculated with the initial estimated parameters;

$K_h = m \cdot \omega_h^2$; $K_\alpha = I \cdot \omega_\alpha^2$; $\omega_\alpha^2 / \omega_h^2 = \varepsilon^2$

$d^2 = K_\alpha / K_h = \varepsilon^2 \cdot I/m \rightarrow d = 210$ mm; in the case of variation of the parameters, d was selected as 250 mm.

The design of the spring was done in such a way that the spring would be always in the elastic range under the dead load and the approximately expected wind load. On the other hand, if the spring stiffness would be so high, no motion of section model could be observed. Finally, the spring having the stiffness of 224 N/m was selected.

4.2.2 Construction of the System

A rectangular section with a length of 790 mm was tested with the section model wind tunnel test as seen in Fig. 4.2, whose flutter derivatives had already been measured by the forced vibration method.

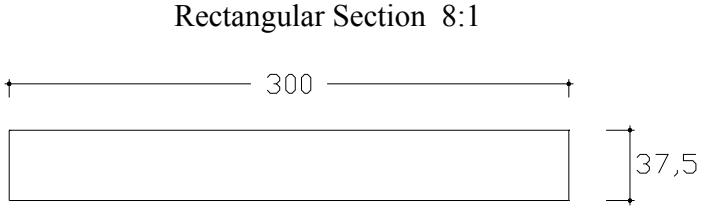

Figure 4.2: Cross section of the model

The experimental set-up is shown in the figures 4.3 and 4.4 in different views. In the Fig. 4.5 the experimental set-up is illustrated without the wind tunnel wooden walls to give general idea about the whole system. The rectangular section model (1) was fixed to a longitudinal bar (3), which was connected to a transversal bar (4) at the outside of the wind tunnel. In order to make the longitudinal bar pass through the wooden walls of the wind tunnel, two rectangular holes were made on the wooden walls of the wind tunnel as seen in the Fig. 4.4. These rectangular holes should be large enough not to affect the motions of the system in both vertical and torsional direction. On the other hand, some turbulence occurred near the openings under the wind flow. To prevent these turbulences, elliptical end plates (2) were connected to the ends of the section model (1). The whole system was suspended by eight equal helical springs (5) from the ends of the transversal bars. In order to obtain displacement time histories of the motion, four position encouders (6) were connected to the transversal bars with a distance of 120 mm at one side. The vertical displacements of the points where the position encouders connected were measured and with the application of relevant calculations vertical and rotational time histories were obtained. Windward and leeward drag wires (8 and 9) were attached to the ends of the longitudinal bar to prevent the motion of the system in the along-wind direction and the motion parallel to the section model. Some additional weights (7) were placed on both longitudinal and transversal bars to adjust the mass and mass moment of inertia of the system.

Only the section model and end plates connected to the section model were placed inside the wind tunnel having a direct contact with the airflow. The rest elements of the experimental setup were placed outside of the wind tunnel not to cause any turbulence.

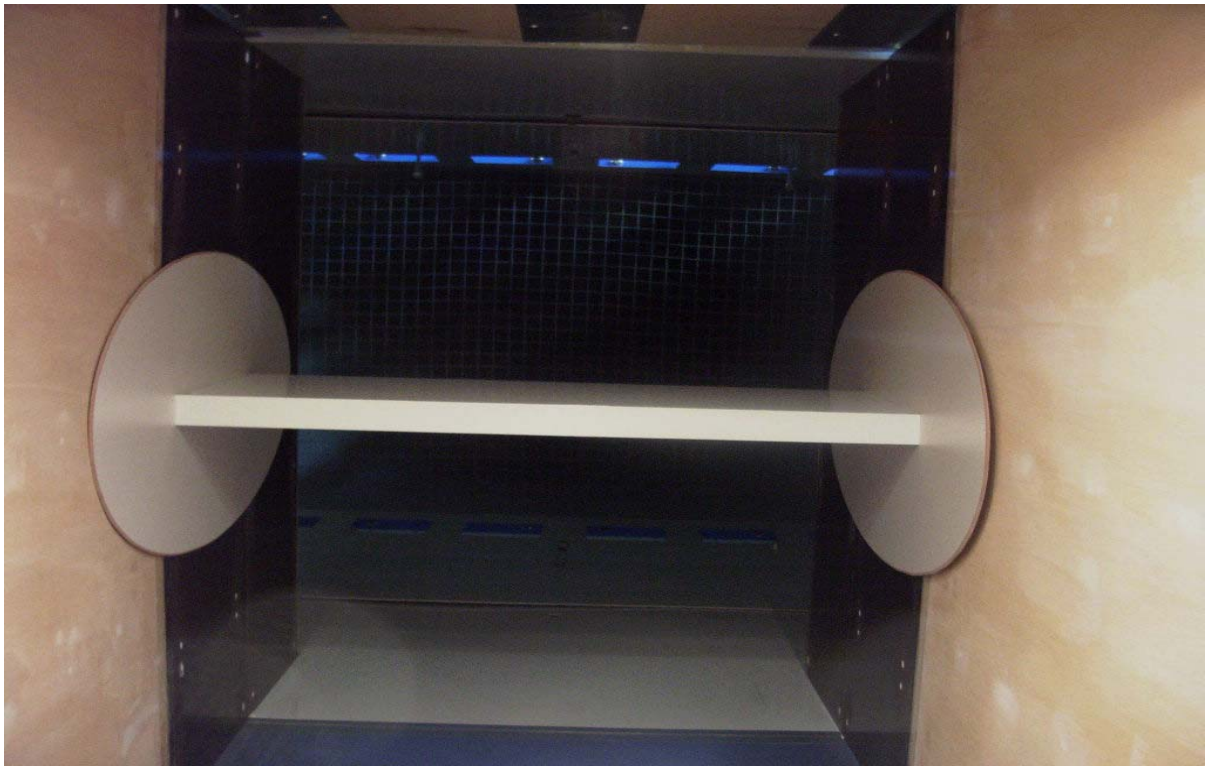

Figure 4.3: Section model in the wind tunnel

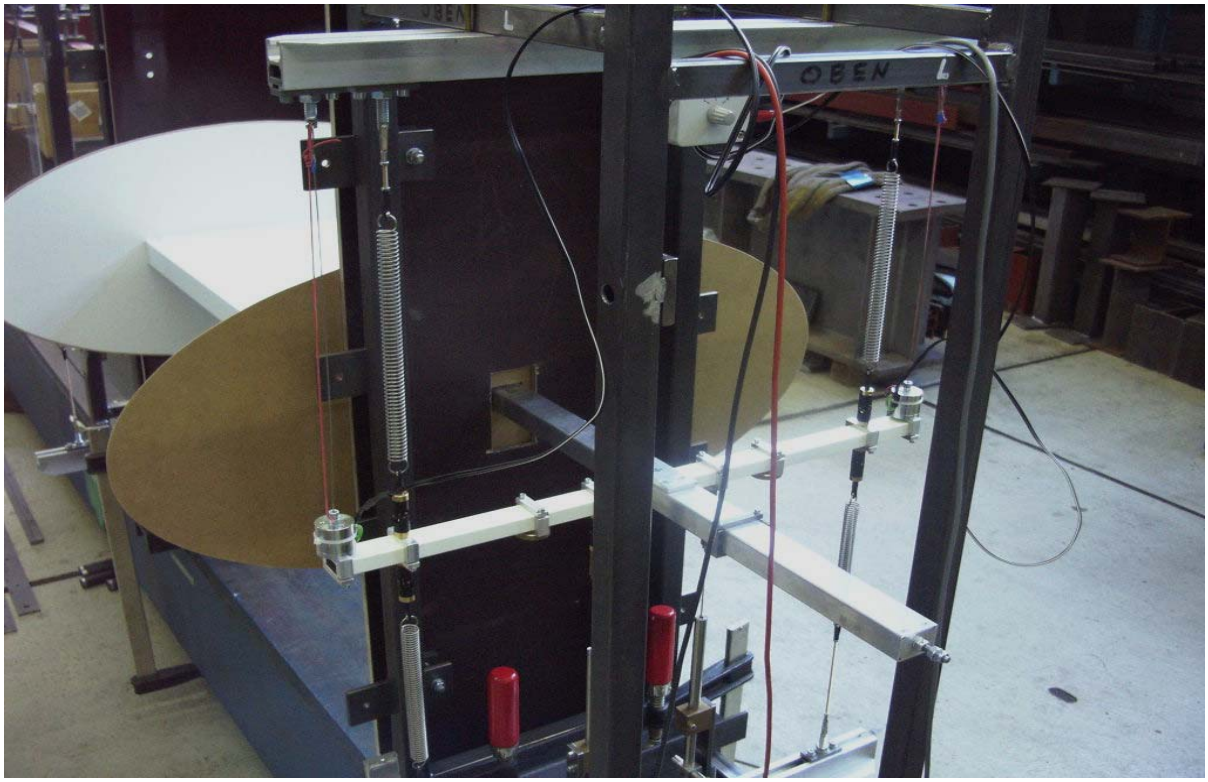

Figure 4.4: Supporting system of the experimental set-up

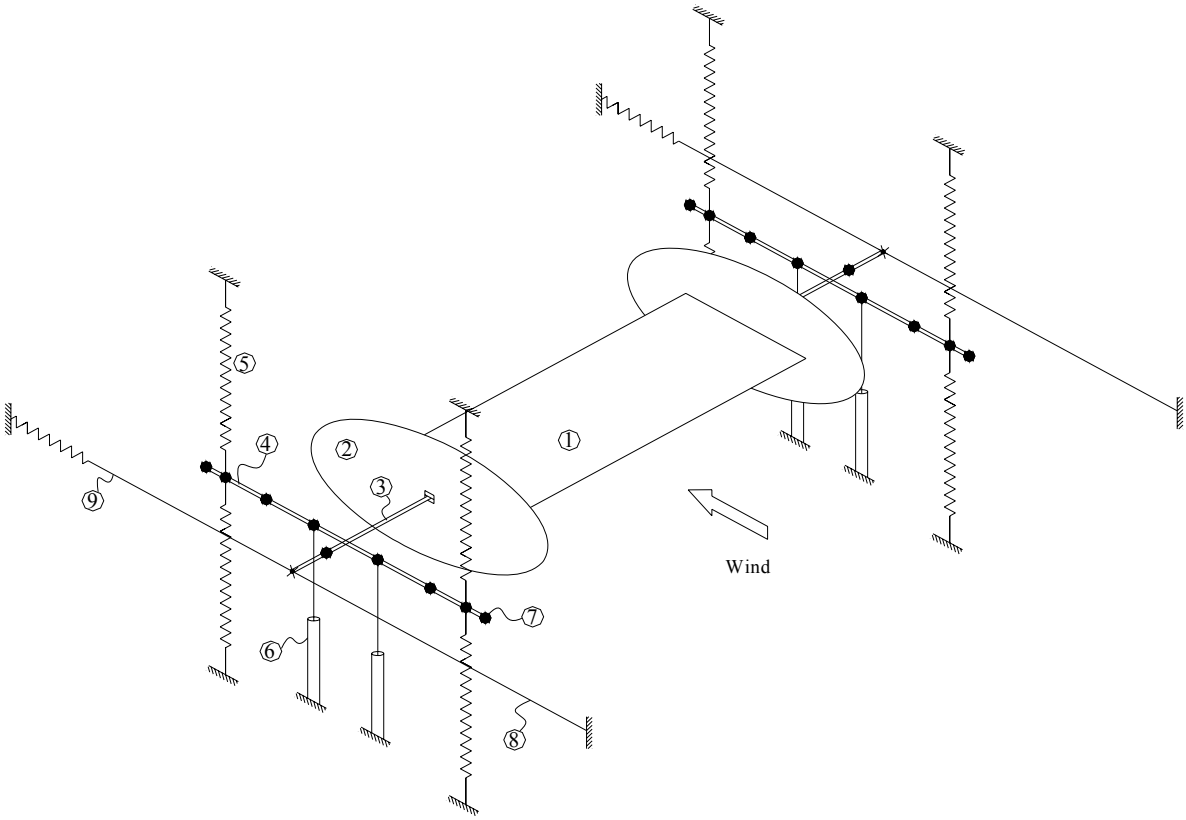

Figure 4.5: Experimental set-up

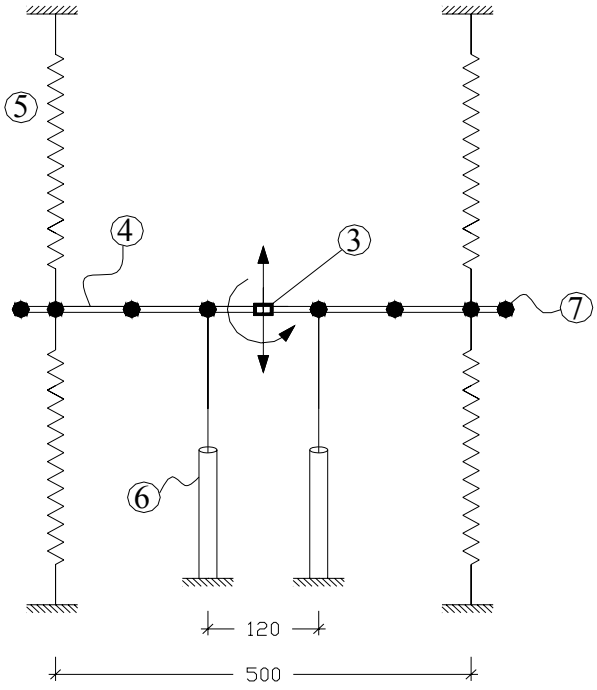

Figure 4.6: Side view of the experimental set-up

Legend:

1. Bridge Section Model (790 mm×300 mm ×4 mm)
2. Elliptical End Plates
3. Longitudinal Bar
4. Transversal Bar
5. Helical Springs
6. Position encouders for measuring vertical displacement
7. Additional Weights
8. Windward drag wire
9. Leeward drag wire with helical spring

The separation between the outside and inside of the wind tunnel was provided by the wooden plate wall. Although the width of the wind tunnel is 1750 mm, it is required to provide 800 mm spacing between the inner faces of the wall at the location where the section model is placed. Therefore, the length of the section model was designed to be 790 mm with the 4 mm thickness of the one end plate and 1 mm spacing in between the end plate and the wall. The distance between the wooden plate walls was decreased along the wind tunnel from 1750 mm to 800 mm continuously to avoid any turbulence flow. But the spacing between the inner faces of the wall is kept constant at the location where the model is mounted.

After the construction of the system, the system was given an initial displacement with the electro magnets and steel wires by lifting the ends of the transversal bars. And the displacement time histories were obtained to get the system parameters for the wind-off case by the MITD method. The diagonal elements of the mechanical stiffness matrix, which correspond to the wind-off case, were used for the calculation of mass moment of inertia with the knowledge of mass of the system m and the half of the distance between springs d, which was selected as 250 mm in the section 4.2.1.

The total weight of the system m is measured as 6.538 kg and the mass moment of inertia I is calculated roughly as 0.1359 $kg \cdot m^2$ by using relevant formulation. The greatest contribution comes from the end plates to the mass moment of inertia of the system with 48.5 % due to their high eccentric weight according to the center of rotation.

The mass moment of inertia can also be calculated from the identified system stiffness matrix as shown below:

$$\overline{K}_{11}^{mech} = m^{-1} \cdot K_h \quad \rightarrow \quad K_h = m \cdot \overline{K}_{11}^{mech}$$

$$\overline{K}_{22}^{mech} = I^{-1} \cdot K_\alpha \quad \rightarrow \quad I = K_\alpha / \overline{K}_{22}^{mech} \text{ , where } K_\alpha = r^2 \cdot K_h \text{ in the Eqn. 4.1.}$$

$$I = r^2 \cdot K_h \,/\, \overline{K}_{22}^{mech} \quad \rightarrow \quad I = m \cdot r^2 \cdot \overline{K}_{11}^{mech} \,/\, \overline{K}_{22}^{mech} \qquad (4.2)$$

If the Eqn. 4.2 is solved for the initial condition case bs_10 under vacuum case, whose mechanical stiffness matrix is given in Table 5.3, the mass moment of inertia of the system is calculated as 0.1348 $kg \cdot m^2$. The difference between the mass moment of inertia values, which are calculated by the structural mechanics formulation and the MITD method, is calculated as

$$\text{Difference in I} = \frac{0.1359 - 0.1348}{0.1359} \times 100 = 0.82\%$$

The small amount difference in the mass moment of inertia calculation results proves the reliability of the MITD method.

4.2.3 Calculation of the Wind Velocity

In the present work, the wind is applied to the section model with zero angle under smooth flow. Wind velocity is known at the entrance location of the tunnel. Because of the change of the wind tunnel cross section due to the wooden plate walls, wind velocity acting on the section model is not known and needs be determined in order to find out the flutter derivatives. According to the fluid mechanics, the continuity principle can be applied to find the wind velocity acting on the section. However since there are some openings at the top of the wind tunnel, this principle is not applicable. A standard pitot-static tube is used for the determination of the horizontal mean wind velocity acting on the section under smooth flow. Wind speed is calculated with a pitot-static tube, which is based on the pressure difference at some specified points on the tube.

Before starting the experiments, a pitot-static tube is placed properly in the middle location of the section model before the installation of the section model in the wind tunnel. The hole at the end of the tube has to be placed with zero angle to the wind direction to measure the pressure difference properly. The tunnel wind velocity U_t is increased from the wind speed of 2.5 m/s with an increment of 0.5 m/s till the wind speed of 10.5 m/s, which is greater than the critical wind speed. The wind speed is measured at the location of pitot-static tube. Each measurement was repeated three times in order to increase the reliability of the measurements and an average value is used for each wind speed. By this way the wind velocity U acting on the section model is obtained with respect to the tunnel wind velocity.

As seen in the Fig. 4.7, there is a linear relation between the applied tunnel wind velocity and the measured velocity at the location of the section model. This linear relationship is calculated as

kv = (measured wind vel.) / (applied tunnel wind vel.) = U/U_t = 1.405

By using this relation, the wind velocity acting on the section model can be calculated for any arbitrary wind tunnel wind speed.

Furthermore, wind velocity distribution along the section model has to be investigated. In order to obtain reliable data, the wind action should be uniform along the section model. Therefore, under the application of a constant tunnel wind velocity, wind velocity from the mid of the section till the end of the section is measured at every 20 mm. The wind velocity distribution is obtained by assuming symmetrical wind velocity distribution for the other side of the section model. An example diagram is drawn for the wind tunnel wind speed 8 m/s in the Fig. 4.8.

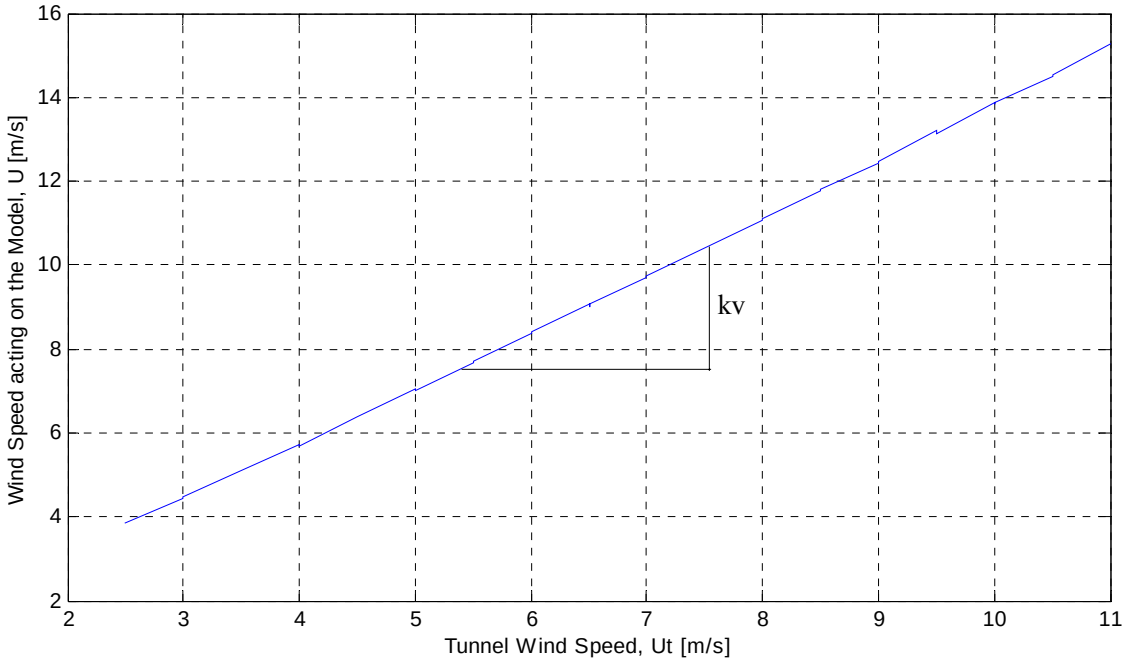

Figure 4.7: Wind speed acting on the section model

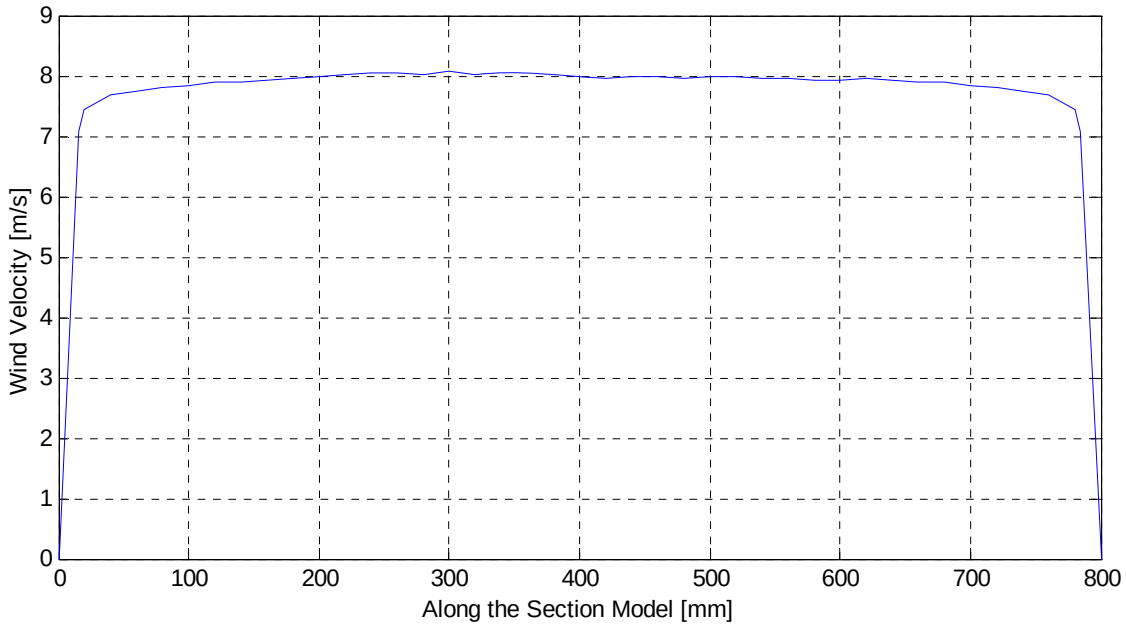

Figure 4.8: Wind speed distribution along the section model

As seen in the Fig. 4.8 wind velocity distribution is not completely constant because of measurement errors or turbulence effects, which are so small that the distribution can be taken as constant.

The wind speed range acting on the section model is obtained 3.85 to 14.53 m/s according to the Fig. 4.7. By using the Eqn. 4.3, it is found out that the Reynolds number varies between 0.75×10^5 and 2.9×10^5 with a constant section model width B of 300 mm.

$$\mathrm{Re} = \frac{UB}{\nu} \quad ; \quad \nu_{air} = 1.5 * 10^{-5} \ \mathrm{m^2/s} \ \text{ at } 20° \qquad (4.3)$$

Compared to the original Reynolds number that is around $1\cdot10^7$, the influence of the Reynolds number in the calculated range is assumed to be negligible. For comparison, Reynolds number of the present experiments is taken as 2.75×10^5, which corresponds to the critical case.

4.2.4 Important Elements of the Experimental Setup

4.2.4.1 Springs

Springs play a very important role in the experiments. They should be selected properly, because they represent the stiffness of the system. Eight tension springs will be used in the experiment, all of which have the same length and stiffness. 4 springs are used in each side of

the tunnel and two of them are connected at the ends of the transversal bars to each other in series. The springs are selected in a way that they should remain in the elastic range under the most unfavorable case during the experiment. The maximum static deformation and the maximum expected deformations due to the vibrations under wind flow should be taken into account and the total calculated deformation should be less than the elastic deformation of the spring. Under these conditions, the stiffness of the spring will not change during the experiments, which affects the quality of the results severely.

Length of the springs is another important design criterion that should be taken into consideration. The distance between the upper and lower fix points and the ends of the transversal beams are covered by the spring and some bar elements in different lengths to adjust the system. Since the above springs carry the weight of the system, they are loaded more than the lower ones. Therefore after deciding the spring length, length of the bar elements are determined to hold the system in the required position. As seen in the Fig. 4.4, longer bar elements are used under the transversal beams and shorter bars are used for the upper part.

4.2.4.2 Drag Wires

When the wind is applied to the section model, it is forced to move in the wind direction due to the drag force caused by the wind pressure. Also due to some random turbulence, the section can move perpendicular to the wind direction. In order to restrain the undesirable motions in the along-wind and perpendicular-wind directions, the ends of the longitudinal bar are connected to the drag wires on the upstream and downstream sides. The drag wires have also a little contribution to the vertical and torsional stiffness of the system. In order to reduce these effects, drag wires are connected to springs, which provide some flexibility to the system, in the downstream of the wind flow. All the drag wires are used in the horizontal plane of the section model without having any turnbuckles, which reduce the tension force on the wire.

4.2.4.3 Electro Magnets

Electro magnets are used to give the initial displacement to the system from the outside of the tunnel. As seen in Fig. 4.4, four magnets are used in the experimental setup, which are placed at the ends of the transversal bars at both sides.

The magnets are connected to a wire, which has a constant length and works only under tension. Besides the tension wire, each magnet is tied to a plastic rubber band, which is shorter than the wire. So that the plastic rubber band will be under tension when the magnets

are connected to the transversal bars. One end of the wires is fixed to the top steel bar and the other end holds the one end of the transversal bar when there is electric current through the electro magnet. By this way, the end of the transversal bar is lifted up to a certain level, which is specified by the length of the wire. In the experiments two sets of wires with different length are used to compare the initial condition effect on the system identification process.

When the electric current cut off through the electro magnet, the system releases from the electro magnets. By this way the system is given an initial displacement and consequently it starts to oscillate with a decaying motion for the wind speeds lower than the critical wind speed. In order to prevent any contact or strike of the electro magnet to the transversal bar or to the springs after the release of the system from the initial condition, the electro magnet is pulled upwards with the tension force on the plastic rubber band.

For each wind velocity electro magnets are attached to the transversal bars in different ways with different length of wires. First, only initial vertical displacement is given to the system by connecting all four magnets to the ends of the transversal bars with different length of wires to lift the system upwards by 10 mm and 20 mm, respectively. Therefore, the effect of the initial vertical displacement on the results of the identified system parameters can be compared. Then, the system is given both vertical and torsional initial displacement by connecting the front two magnets to the ends of the transversal bars to lift the windward side of the system 10 mm upwards.

For each set of initial condition case, the section model should be given exactly the same vertical and torsional displacements in all the experiments performed under different wind speeds. Otherwise, the results of the identified system parameters will not be consistent. Because the maximum amplitudes of the oscillation, which is given to the system by the initial displacement, play a very important role in the identification of system parameters for the free vibration tests. All the tests were carried out for three different initial condition cases with respect to each wind velocity to investigate the initial condition effect. Also for each wind speed and initial condition case, the tests were repeated for five times and their results were averaged to get more reliable results.

4.2.5 Data Acquisition

A suitable sampling rate should be selected to record the data. A low sampling rate is not convenient for the system identification method. On the other hand a high sampling rate not only requires greater disk space at the computer, but also it requires more time to identify the

system parameters. Therefore, 1/100 sampling rate is selected to record the data and the identification of the system parameters will be done with respect to this sampling rate.

Four position encouders are placed symmetrically according to the center of the model on each side of the transversal bars with a distance of 120 mm as seen in the Fig. 4.6. The vertical displacement of the points, where the position encouders are connected on the transversal bar, are measured with respect to the specified sampling rate. Multi channel data acquisition system and data acquisition Software HBM-Catman are used. The section model is given a fixed initial displacement by the electro magnets and it starts to oscillate both in vertical and rotational direction. Time history data are obtained by the software with five channels. First one represents the time at which the displacements are measured and the rest four channels represent the displacement data of the four points, where the position encouders are connected to the transversal bars. From these data points the vertical and the torsional displacement time histories of the section model are calculated.

4.3 Suggestions for the Future Experiments

The deficiencies of the present experimental set-up will be discussed and some appropriate suggestions are given for the future works to increase the efficiency and to improve the quality of the experimental data, which provides more reliable input data for the identification of the system parameters.

- For the free vibration tests under different wind speeds, the maximum amplitude of the oscillation of the section model should be the same for each set of experiment that are carried out with the same initial displacement condition. In other words the section model should be released from the same position. This condition is partially fulfilled by suspending the section model to the upper fix points by tension cables. However, before the section model is released from its initial position, it is affected by the wind pressure in upward and downward directions, when the air is flowing through it. For the lower wind speeds, the wind pressure is so small that it can be neglected, which is not the case for higher wind speeds. Since the wires do not work under compression, the section model is lifted upward by the wind pressure at the high wind speeds and different initial displacement is given to the system for different wind speeds. To prevent the movement of the section model before releasing, it should be fixed to the upper and lower fix points by the wires at the same time; or instead of cables, compression bars can be used to hold the section model to the upper fix point.

- The selected sampling rate of the data is very important, because it directly affects the length of the data. All the experimental data are obtained with the same sampling rate of 1/100 second. In order to investigate the effect of the sampling rate on the identification of system parameters and to find out the most appropriate sampling rate, it would be better if the data are obtained with two more different sampling rates such as 1/200 s and 1/400 s at least for the wind-off case.
- The number of useful data affects the quality of the identified system parameters. The more number of experimental data, the better quality for the identified parameters. Therefore, if the system is given greater initial displacements, the length of the data will be longer and the quality of the identified parameters will be better. The length of the useful data also depends on the aerodynamic damping of the motions in the corresponding degrees of freedom. Therefore, the system with lower damping ratio can result in better results especially at the higher wind speeds. The friction in the position encouders not only decreases the reliability of the experimental data, but also gives additional damping to the system. For that reason, the friction in the position encouders should be decreased to the minimum level or time histories of the motions should be obtained with different type of instruments, which give less damping to the system.
- At higher wind speeds, there is a considerable scatter in the identified flutter derivatives, which will be discussed in the following sections. In order to reduce the scatter in the results, Iwamoto [9] suggested to make the experiments with a heavier section model having high mass moment of inertia as long as the supporting system has sufficient capacity. Otherwise, the springs will not be in the elastic range, which is not desirable in the wind tunnel tests.
- In order to understand the complete physical mechanism of the bridge desk section to wind loading, all flutter derivatives related with the vertical, torsional and lateral motions should be considered. 3-degree of freedom section model wind tunnel tests and the application of system identification method with respect to a 3-dof system are required to find out all 18-flutter derivatives. Furthermore, the direct flutter derivatives can be extracted from single degree of freedom systems. The results of the single degree of freedom motion tests provide the opportunity to compare the direct flutter derivatives identified from the results of the coupled motion wind tunnel tests.
- The geometrical shape of the section model has a very big influence on the determination of flutter derivatives. Using different cross sections, such as

streamlined and bluff bodies, provide the opportunity to compare behavior of such cross sections from the aerodynamic point of view. Especially, the theoretically calculated flutter derivatives from a thin plate could be compared with the ones for the corresponding section models, to investigate the applicability of the theoretical formulation of the flutter derivatives.

4.4 Summary

Since the section-model wind tunnel tests are easier and more economical than the other types of wind tunnel tests, they are used widespread for the design of long span bridges. In order to obtain reliable results, care should be given to each step of the procedure, from model construction till the acquisition of data and the identification of system parameters with the help of the system identification method.

In this chapter the experimental set up is discussed in a detailed way. In order to make a successful experiment, all the members of the section model should be designed and selected properly. Also a proper construction of the system in the wind tunnel is very important for the success of the experiment and the quality of the obtained data.

It is impossible to remove all the friction from the system. There will be certainly some unavoidable friction, which is treated as additional noise in the data. Such as the friction in the position encouders, the friction between the end plates of the section and the walls of the wind tunnel. The end plates should be very close to the wind tunnel walls to prevent the aerodynamic end effects, but also there should be sufficient space between them to prevent the end plates touch the wall.

Electro magnets are used in this experiment for giving an initial displacement to the section model. For all experiments with different wind speed, same initial displacement should be given to the model. Therefore the release system has to be properly designed to give consistent initial displacement for all experiments.

The test involves the measurement of the decay in amplitude in time with an initial displacement of the bridge deck motion in vertical and torsional direction for various wind speeds in smooth flow. In order to get good results from the experiments, each set of experiment is repeated 5 times and system identification process is carried out for each set of experimental data and finally the average of the results are used to find out the parameters of that experiment. By this way, the error level could be decreased to a better percentage.

5 EXTRACTION OF FLUTTER DERIVATIVES

The flutter derivatives cannot be extracted directly from the experimental results. First, the useful displacement time histories of the motions should be obtained from the wind tunnel experiment results that are carried out under smooth flow. After then, by using the time histories, all eight-flutter derivatives can be calculated simultaneously.

5.1 Calculation of the Time Histories

Displacement time histories are required as input data of the system identification method. In order to investigate the vertical and rotational motion of the system, first the system is given an initial displacement. For comparison the experiments are done under three different initial condition cases that are named as bs_10, bs_20 and os_10 where the terms 'bs' and 'os' mean 'both sided' and 'one sided', respectively. The system is suspended to the fix points on the wind tunnel with different length of wires in different combinations to apply different initial conditions to the system. In the wind tunnel tests, the main emphasis is given to the initial condition cases bs_10 and os_10. For the initial condition case bs_20, the wind tunnel tests are not carried out for all wind speeds as done for the other initial condition cases. Therefore, the results of the bs_20 are used only for comparison.

For bs_10 and bs_20, both ends of the transversal bars are suspended with the different length of wires to lift the system upwards by 10 mm and 20 mm, respectively. For os_10, only the front ends (on the windward side) of the transversal bar are lifted upwards by 10 mm to give both vertical and torsional displacement. The initial displacement values, which are given in Table 5.1, are calculated from the first data points of the displacement time histories.

Initial Condition	bs_10	bs_20	os_10
h_o [mm]	8.940	18.570	4.160
α_o [grad]	0.275	0.170	1.150

Table 5.1: Initial displacement values for different cases

The displacement of the points where the position encouders are connected on the transversal bars, are obtained at every 1/100 second time interval. For each set of experiment, 4 sets of data are available from the data acquisition software; time histories of the 4 points, 2

at windward and 2 at leeward side of the section model with a distance of 120 mm in between. The corresponding points are named as shown in the Fig. 5.1 with respect to their locations according to the section model. By using these data points the displacement time history data X(t), which are the vertical displacement time history h(t) and the torsional displacement time history $\alpha(t)$, are obtained.

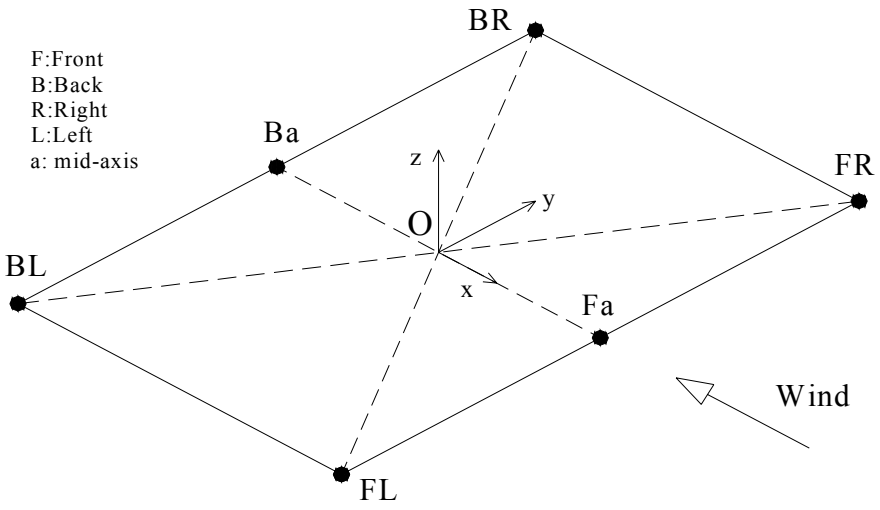

Figure 5.1: Measurement points on the system

During the experiments, before starting to obtain the displacement time histories of the section model through the four points shown in Fig. 5.1, a zero location, which is the stable position of the section model, should be specified for the data acquisition software. After the system is given an initial displacement, it starts to oscillate around the zero location. Above the zero location, the displacement time history is assigned as negative and positive under the zero location. However, this not the case after certain wind speeds due to the wind pressure acting on the section model. After the wind tunnel wind velocity U_t = 7.0 m/s, first the section model is suspended from fix points and than zero location is defined. Since downward displacement of the section model is assigned as positive, it oscillates in the positive side of the displacement time history, rather than oscillating around the zero displacement. Therefore, the average of X(t) is deducted from its values to shift X(t) to the zero displacement ordinate in order to make X(t) oscillate around the zero displacement, which will be used in the MITD method.

5.1.1 Vertical Displacement Time History, h(t)

The main subject of this section is to obtain the least noisy vertical time history data of the section model. So that 7 different combinations are calculated by using the data points on the corners shown in the Fig. 5.1 to get the best vertical time history. Some abbreviations are used to represent the combinations of time histories as follows

1) VR : The average displacement of the points (FR & BR) on the right side of the model.
2) VL : The average displacement of the points (FL & BL) on the left side of the model.
3) VF : The average displacement of the points (FR & FL) on the front side of the model.
4) VB : The average displacement of the points (BR & BL) on the back side of the model.
5) VD1 : The average displacement of the points (FR & BL) on the first diagonal of the model.
6) VD2 : The average displacement of the points (FL & BR) on the second diagonal of the model.
7) Vave : The average displacement of all the four points (FR, FL, BR, BL) of the model.

7 different vertical displacement time histories are calculated and shown in the Fig. 5.5 according to the experimental data v5.0_20_01. Three sets of comparisons are carried out between the three different h(t) distributions of 'Vave with VR and VL', 'Vave with VF and VB' and 'Vave with VD1 and VD2' in the figures 5.5a, 5.5b, 5.5c, respectively. In all comparisons, Vave data are always in between the other two time histories. The time histories of the diagonals almost fit with the Vave data and for the time histories of front and back sides of the model nearly fit with Vave except for the peak values. However, the time histories calculated according to the right and left side of the section model have big discrepancies to the Vave data. Some unavoidable motions such as torsional motion in x and z direction and sway motions in x and y direction shown in the Fig. 5.1, cause the discrepancies in the displacement time histories. Since the effects of such unavoidable motions are partially eliminated for the Vave by using the four data points, its results are evaluated to be the best among the other combinations of the time histories. Therefore, Vave values are used for the vertical displacement time history for the each experimental result.

5.1.2 Torsional Displacement Time History, $\alpha(t)$

The necessary set of data for the calculation of torsional time history, $\alpha(t)$ should be the same with the ones used for the calculation of h(t) data to obtain consistent results. Therefore, the displacements of the points Fa and Ba as seen in the Fig. 5.1, are calculated by

taking the average values of front and back side of the section model, respectively. The average values Fa and Ba and the difference between these two points, which is 120 mm, are the necessary information in the calculation of $\alpha(t)$.

A proper sign convention should be specified for $\alpha(t)$ data. In the present work, it is specified that the rotation of the section model in the counterclockwise direction is negative and the clockwise direction is positive. So that the calculation of $\alpha(t)$ is done for two different cases according to the position of the points Fa and Ba as shown in Fig. 5.2

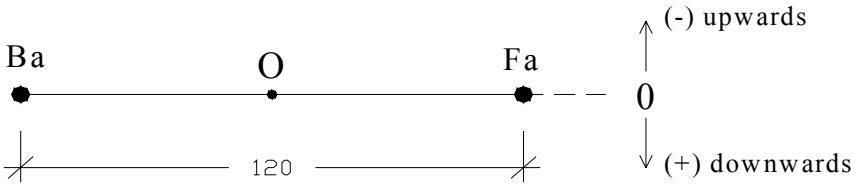

Figure 5.2: The vertical motion sign convention of the mid of the section model

Calculation of the $\alpha(t)$ is done with respect to two different cases

case-1) When Ba(t) > Fa(t), $\alpha(t)$ value will be negative

$$\alpha(t) = - \text{asin} [\text{abs}\{ \text{abs}(Ba(t)) - \text{abs}(Fa(t)) \}/120]$$

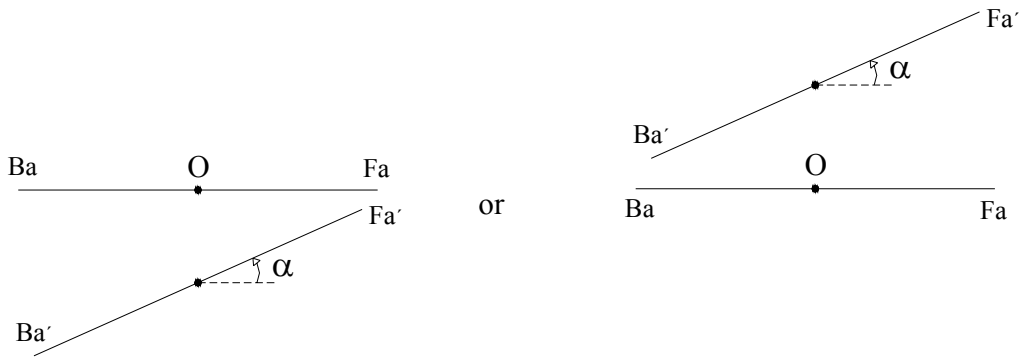

Figure 5.3: Negative $\alpha(t)$

case-2) When Fa(t) > Ba(t), $\alpha(t)$ value will be positive

$$\alpha(t) = \text{asin} [\text{abs}\{ \text{abs}(Fa(t)) - \text{abs}(Ba(t)) \}/120]$$

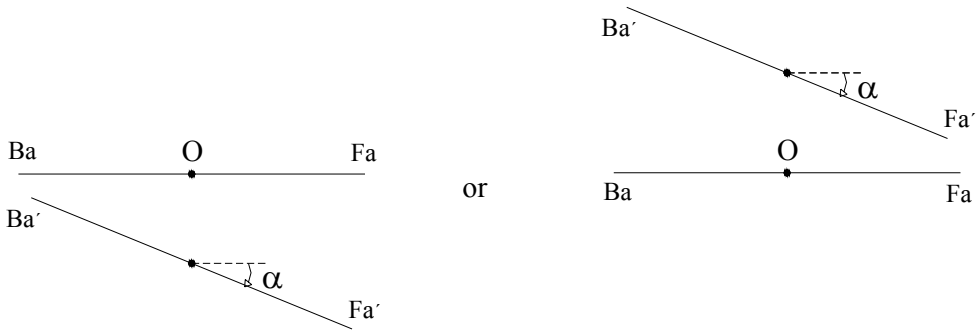

Figure 5.4: Positive $\alpha(t)$

5.1.3 Length of the Displacement Time Histories

The length of the data affects quality of the identified parameters and useful length of data should be decided properly for each test. The calculated vertical and torsional time histories cannot be applied directly to the system identification method. In the case of decaying motions, the amplitude of the motion decays according to the damping ratio of the system and the relative noise level in the motion increases with the decaying motion. Therefore, the end of the data should be cut off at a limit value, whose relative noise level is acceptable.

Besides, the time just after the system is released, the relative noise level of the displacement time histories is higher for that time interval. Moreover, in order to get better results, the displacement time histories should start with their maximum amplitude values. Because of these reasons, some of the data at the beginning of the time history is eliminated when necessary.

In order to apply any system identification method to a two-degree of freedom coupled motion, the length of the both displacement time histories of the corresponding degrees of freedom should be the same. The length of the both data is decided according to the degree of motion with shorter length of data, which is h(t) in the higher wind speed tests.

The length of the useful displacement time history data decreases with the increasing wind velocity. The vertical motion is damped more rapidly than the torsional motion due to its increasing damping ratio with the increasing wind velocity. The vertical time histories for the wind velocities 3.84 m/s, 8.39 m/s, and 12.46 m/s of the initial condition case bs_10 are plotted in the Fig. 5.6. As seen in the Fig. 5.6, the useful length of time history decreases

with the increasing wind velocity. Especially for some initial condition cases, at the flutter speed and after the flutter speed the number of useful data is not sufficient to calculate the flutter derivatives with the system identification methods, which is also mentioned by Iwamoto [9], Chen [13], Wienand [4]. Therefore, at higher wind speeds the quality of the identified parameters decreases due to the limited data points.

5.1.4 Filtering of the Data

The calculated displacement time history data can be filtered before application of the data to the system identification method to reduce the noise level of the data. The noisy data with the frequency of a particular value can be eliminated by using lowpass filters. The specified frequency value after which the data will be cut, influence the quality of the filtered data. If a high frequency is specified for the filtering, then the filtering does not change the noise level so much. On the other hand, if a low frequency is specified for the filtering, then it may completely change the properties of the data, which is undesirable. In the present work in order to make the comparison between the filtered and the without filtered data, a filter with an upper cut-off frequency of 10 Hz is used, where the vertical and torsional motion frequencies at zero-wind condition are 2.64 and 4.59 Hz, respectively. That means, the data having the frequency of 10 Hz or more will be removed.

In most of the cases the results of the identified parameters are almost equal to each other calculated with filtered data and without filtered data. It has been proven that the MITD method works well even with the noisy data, so that the necessity for filtering will be investigated with the torsional displacement time history data v7.5_10_01, whose data have considerable amount of noise. Since the filtering removes some part of the data, which changes the structure of the data, the curve fit calculated by system identification method of the filtered data is even worse than the curve fit of the without filtered data as seen in the Fig. 5.7a and 5.7b. Especially at the peak points of the filtered data do not fit properly, whereas the without filtered data even with noisy data points fit very well.

The results of the identified parameters for filtered and without filtered data v7.5_10_01 are presented in the Table 5.2.

	λ_h	λ_α	ω_h [1/s]	ω_α [1/s]	[*C*]		[*K*]	
With filter	-1,023	-0,241	17,219	27,947	1,931	-0,232	297,783	13,337
					-3,702	0,598	24,310	781,559
Without filter	-1,022	-0,259	17,219	27,952	1,929	-0,238	297,797	13,650
					-3,552	0,632	24,421	781,775
Difference [%]	0,186	6,729	0,001	0,015	0,104	2,435	0,005	2,293
					4,226	5,273	0,457	0,028

Table 5.2 : System parameters calculated with filtered and without filtered data

As seen in the Table 5.2, the difference between the two results is in the allowable range. Therefore, in order to reduce the calculation time and not to disturb the original data, no filtering is applied to the displacement time history data.

5.2 Uniqueness Problem

The aerodynamic forces L_h and M_α are rewritten by converting the wind velocity U and reduced frequency K terms into the circular frequency ω and the deck width B terms by using the equation $K = B \cdot \omega / U$. Then the Eqns. 2.6 and 2.7 are written as

$$\begin{aligned} L_h &= \frac{1}{2}\rho B^3 \omega^2 \left[H_1^*(K)\frac{\dot{h}}{B\omega} + H_2^*(K)\frac{\dot{\alpha}}{\omega} + H_3^*(K)\alpha + H_4^*(K)\frac{h}{B} \right] \\ M_\alpha &= \frac{1}{2}\rho B^4 \omega^2 \left[A_1^*(K)\frac{\dot{h}}{B\omega} + A_2^*(K)\frac{\dot{\alpha}}{\omega} + A_3^*(K)\alpha + A_4^*(K)\frac{h}{B} \right] \end{aligned} \qquad (5.1)$$

The section model system has a coupled motion, oscillating in vertical and rotational direction with the circular frequencies of ω_h and ω_α, respectively. Therefore, the problem arises that which modal frequency will be used in the Eqn. 5.1 and in the calculation of the reduced frequency. By taking both the model frequencies into account, the complete aerodynamic forces can be written as

$$L_h = \frac{1}{2}\rho B^3 \omega_h^2 \left[H_1^*(K_h)\frac{\dot{h}}{B\omega_h} + H_2^*(K_h)\frac{\dot{\alpha}}{\omega_h} + H_3^*(K_h)\alpha + H_4^*(K_h)\frac{h}{B} \right] + \frac{1}{2}\rho B^3 \omega_\alpha^2 \left[H_1^*(K_\alpha)\frac{\dot{h}}{B\omega_\alpha} + H_2^*(K_\alpha)\frac{\dot{\alpha}}{\omega_\alpha} + H_3^*(K_\alpha)\alpha + H_4^*(K_\alpha)\frac{h}{B} \right] \quad (5.2)$$

$$M_\alpha = \frac{1}{2}\rho B^4 \omega_h^2 \left[A_1^*(K_h)\frac{\dot{h}}{B\omega_h} + A_2^*(K_h)\frac{\dot{\alpha}}{\omega_h} + A_3^*(K_h)\alpha + A_4^*(K_h)\frac{h}{B} \right] + \frac{1}{2}\rho B^4 \omega_\alpha^2 \left[A_1^*(K_\alpha)\frac{\dot{h}}{B\omega_\alpha} + A_2^*(K_\alpha)\frac{\dot{\alpha}}{\omega_\alpha} + A_3^*(K_\alpha)\alpha + A_4^*(K_\alpha)\frac{h}{B} \right] \quad (5.3)$$

where $K_h = B\cdot\omega_h/U$ and $K_\alpha = B\cdot\omega_\alpha/U$

As seen in the Eqns. 5.2 and 5.3, there are totally 16 flutter derivatives; $H_i^*(K_h)$ and $H_i^*(K_\alpha)$, i = (1-4) for self-excited aerodynamic lift force L_h and $A_i^*(K_h)$ and $A_i^*(K_\alpha)$, i = (1-4) for self-excited aerodynamic moment M_α. It is not possible to identify all the unknown flutter derivatives simultaneously due to the lack of information. From the system identification method, it is only possible to get information for 8 parameters, which are two sets of modal frequencies, modal damping ratios, amplitudes and phase shifts for both degrees of freedom. Therefore, the number of unknown flutter derivatives is more than the number of known parameters, which is called the uniqueness problem.

In order to solve uniqueness problem, the number of unknowns should be decreased to the same number of identified parameters. As done by Iwamoto [9], the level of coupling between the vertical and torsional motions should be investigated. As an example, the displacement time histories of the section model for the tunnel wind speed U_t = 7 m/s are investigated. It can be interpreted from the Fig. 5.8 that the coupling between these two motions is assumed to be weak because the vertical motion and the rotational motion do not behave in the same manner, for example both motions are not prevailing at the same time or the other way around. Therefore, the number of unknown flutter derivatives can be reduced to 8 by neglecting the terms α and $\dot{\alpha}$ related with ω_h and the terms h and $\dot{h}$ related with ω_α. By this way both the number of unknown parameters and the number of information will be equal to each other, which prevents the uniqueness problem.

Besides, Sarkar [3] suggested that the flutter derivatives H_1^*, H_4^*, A_1^*, A_4^* associated with the vertical motion are calculated by using the circular frequency ω_h, and the flutter

derivatives H_2^*, H_3^*, A_2^*, A_3^* associated with the torsional motion are calculated by using the circular frequency ω_α. Because according to the calculations of Sarkar [3], the vertical circular frequency calculated with respect to the single-degree of freedom motion and the two-degree of freedom motion are close to each other, which is the same case for the torsional circular frequency. And also in the same work, the direct flutter derivatives extracted from single degree of freedom motion and coupled motion match very well, which proves that the torsional motion has no influence on the flutter derivatives related with the vertical motion and vice versa. According to this simplification, which is suggested and proved by Iwamoto [9] and Sarkar [3], Eqns. 5.2 and 5.3 can be written as

$$L_h = \frac{1}{2}\rho B^3 \omega_h^2 \left[H_1^*(K_h)\frac{\dot{h}}{B\omega_h} + H_4^*(K_h)\frac{h}{B} \right] + \frac{1}{2}\rho B^3 \omega_\alpha^2 \left[H_2^*(K_\alpha)\frac{\dot{\alpha}}{\omega_\alpha} + H_3^*(K_\alpha)\alpha \right] \quad (5.4)$$

$$M_\alpha = \frac{1}{2}\rho B^4 \omega_h^2 \left[A_1^*(K_h)\frac{\dot{h}}{B\omega_h} + A_4^*(K_h)\frac{h}{B} \right] + \frac{1}{2}\rho B^4 \omega_\alpha^2 \left[A_2^*(K_\alpha)\frac{\dot{\alpha}}{\omega_\alpha} + A_3^*(K_\alpha)\alpha \right] \quad (5.5)$$

According to the Eqns. 5.4 and 5.5 it is possible to identify all the flutter derivatives simultaneously from the free vibration test results.

5.3 Calculation of the Flutter Derivatives

The following calculation procedure is applied to extract the flutter derivatives. In case of any calculation or logical error at one step can result in big errors in the calculation of flutter derivatives. Therefore, care should be given in each step in order to get better results.

step (1) By using the electro magnets the section model is given a fix initial displacement in vertical or rotational direction or both. Then, the useful free vibration time histories of the two motions are calculated as explained in the section 5.1. The noise level in the displacement time histories affect the identified parameters. Therefore, this step has the greatest importance among the others.

step (2) Time Shifts N_1 and N_2 of the motion is required for the MITD method. As explained in Section 3.3.3.1, time shifts are calculated with respect to an empirical

formula for each experiment. Time shifts affect both the quality of the identified parameters and the number of iterations required to converge.

step (3) First, the system identification method is carried out for the wind-off case to calculate the mechanical system matrices $\overline{K}^{mech}$ and $\overline{C}^{mech}$ and the system parameters λ_h, λ_α, ω_h, ω_α of the two-degree of freedom system from the free vibration time histories. In order to increase the quality of the results, each set of experiment is carried out five times and therefore, five free vibration displacement time histories having the same data length are obtained. So that this step is repeated five times and an average value of the mechanical system matrices and the system parameters are obtained.

step (4) Next, all the previous steps are repeated for the wind-on cases for the calculation of the effective system matrices $\overline{K}^{eff}$ and $\overline{C}^{eff}$ and the system parameters λ_h, λ_α, ω_h, ω_α. The only difference is that the free vibration time histories are obtained from the experimental results that belong to a particular wind speed. The wind speed U values used in the calculations have an increment of 0,7 m/s (U_t = 0.5 m/s) from 3.84 m/s (U_t = 2.5 m/s) up to the wind speed that has sufficient time history data for the system identification method. The modal frequencies ω_h, ω_α identified from the free vibration data of the wind-on case are more important than the other system parameters, because both modal frequencies will be used in the calculation of the flutter derivatives and their corresponding reduced velocities in the Eqns. 5.4 and 5.5.

step (5) The flutter derivatives for a particular wind speed are calculated by using the identified effective and mechanical system matrices and the modal frequencies of the corresponding wind speed.

step (6) In order to compare the effect of the initial displacement conditions on the flutter derivatives, the section model is given three different initial conditions. Therefore, all the steps from 1 to 5 should be repeated for each initial condition case and three different sets of flutter derivatives are extracted for comparison.

5.3.1 The Effect of Initial Condition

System parameters and mechanical system matrices of wind-off cases are obtained for three different initial condition cases. In the Table 5.3, the average values of these parameters among the five different experimental results are presented as

Initial Condition	λ_h	λ_α	ω_h [1/s]	ω_α [1/s]	$\overline{C} = M_s^{-1} \cdot C_s$		$\overline{K} = M_s^{-1} \cdot K_s$	
bs_10	-0.133	-0.324	16.600	28.904	0.267	-0.004	275.544	-0.625
					-0.368	0.647	14.147	835.542
bs_20	-0.096	-0.385	16.552	28.840	0.193	-0.005	273.950	-1.356
					-0.084	0.770	10.326	831.939
os_10	-0.245	-0.423	16.597	28.411	0.492	-0.012	275.529	-0.525
					-1.542	0.844	-14.503	807.374

Table 5.3: System parameters and matrices for the wind-off case

The system parameters are expected to be the same for any initial condition, because the properties of the system, such as the damping ratio, circular frequency should be independent of the initial condition. However, as seen in the Table 5.3 this not the case for the results of the experiments. The maximum difference between the circular frequencies, presented in the Table 5.3 is less than 2 % but for the decay rates, the difference is relatively high compared to the circular frequencies. The identification results of the system damping properties are less reliable than for the stiffness properties of the system.

Furthermore, the mechanical damping and the mechanical stiffness matrices should be diagonal matrices. In other words, off-diagonal elements should be zero. Most of the off-diagonal elements are very small compared to their corresponding diagonal elements except for some elements. Especially for the initial condition cases bs_10 and os_10, the element $\overline{C}_{21}$ is even greater than the diagonal elements. $\overline{C}_{21}$ represents the effect of vertical motion on the rotational damping of the system. The differences in the initial vertical displacements of each initial condition case can be the reason for the discrepancy in the element $\overline{C}_{21}$, which is affected by the vertical motion. As given in the Table 5.1, bs_20 has the highest initial vertical displacement and the element $\overline{C}_{21}$ of bs_20 case has the smallest value among the other initial condition cases. On the other hand for the case os_10, the condition is completely opposite compared to the bs_20. Therefore, it can be interpreted that the quality of the mechanical system matrices increase with the application of higher initial vertical displacements, which also affect the length of the useful data. The second reason for these discrepancies can be the different length of useful data and the noise level of the data, both of which are different for each initial condition case.

Because of these discrepancies in the results of the mechanical system matrices, it is not possible to use the average of the three results as the mechanical system matrices of the general system in the calculation of flutter derivatives. Therefore, it is suggested to use each mechanical system matrices $\overline{K}^{mech}$ and $\overline{C}^{mech}$ with its corresponding effective system matrices $\overline{K}^{eff}$ and $\overline{C}^{eff}$. So that three sets of flutter derivatives are calculated for each initial condition case. That means any error made in the calculation of mechanical system matrices will also appear in the effective system matrices for the same initial condition. By this way the errors occurred in both matrices will be automatically eliminated, because the flutter derivatives are calculated by taking the difference between the mechanical and effective system matrices of each initial condition case.

5.3.2 Extraction of Flutter Derivatives

In order to define the aerodynamic behavior of the rectangular section model, all flutter derivatives are obtained from a two-degree of freedom motion under smooth wind flow with zero angle of incidence. As explained before, since the mechanical properties of each initial condition case is different from each other, three sets of flutter derivatives will be calculated by using the corresponding mechanical system parameters. The necessary parameters for the calculation of the flutter derivatives are presented in the Table 5.3 for each initial condition case. Also the following parameters are used in common for each set of flutter derivatives.

m = 6.538 kg (mass of the total system)
I = 0.1359 kg·m^2 (mass moment of inertia of the total system)
B = 0.3 m (width of the rectangular section model)
ρ = 1.20 kg/m^3 (standard air density at 20°, 1013.25 mbar and 50 % relative humidity)

The flutter derivatives can be calculated after the calculation of mechanical and effective system matrices by the MITD method from free vibration response of the system with respect to the wind-off and wind-on cases, respectively. The flutter derivative terms, which form the loading term on the right side of the equation of motion at Eqn. 2.1, manifest themselves in the system matrices in order to set the right side of the equation of motion into zero. By this way, system identification method can be applied with respect to the free vibration response of the system. The equation of motion for free vibration is written as

$$\ddot{x} + \overline{C}\dot{x} + \overline{K}x = 0 \qquad (5.6)$$

where $\overline{K} = M_s^{-1}K_s$ and $\overline{C} = M_s^{-1}C_s$

According to the Eqn. 5.6, the effective damping and stiffness matrices can be formed as

$$\overline{C}^{\,eff} = \begin{bmatrix} \overline{C}_{11}^{mech} - \dfrac{\rho B^2 \omega_h}{2m} H_1^* & \overline{C}_{12}^{mech} - \dfrac{\rho B^3 \omega_\alpha}{2m} H_2^* \\ \overline{C}_{21}^{mech} - \dfrac{\rho B^3 \omega_h}{2I} A_1^* & \overline{C}_{22}^{mech} - \dfrac{\rho B^4 \omega_\alpha}{2I} A_2^* \end{bmatrix} \qquad (5.7)$$

$$\overline{K}^{\,eff} = \begin{bmatrix} \overline{K}_{11}^{mech} - \dfrac{\rho B^2 \omega_h^2}{2m} H_4^* & \overline{K}_{12}^{mech} - \dfrac{\rho B^3 \omega_\alpha^2}{2m} H_3^* \\ \overline{K}_{21}^{mech} - \dfrac{\rho B^3 \omega_h^2}{2I} A_4^* & \overline{K}_{22}^{mech} - \dfrac{\rho B^4 \omega_\alpha^2}{2I} A_3^* \end{bmatrix} \qquad (5.8)$$

As seen in the Eqns. 5.7 and 5.8, the flutter derivatives for any wind speed can be calculated by taking the difference between the effective system matrices, which are calculated with respect to the corresponding wind speed, and the mechanical system matrices. Both circular frequencies ω_h and ω_α are used in the calculation of flutter derivatives for the corresponding wind speed.

$$H_1^*(K) = -\frac{2m}{\rho B^2 \omega_h}(\overline{C}_{11}^{eff} - \overline{C}_{11}^{mech}) \; ; \qquad A_1^*(K) = -\frac{2I}{\rho B^3 \omega_h}(\overline{C}_{21}^{eff} - \overline{C}_{21}^{mech})$$

$$H_2^*(K) = -\frac{2m}{\rho B^3 \omega_\alpha}(\overline{C}_{12}^{eff} - \overline{C}_{12}^{mech}) \; ; \qquad A_2^*(K) = -\frac{2I}{\rho B^4 \omega_\alpha}(\overline{C}_{22}^{eff} - \overline{C}_{22}^{mech})$$

$$H_3^*(K) = -\frac{2m}{\rho B^3 \omega_\alpha^2}(\overline{K}_{12}^{eff} - \overline{K}_{12}^{mech}) \; ; \qquad A_3^*(K) = -\frac{2I}{\rho B^4 \omega_\alpha^2}(\overline{K}_{22}^{eff} - \overline{K}_{22}^{mech})$$

$$H_4^*(K) = -\frac{2m}{\rho B^2 \omega_h^2}(\overline{K}_{11}^{eff} - \overline{K}_{11}^{mech}) \; ; \qquad A_4^*(K) = -\frac{2I}{\rho B^3 \omega_h^2}(\overline{K}_{21}^{eff} - \overline{K}_{21}^{mech}) \qquad (5.9)$$

The same calculation procedure is applied to all wind speed case, which has sufficient length of data points to apply the system identification method. The length of useful data decreases with the increasing wind velocity. Because the higher the wind speed, the shorter will be the length of data. Especially, near the flutter onset wind velocity the aerodynamic damping of the vertical motion is very high, so that the vertical motion is damped faster and the useful vibration data is consequently shorter. Therefore, accuracy of the identified flutter

derivatives and system parameters decrease with the increasing wind velocity. In order to reduce the effect of this problem, Iwamoto [9] suggested using heavier section models having greater mass moment of inertia for the free vibration tests. Therefore, in order to get better results, the rectangular section model used in the experiments has relatively high mass and mass moment of inertia.

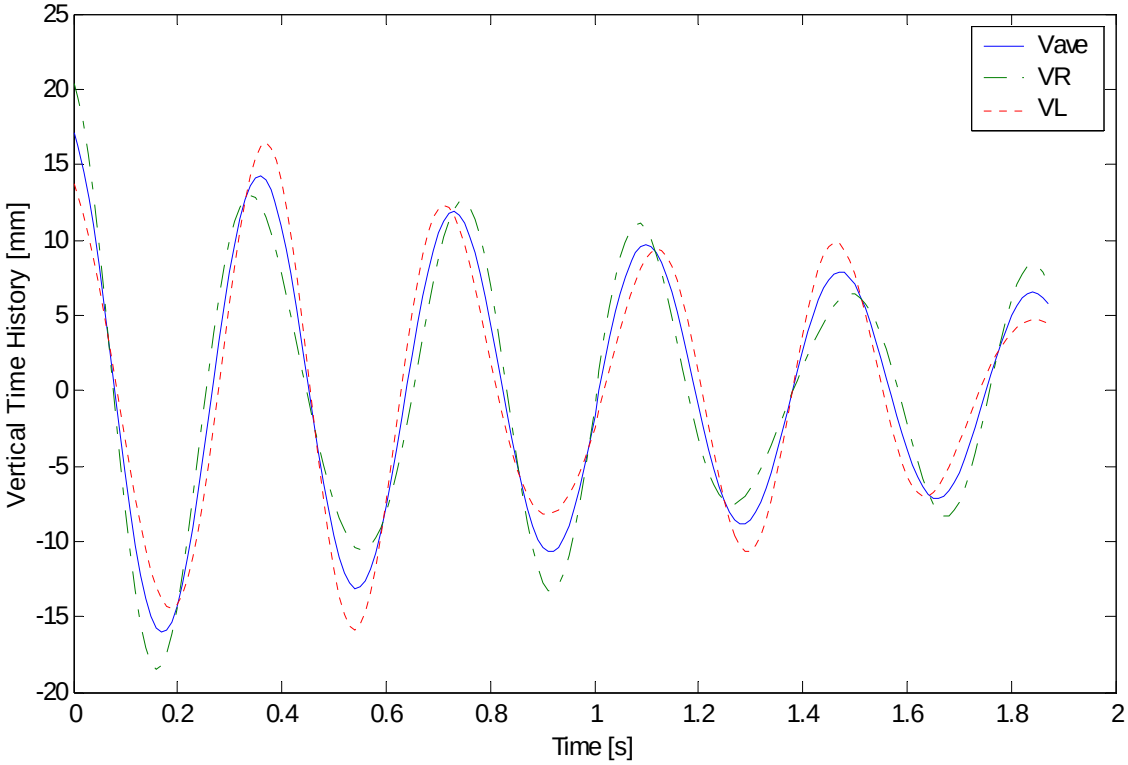

Figure 5.5a: Comparison of the vertical time histories Vave, VR, VL

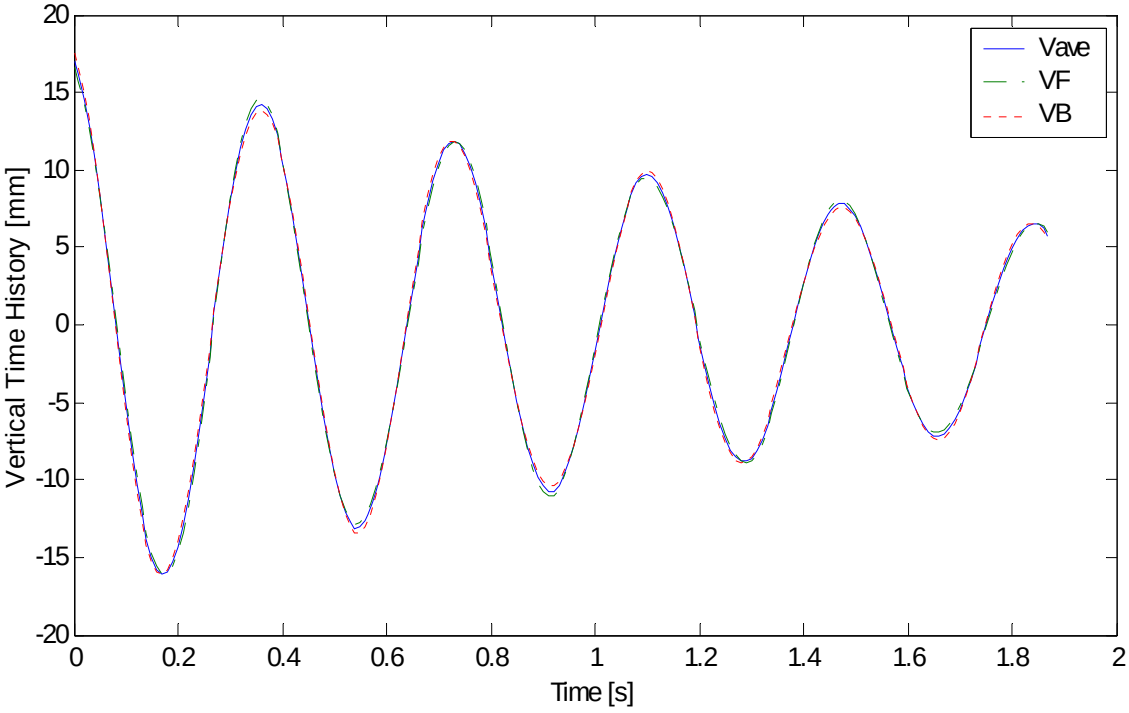

Figure 5.5b: Comparison of the vertical time histories Vave, VF, VB

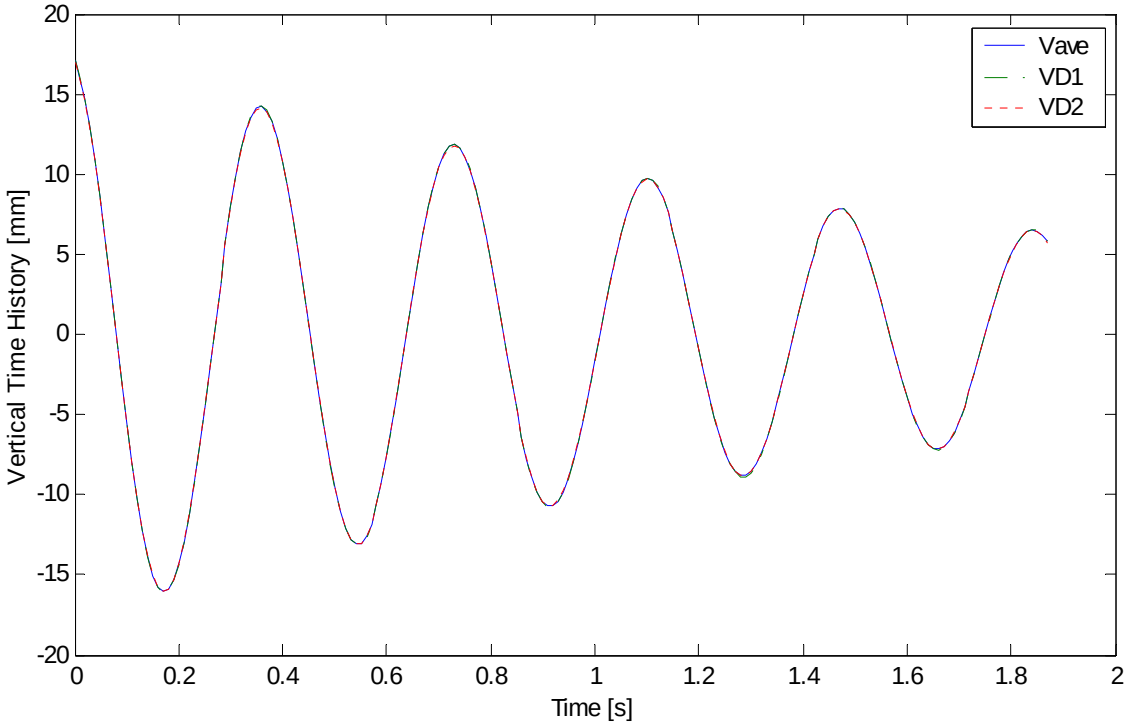

Figure 5.5c: Comparison of the vertical time histories Vave, VD1, VD2

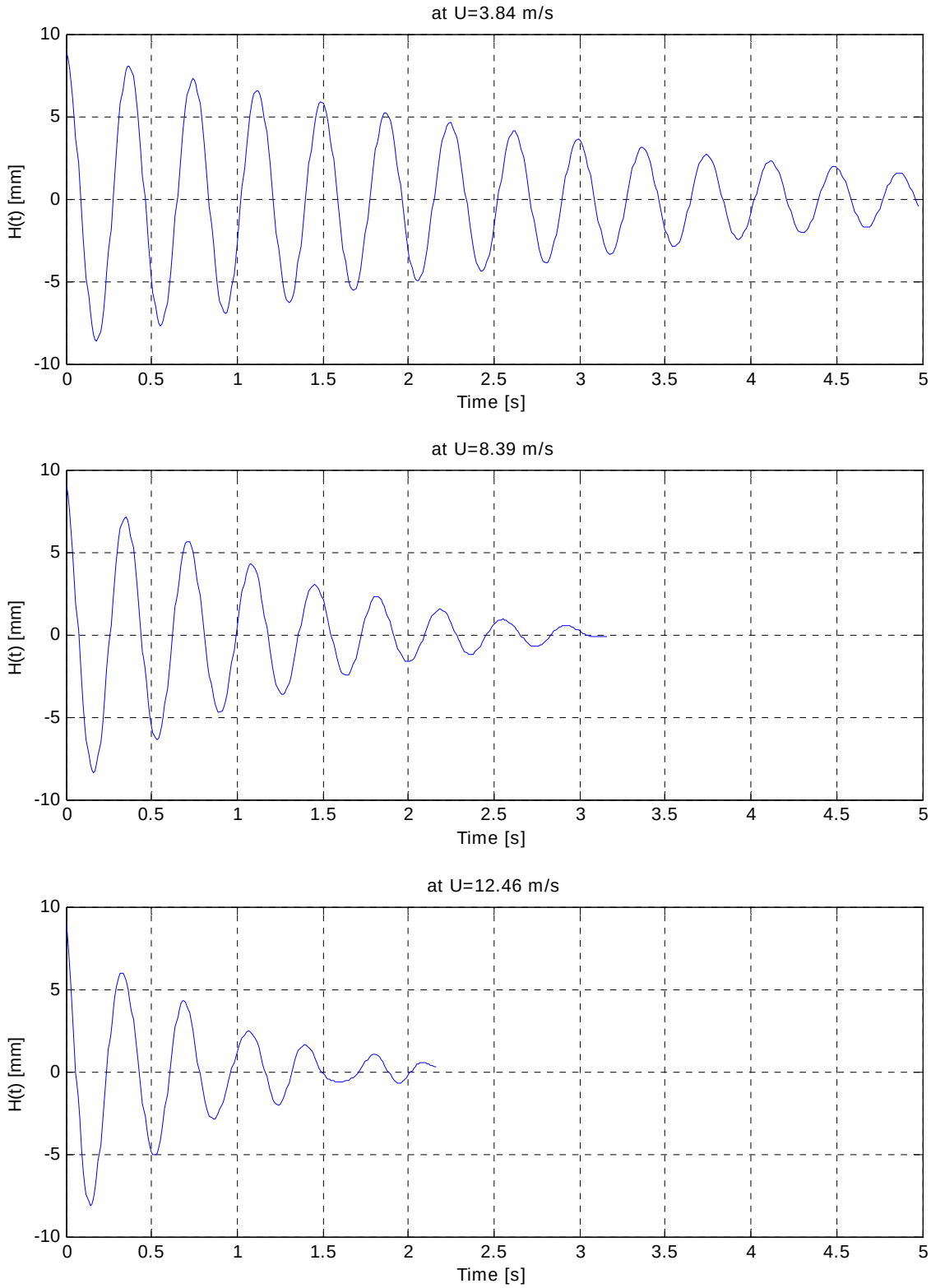

Figure 5.6: Vertical time histories at 3.84 m/s, 8.39 m/s, 12.46 m/s

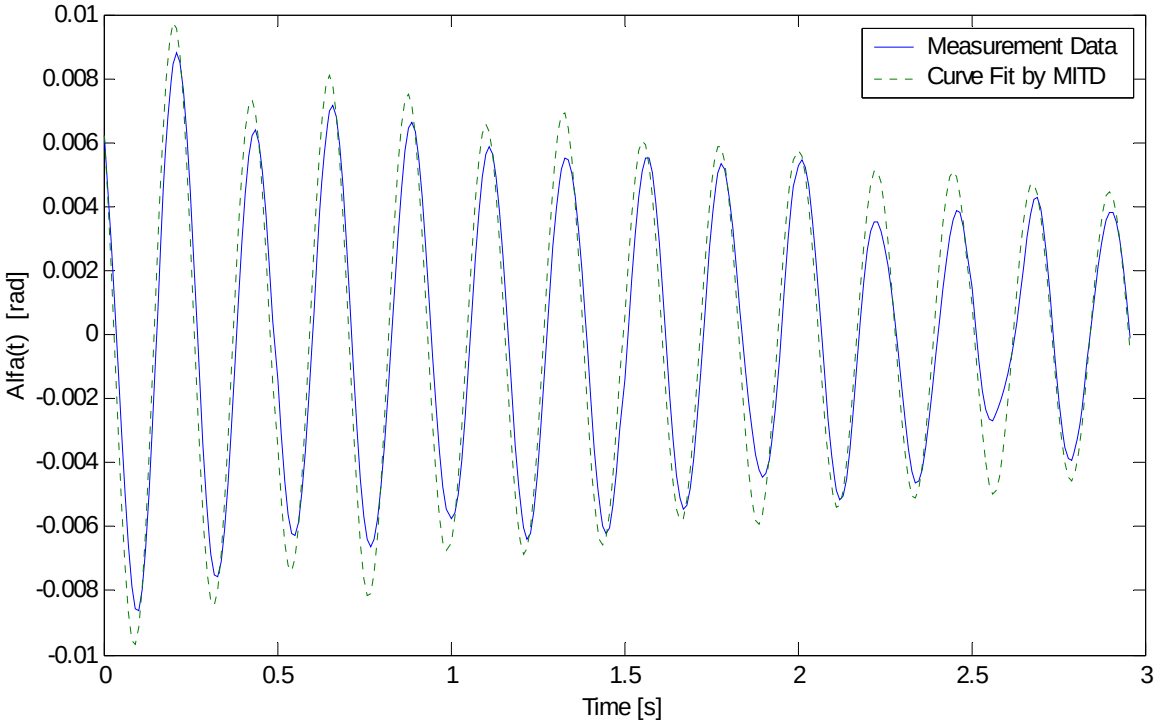

Figure 5.7a: Curve fit with respect to the filtered measurement data

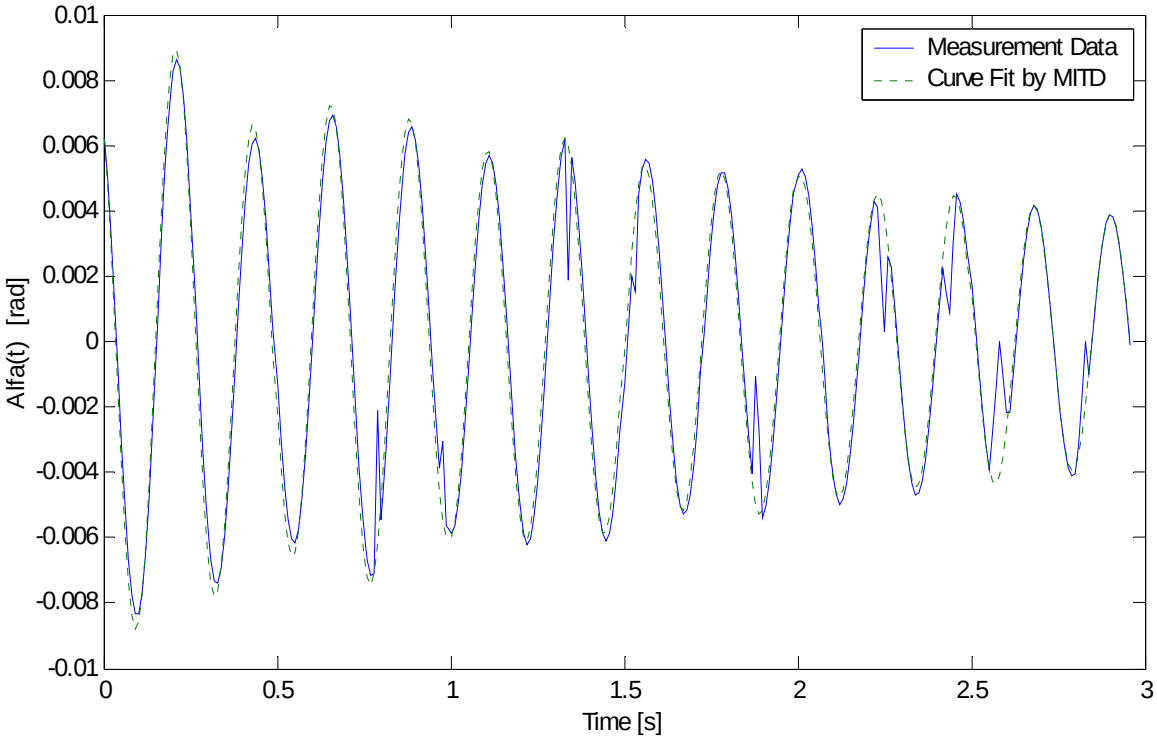

Figure 5.7b: Curve fit with respect to the measurement data without filtering

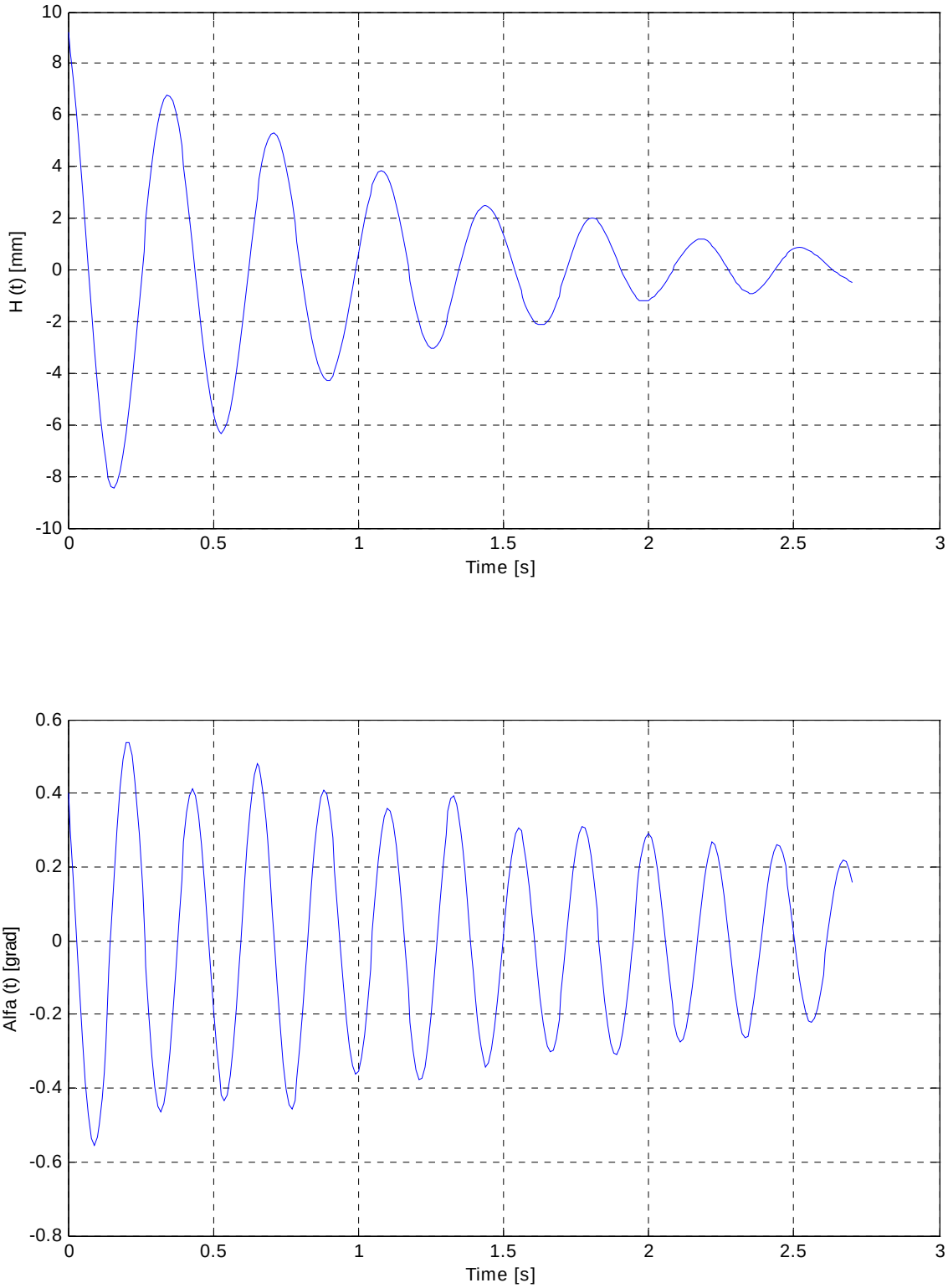

Figure 5.8: Displacement time histories, h(t) and $\alpha(t)$ at U_t = 7.0 m/s

6 RESULTS AND DISCUSSION

This chapter is devoted to present and interpret the results obtained from the wind tunnel tests of a rectangular section model with an aspect ratio of 1:8 under smooth wind flow with zero angle of incidence. The interpretation is done by comparing the free vibration test results with two sets of forced vibration test results, which provide the possibility to check the results of both techniques.

6.1 Flutter Derivatives

As explained in chapter five, flutter derivatives are determined from the results of the wind tunnel tests with the Reynolds number of 2.75×10^5. The maximum wind speed, which is used in the determination of the flutter derivatives, is about 1 m/s greater than the critical wind speed in order to observe the flutter effect on the system parameters providing sufficient length of useful data. The test, which is performed under the maximum wind speed, has enough length of displacement time history data for the application of the system identification method to identify the flutter derivatives. Although the torsional motion has a constant or growing oscillation time history at higher wind speeds, the length of useful data is determined with respect to the length of the h(t), which has a higher damping ratio.

On the other hand at very high wind speeds greater than the flutter limit, there is a relatively big difference between the vertical and torsional oscillation data, which makes the instrumental matrices Φ and $\hat{\Phi}$ defined in the Eqns. 3.9 and 3.10, singular and the system parameters cannot be identified any more. Also, after a short time with the application of initial displacement, both vertical and torsional motion has growing oscillation time histories with the same circular frequencies at very high wind speeds greater than the flutter limit. Furthermore, the vertical motion has two different types of motion with different frequencies; after the initial displacement is given to the system, vertical motion first starts to decay with a lower frequency up to certain time, after then it grows continuously with a higher frequency, which is exactly the same with the frequency of torsional motion. Therefore it is not possible to identify the flutter derivatives with the MITD method at very high wind speeds, where both of the motions have the same circular frequency.

As an example, the vertical and torsional displacement time histories of the wind tunnel test v11.5_10_01, which is performed under the wind speed much higher than the flutter limit, are presented in Fig. 6.2a. The frequencies of the both motion are calculated by the fast fourier transformation (fft) method and the results are presented in the Fig. 6.2b. As seen in

the Fig. 6.2a, after the application of initial displacement, oscillation of the torsional motion grows continuously with the torsional frequency of 4.21 Hz. However, at first the vertical motion has a decaying oscillation for 2 seconds with the frequency of 2.96 Hz, after then it starts to grow continuously with the frequency of 4.21 Hz, which is exactly the same as the torsional frequency. In the Fig. 6.2b, two peak points with different frequency values arise for the frequency analysis of the vertical motion. The smaller frequency represents the decaying oscillation, where the bigger one represents the growing oscillation.

In section 5.2, it is proved that the effect of the vertical motion on the flutter derivatives associated with the torsional motion is very small and vice versa. So that these effects are neglected to overcome the uniqueness problem in the calculation of flutter derivatives. At the higher wind speeds greater than the flutter limit this assumption is no more valid, because the two motions cannot be separated between each other and they are not independent any more. Both the vertical and the torsional motion have a growing oscillation with the same frequency.

6.1.1 Curve Fitting for Flutter Derivatives

In order to improve the quality and the reliability of the flutter derivatives identification results, all the tests are performed 5 times for the same wind speed and initial condition. After the calculation of all the flutter derivatives with respect to the reduced wind velocity $U_{red}=U/(B\cdot f)$ for each test result, a least square method with an order of five is applied to fit a curve through the identification results, which will give the best result for the flutter derivatives. The least square technique uses all the data points to get the best fit for the flutter derivatives, which eliminates the obvious outliers throughout the distribution of the results represented by the points as seen in the Fig. 6.3 for the initial condition case bs_10. The effect of the useful time history length on the flutter derivatives results can be seen clearly in the Fig. 6.3. Since the useful length of the response data is getting shorter with the increasing reduced wind velocity, there is a large scatter of the results at the high reduced wind velocities around the stability border, especially for the flutter derivative A_4^*. The reason for the scatter of the results is not only the limited length of response data but also the nature of the corresponding flutter derivative, which is hard to identify exactly. This phenomenon will be explained in the next section in detail.

6.2 Comparison of the Results

Three sets of flutter derivatives are calculated for three different initial condition cases from the free vibration tests having the Reynolds number of 275.000. All these results will be compared with the forced vibration test results. The results of forced vibration tests can also contain some error, because they are also calculated from the experimental results. Therefore, two different forced vibration results are considered for the comparison of the free vibration test results, which provides the opportunity to check the forced vibration test results at the same time.

The first set of forced vibration test results are obtained from the tests of Hortmanns [23], which have the Reynolds number of 100.000. The second set is obtained from the tests of Bergmann [22], which are carried out for the rectangular section model with the Reynolds number of 200.000. Bergmann test results are presented with three different initial displacement conditions, which are given to the section model separately for each motion. The three different initial vertical and torsional displacement amplitudes given to the section model are 2 mm, 4 mm, 8 mm and 2°, 5°, 8°, respectively. In order to make a consistent comparison between the different sets of results, all the flutter derivatives are converted to the current Scanlan notations [2] according to the Table 2.1.

6.2.1 Comparison of the Flutter Derivatives

The results of the free vibration tests for each initial condition and the forced vibration test results are presented in Appendix A, in the figures A.1 – A.12. The results of the flutter derivatives H_3* and A_3* are in good agreement for all cases. The flutter derivatives H_1^* and A_1^* of the initial conditions bs_10 and bs_20 match very well with the forced vibration results, which is not the case for the initial condition case os_10. This shows the weakness of the experimental results for the initial condition case os_10, not for the system identification method. However, the results of the flutter derivative H_2^* for all initial condition case show the same discrepancy compared with the forced vibration test results, which can be a proof of the weakness of the system identification method in calculating the flutter derivative H_2^*. In fact, at the low reduced wind velocities, H_2^* results for each technique show good agreement. However, with increasing U_{red}, the discrepancy increases considerably between the results of free vibration and forced vibration tests. This discrepancy can be taken as under the acceptable limits compared to the discrepancies in the flutter derivatives H_4^* and A_4^*.

Since the rectangular section model does not have a streamlined cross section, the torsional aerodynamic damping coefficient A_2^* dominates the aeroelastic performance of the

section. As in the results of initial condition cases bs_10 and bs_20, A_2^* exhibits sign change at a particular reduced wind velocity, which indicates the tendency of the section model to the torsional flutter. For the initial condition case os_10, after a certain reduced wind velocity A_2^* exhibits an irregular distribution, which has a completely different behavior compared to the A_2^* distributions of the other initial condition cases.

On the other hand, there is an evident discrepancy in the A_2^* results of the forced vibration test results. The free vibration test results of A_2^* are in good agreement with the wind tunnel test results of Hortmanns [23], but there is big discrepancy with the results of forced vibration wind tunnel test results of Bergmann [22]. Almost the same results are obtained according to the numerical approach using the Computational Fluid Dynamics (CFD) by Thiesemann et al. [21]. The numerical results are in good agreement with the results of Hortmanns, but there is a considerable discrepancy between the numerical results and the results of Bergmann for the forced vibration tests. Therefore, the discrepancy in the forced vibration test results should be further investigated in order to make reliable comparisons.

As seen in the figures in appendix A, there is a relatively high difference in the flutter derivatives H_4^* and A_4^* calculated with the free vibration test results and the forced vibration test results. The discrepancy in the flutter derivatives H_4^* and A_4^* is not only in between the free vibration test results for different initial condition cases, but there is also an obvious disagreement between the forced vibration test results, especially for the A_4^*. As mentioned earlier, due to the high damping ratio of the vertical motion at the higher reduced wind speeds, the length of useful time history is very short, which makes the identification of flutter derivatives H_4^* and A_4^* difficult and inconsistent. The second reason for the disagreement is that, as given in the Eqn. 5.9, H_4^* and A_4^* are calculated by taking the difference between the effective and mechanical stiffness matrices $\overline{K}_{11}$ and $\overline{K}_{21}$, respectively, which are directly related with the natural circular frequency of the vertical motion. As seen in the Fig. 6.5, the change in ω_h is very small with the increasing reduced wind velocity. Therefore, the calculation of the flutter derivatives H_4^* and A_4^* is very sensitive to the noise level of the input data and even small errors in the identification of the corresponding stiffness matrices can result in big differences in H_4^* and A_4^*.

In general the results show that, even for the high-reduced wind speeds, the free vibration test results and the forced vibration test results are in good agreement in between except for the flutter derivatives H_4^* and A_4^*, which is also stated by Iwamoto [9], Sarkar [3]. Furthermore, it has been confirmed that the errors occur at the flutter derivatives H_4^*, A_4^* do

not affect the flutter behavior of the system so severely. Because of this reason these flutter derivatives are not presented in the original work of Scanlan and Tomko [10].

The results of flutter derivatives calculated by free vibration test results for the initial condition case bs_10, are proved to be the best results among the other initial condition cases by comparing the forced vibration test results in the figures Fig. A.1 - Fig. A.4. Also, bs_10 results contain more flutter derivatives with different reduced wind speed values than the other initial condition cases. Therefore, the calculation of the critical wind speed and the other comparisons are done with respect to the results of initial condition case bs_10.

6.2.2 Comparison of the Rectangular Section with the Flat Plate

In chapter 2 the theoretical values of the flutter derivatives of a flat plate are calculated in terms of Theodorsen function. These theoretical results are compared with the results of the rectangular section model calculated by the system identification method from the free vibration test results for the initial condition case bs_10. The comparison provides the opportunity to find out similarities and discrepancies of the rectangular section to the plate-like sections from the aerodynamic point of view. The streamlined cross sections used in the long-span bridge construction show almost the same aerodynamic behavior as the flat plate section, proved by Scanlan [2]. As seen in the Fig. 6.4, the discrepancy between the flutter derivatives of the flat plate and the rectangular section is relatively high. Especially, the discrepancy in the flutter derivative A_2^* exhibits the main difference between aerodynamic behavior of the two sections. A_2^* of the flat plate does not show any sign change like A_2^* of the rectangular section and it stays on the negative side for all reduced wind speeds. Therefore the flat plate sections or namely streamlined sections do not show pure torsional flutter. On the contrary the rectangular section is prone to the torsinal flutter. Finally, it is interpreted that the theoretical calculations of the flutter derivatives are no more valid for the rectangular section with an aspect ratio of 1:8.

6.2.3 Calculation of Critical Wind Speed

Another way of inspection for the reliability of the MITD method and the analysis results is making a comparison between the measured critical wind speed during the wind tunnel tests and the theoretically calculated critical wind speed by using the identified flutter derivatives. The tunnel wind speed U_t is measured as 10.0 m/s at the stability border of the section model. The corresponding wind speed acting on the section model is calculated as 13.857 m/s from the Fig. 4.7. As explained in section 2.3.1, the critical wind speed is

calculated by using the identified flutter derivatives according to the theoretical calculations derived by Starossek [1].

The system parameters δ_h, δ_α, ω_h, ω_α are already calculated with the MITD method from the experimental results. In order to make a second comparison, the system parameters are obtained with respect to the theoretical calculations by using the identified flutter derivatives and the following mechanical system parameters for the initial condition case bs_10.

$\lambda_h = -0.1334$, $\lambda_\alpha = -0.3236$, $\omega_h = 16.5995$ [1/s], $\omega_\alpha = 28.9036$ [1/s] ; (Table 5.3)

$\xi_h = |\lambda_h/\omega_h| = 0.00804$, $\xi_\alpha = |\lambda_\alpha/\omega_\alpha| = 0.0112$; damping ratio-to-critical

$g_h = 2\cdot\xi_h = 0.01608$, $g_\alpha = 2\cdot\xi_\alpha = 0.0224$; damping coefficient, Starossek [1]

$\varepsilon = \omega_\alpha/\omega_h = 1.7412$; frequency ratio

$\mu = 77.078$; relative mass, Eqn. 2.22

$r = 0.957$; reduced mass radius of gyration, Eqn. 2.22

Flutter derivatives associated with torsinal and vertical motion has different U_{red} values. Therefore in the calculation of system parameters and critical wind speed, the flutter derivatives having the common U_{red} values are taken into account.

In the Fig. 6.5, experimental values and calculated values of the system parameters are presented. Except for the vertical motion damping δ_h, both calculated and experimental values of the system parameters fit very well. Since the discrepancy in the δ_h results is not so severe, the difference in the results are accepted to be in the allowable range. Therefore, the reliability of the theoretical formulations is proved for the calculation of the system parameters by using the flutter derivatives.

The critical wind speed can be calculated with respect to the point where the calculated damping ratio of the torsional motion δ_α is equal to zero or namely at the stability border of the section model. According to the Fig. 6.5, the calculated δ_α curve crosses the zero ordinate at $U_{red} = 10.483$ and the corresponding torsional circular frequency is obtained as 27.319 1/s. The critical wind speed is calculated as

$$U_{critical} = U_{red}\cdot B\cdot f_\alpha = 10.483\times 0.3\times(27.319/(2\cdot\pi)) = 13.674 \text{ m/s}$$

The difference between the measured critical wind speed 13.857 m/s and calculated critical wind speed 13.674 m/s is 1.32 %. Both measured and calculated critical wind speed

values should be identical, because the critical wind speed is calculated by using the results of the measurement data. The small amount of difference, which is only due to numerical reasons, proves the applicability of the formulas used for the calculation of the critical wind speed.

Moreover, the critical wind speed is calculated with respect to the forced vibration test results of Hortmanns and Bergmann by using the same procedure explained in section 2.3.1. The flutter derivatives for the forced vibration test results are available, whereas the mechanical system parameters are not provided. However, it should be pointed out that the mechanical properties of the system are independent of the technique used for the identification. In order to make a rough comparison, the system parameters that are obtained from the MITD method for the initial condition case bs_10, are used in the theoretical calculation of the critical wind speed by applying the flutter derivatives calculated from the forced vibration test results.

Bergmann's forced vibration test results are available for different initial condition cases. The initial condition case (α_0=8° and h_0=8 mm) is selected whose results show the best agreement with the free vibration test results.

The system parameters obtained from the free vibration test results and the ones calculated by using the flutter derivatives determined from the forced vibration test results of Hortmanns and Bergmann are compared in the Fig. 6.6 and 6.7, respectively. The discrepancies between the related system parameters shown in the Fig. 6.6 and 6.7 are greater than the ones shown in the Fig. 6.5.

The critical wind speed obtained from the experiments is compared with the critical wind speed obtained from the calculations by using the flutter derivatives identified from the free vibration test results and the forced vibration test results of Hortmanns and Bergmann. These results are presented in the Table 6.1 and the percentage difference is calculated with respect to the critical wind speed 13.857 m/s, measured from the wind tunnel tests.

		Re	U_{red}	ω_α [1/s]	f_α [Hz]	$U_{critical}$ [m/s]	Diff. [%]
Free Vibration Tests		$2{,}75\times10^5$	10,48	27,32	4,35	13,67	1,32
Forced Vibration Tests	Hortmanns	$1{,}0\times10^5$	9,35	27,17	4,32	12,13	12,47
	Bergmann	$2{,}0\times10^5$	11,93	27,14	4,32	15,45	11,53

Table 6.1: Comparison of the critical wind speed of the rectangular section model

As seen in the Table 6.1, the difference for the free vibration test result is almost negligible, because the flutter derivatives are identified exactly from the present experiment. Although the flutter derivatives of the forced vibration tests are obtained from different experiments with different Reynolds numbers, the difference for both forced vibration test results are in the acceptable limits.

6.2.4 Simplified Flutter Prediction

For the non-streamlined bridge cross sections, a simplified flutter prediction method is developed by Starossek [1] to estimate the critical wind speed roughly. The simplified method results are in good agreement for the bluff sections, which are prone to the uncoupled, pure torsional flutter. The greatest advantage of the simplified method is the reduction in the calculation process, because only the flutter derivatives $c_{\alpha\alpha}''$ ($= 8/\pi \cdot A_2^*$) and $c_{\alpha\alpha}'$ ($= 8/\pi \cdot A_3^*$) are required. The simplified method is applied to the rectangular section model in order to investigate the behavior of the model, whether it exhibits a pure torsional flutter or not.

When the Eqn. 2.20 is arranged with respect to the uncoupled torsional motion, the following formulation is derived as

$$c''_{\alpha\alpha} = g_\alpha (\mu \cdot r^2 + c'_{\alpha\alpha}) \qquad (6.1)$$

The section reaches to the stability border and oscillates with a harmonic motion when the Eqn. 6.1 is in equilibrium. Then the critical wind speed is calculated according to the reduced wind velocity at the corresponding point. Therefore, the left and the right side of the Eqn. 6.1 are plotted with respect to the reduced wind velocity in the Fig 6.8 by using the mechanical system parameters and flutter derivatives identified from the free vibration test results for the initial condition bs_10. The intersection point of the two curves results in the reduced wind velocity, by which the critical wind speed can be calculated.

As seen in the Fig. 6.8, the two curves do not intersect due to insufficient number of flutter derivatives, but they seem to intersect nearly at $U_{red} = 12.0$ which is greater than the theoretically calculated stability border $U_{red} = 10.48$, obtained in the Fig. 6.5. This result shows that the coupled motion flutter for the rectangular section is more critical than the pure torsional flutter. Therefore, it can be interpreted that, the rectangular section model (1:8)

behaves in between the streamlined and bluff cross sections from the aerodynamic point of view.

6.2.5 Phase Shift (φ_α) and Amplitude Ratio (R_α)

During the wind tunnel tests, at the flutter case the section model was observed to move around a particular point, which is at the windward side. The presence of phase shift between the two motions force the rotation axis of the section model move apart from the center of the model. It is obviously observed from the experiments that with the increasing wind speed, the location of the center of rotation of the section moves away from the center of the section to the windward direction.

The phase shift and the amplitude ratio of the motions at the stability limit are calculated by using the system parameters and the flutter derivatives at the flutter case according to the Eqns. 2.31 and 2.32 as follows

$$R_\alpha = 1.9645 \text{ and } \varphi_\alpha = 0.3557 \text{ [radians]} = 20.38°$$

The phase shift and the amplitude ratio are represented in the Fig. 6.1. The two vectors α and h/b rotate in the complex plane with a constant angular velocity ω in counterclockwise direction with a constant amplitude ratio and phase shift.

The location of the rotation axis T is simply calculated from geometry, in the Fig. 6.1 as

$$z = \frac{\tilde{h}}{\tan\tilde{\alpha}} = b\frac{\tilde{h}/b}{\tan\tilde{\alpha}} \cong b\frac{\tilde{h}/b}{\tilde{\alpha}} = b\frac{1}{R_\alpha} = \frac{0.15^m}{1.9645} = 7.6cm$$

The rotation axis lies 7.6 cm away from the center of the section model in the windward side for the flutter condition, which is already observed in the experiments.

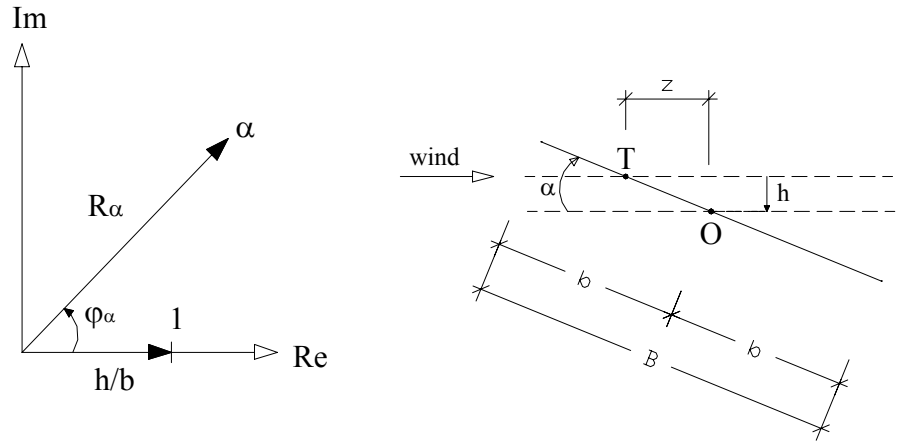

Figure 6.1: Normalized displacement vectors and the motion of the section model

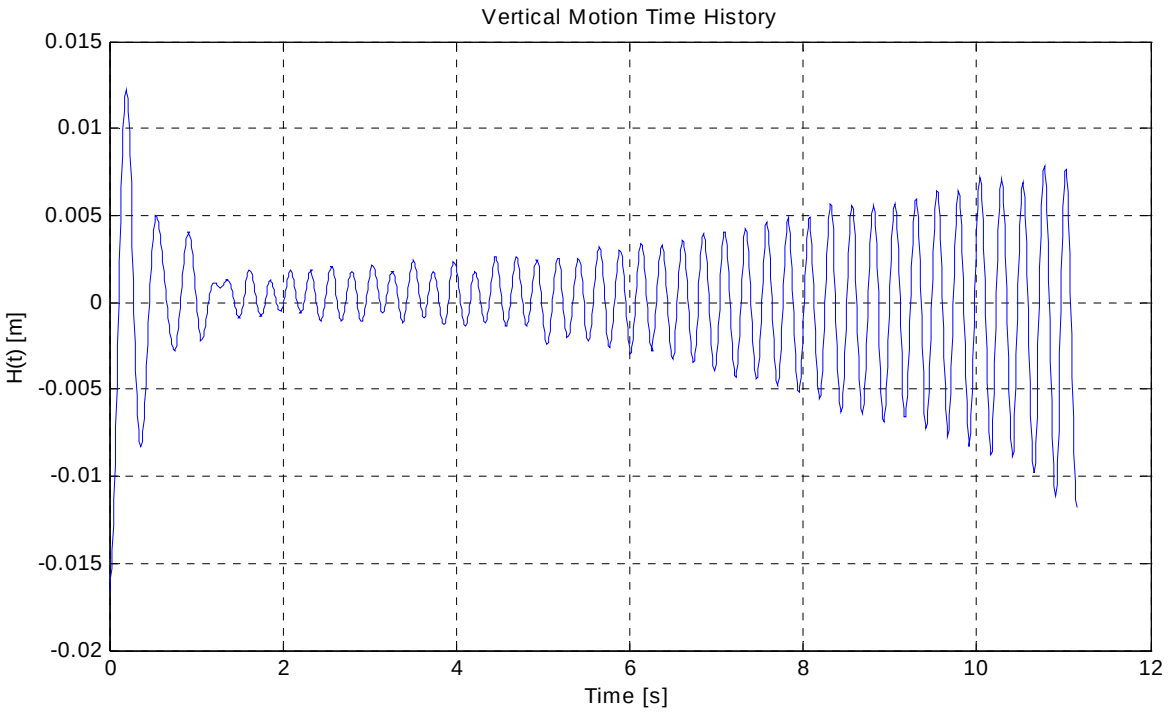

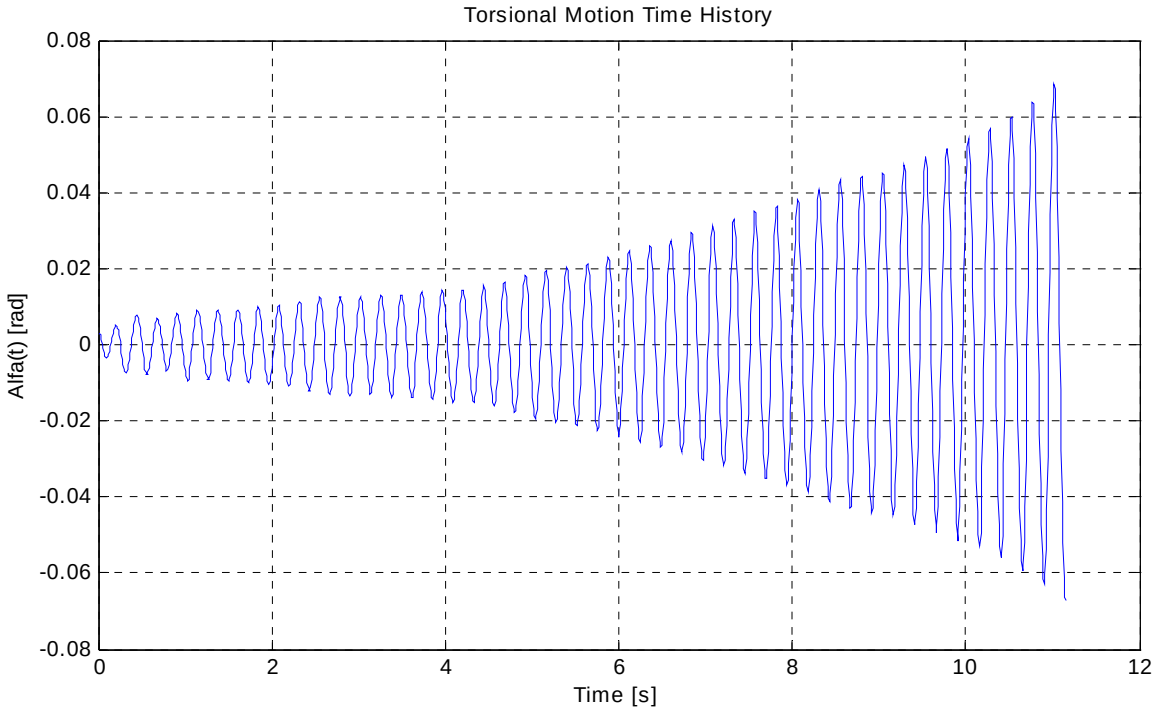

Figure 6.2a: h(t) and $\alpha(t)$ for U_t = 11.5 m/s greater than flutter limit

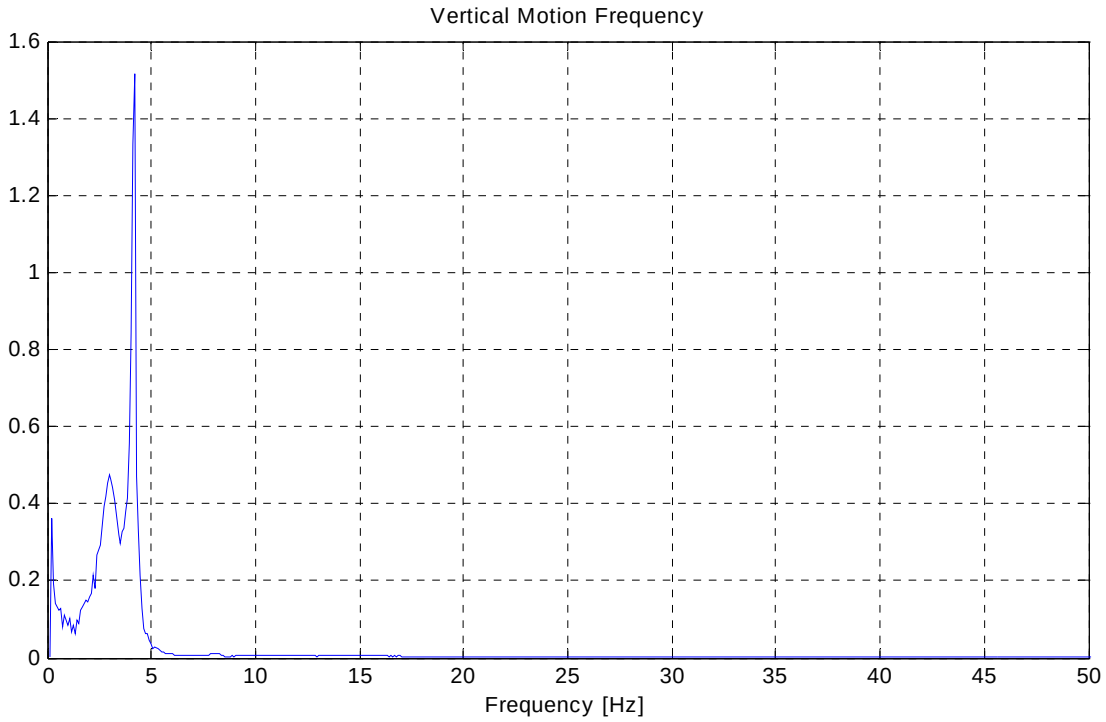

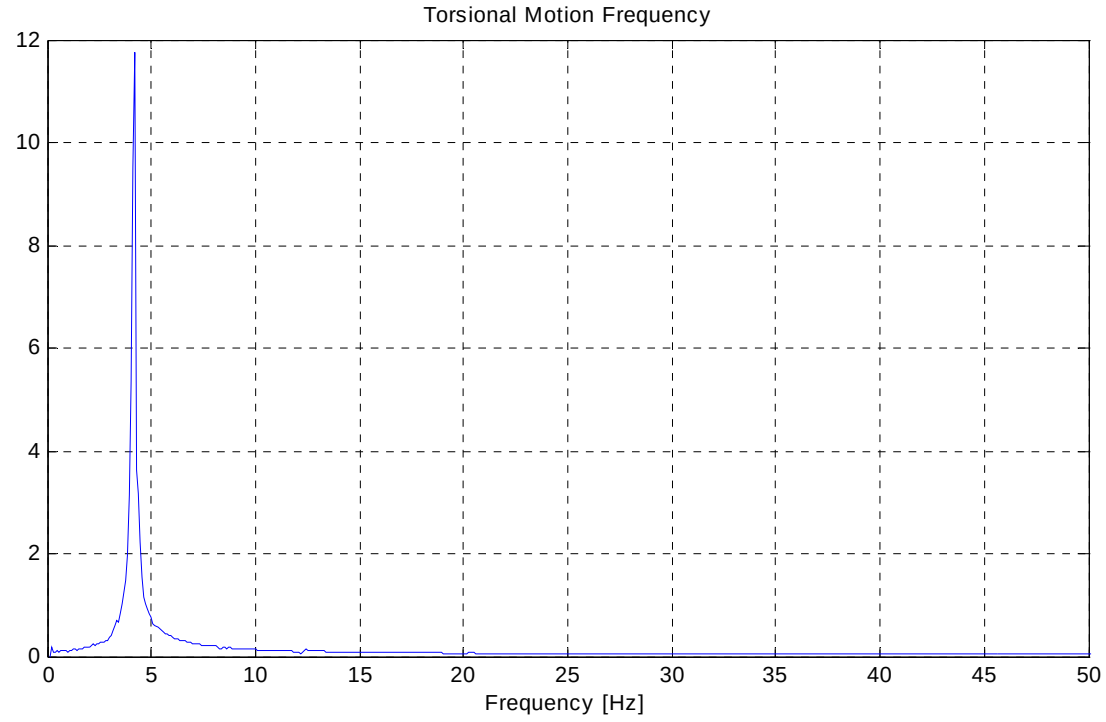

Figure 6.2b: Frequency analysis of the h(t) and α(t) for U_t = 11.5 m/s

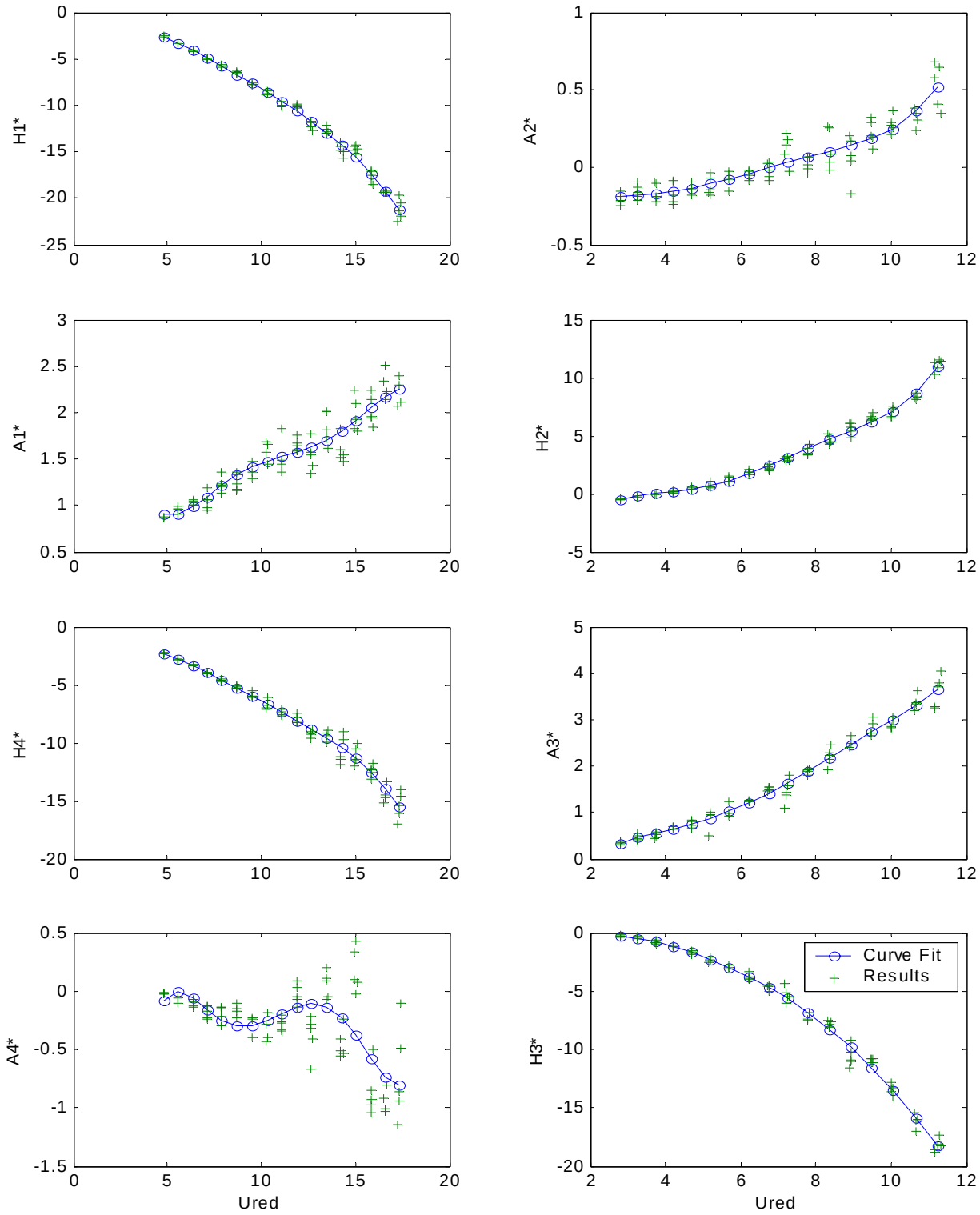

Figure 6.3: Curve fit for the flutter derivatives of the initial condition case bs_10

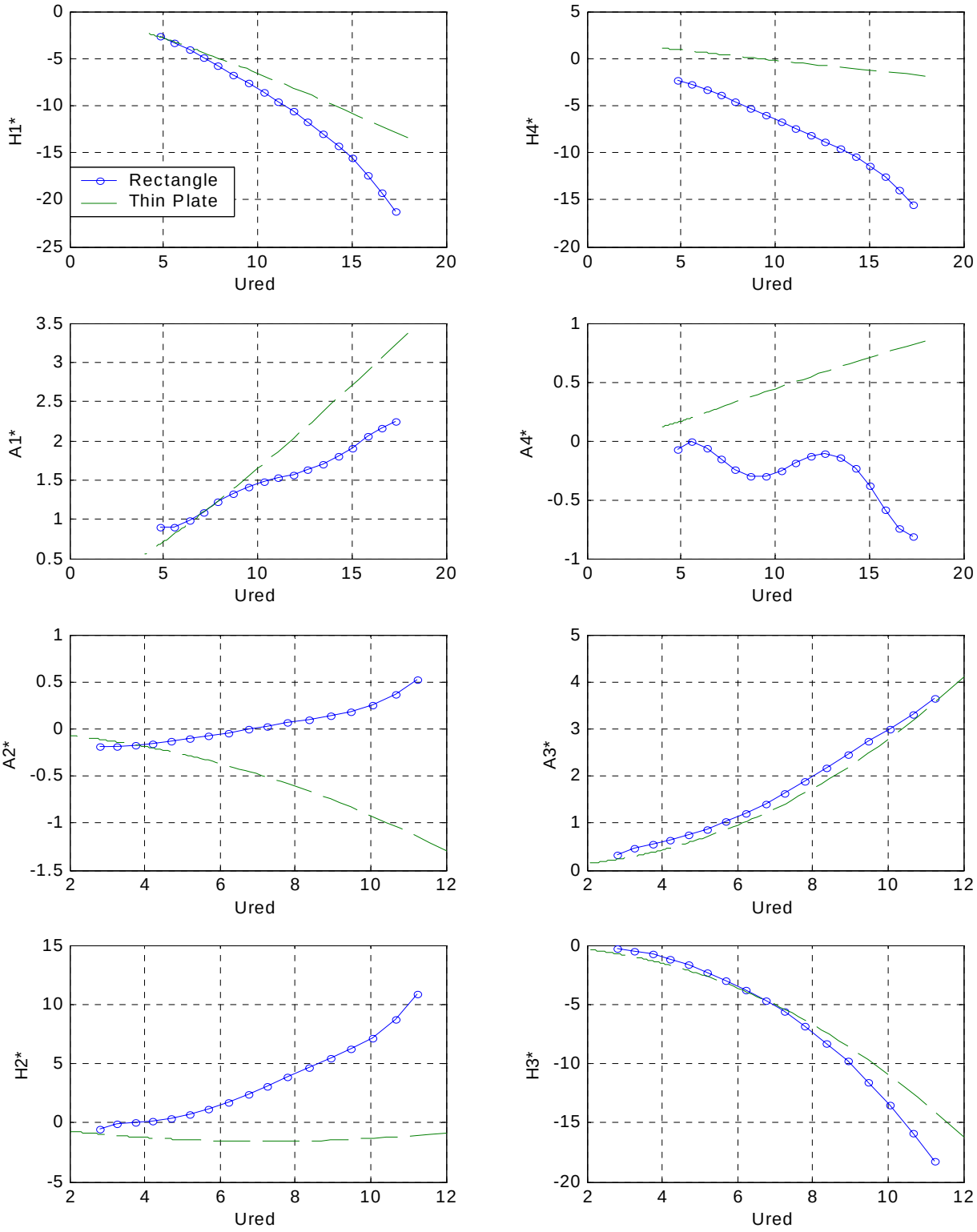

Figure 6.4: Flutter derivatives of the rectangular section (1:8) and the thin plate

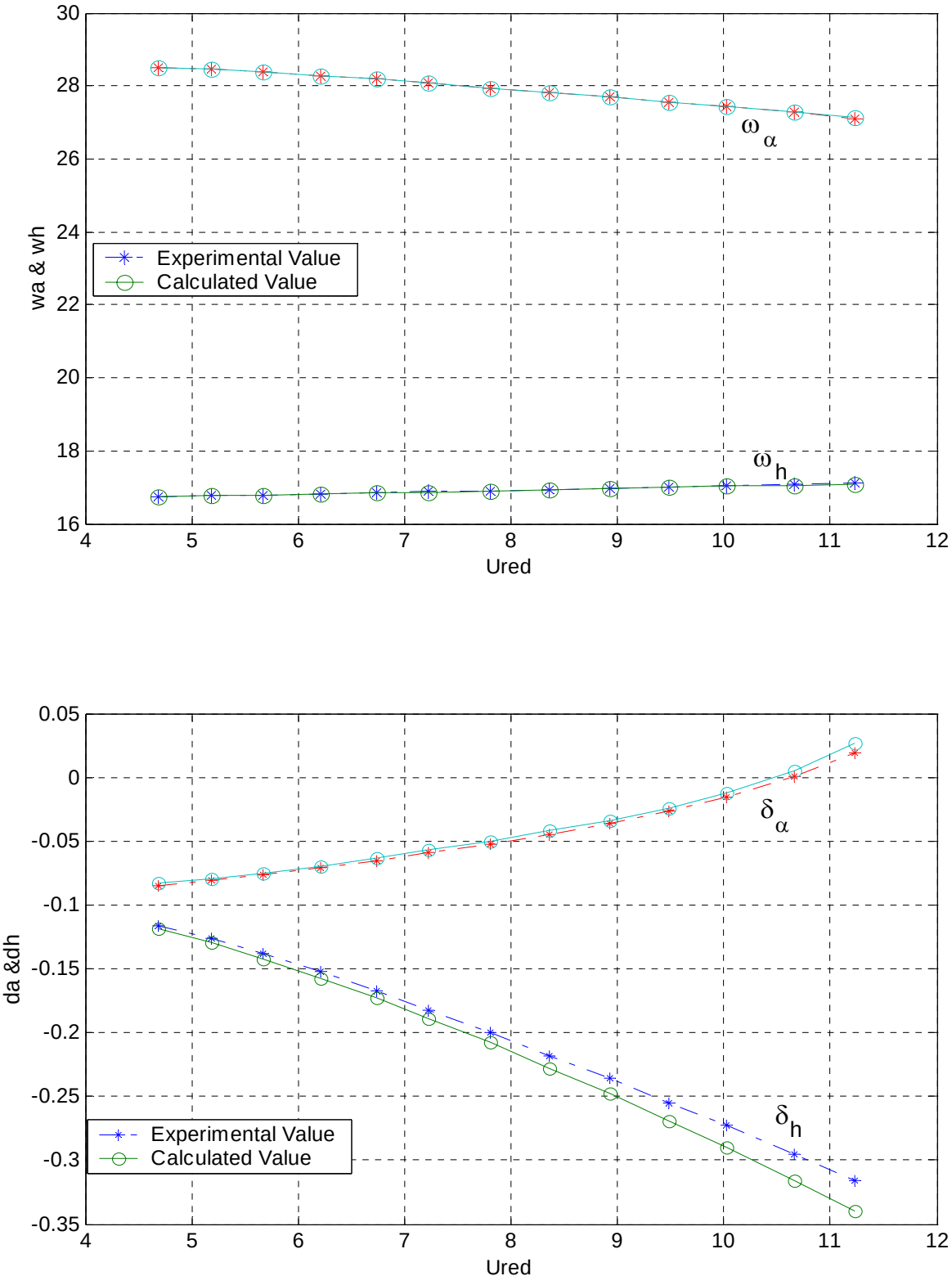

Figure 6.5: System parameters according to the free vibration test results

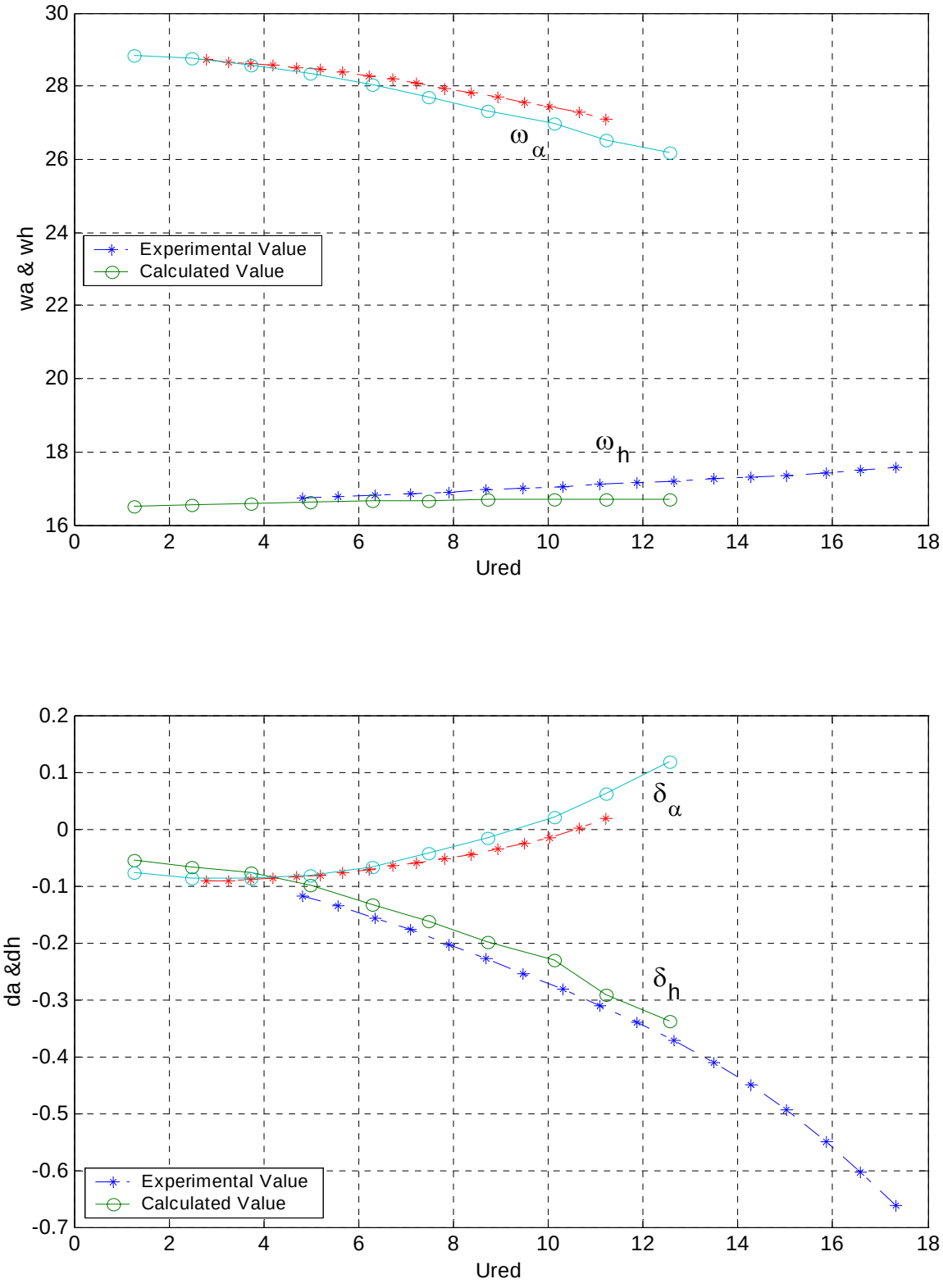

Figure 6.6: System parameters according to the results of Hortmanns

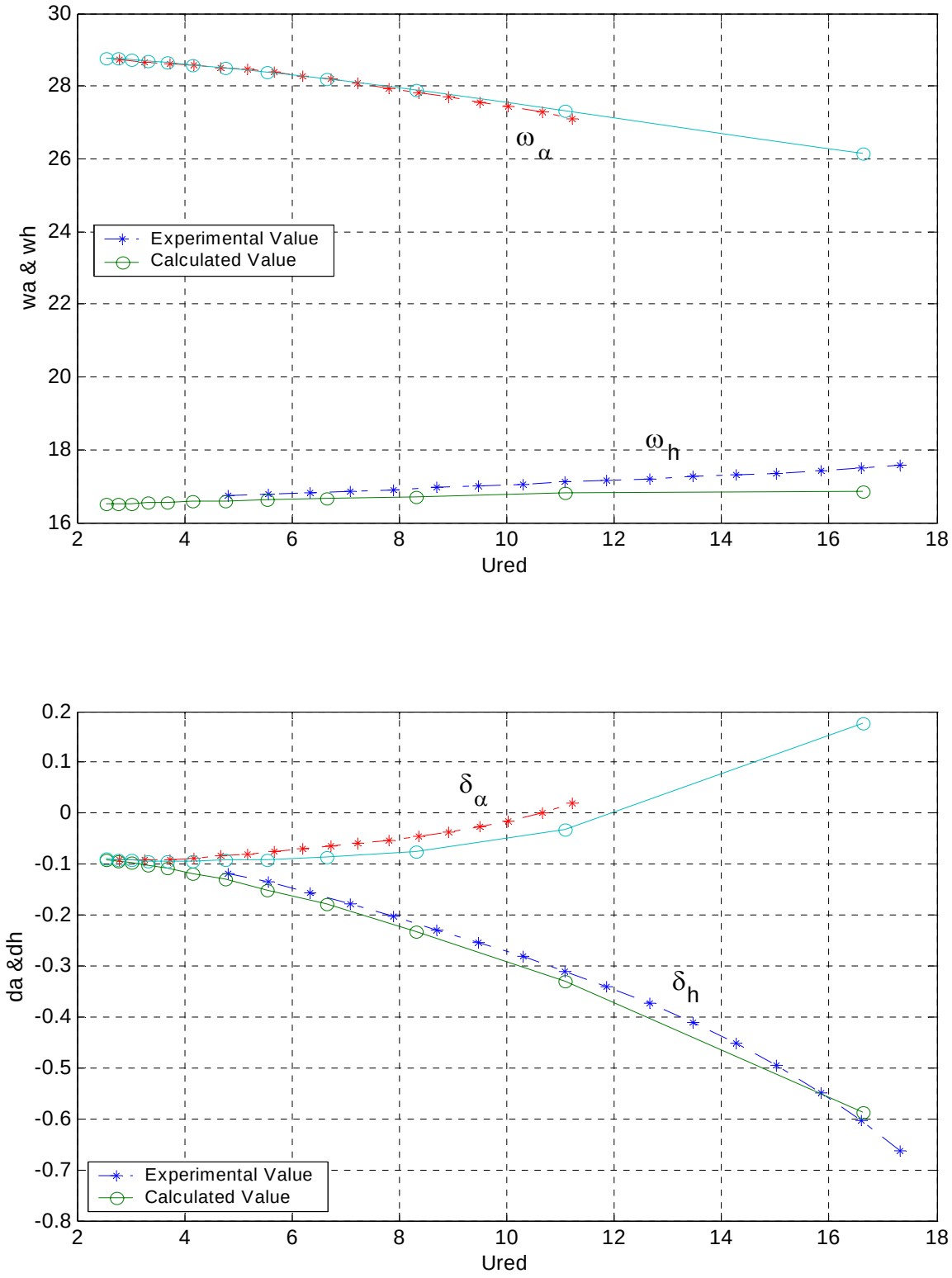

Figure 6.7: System parameters according to the results of Bergmann

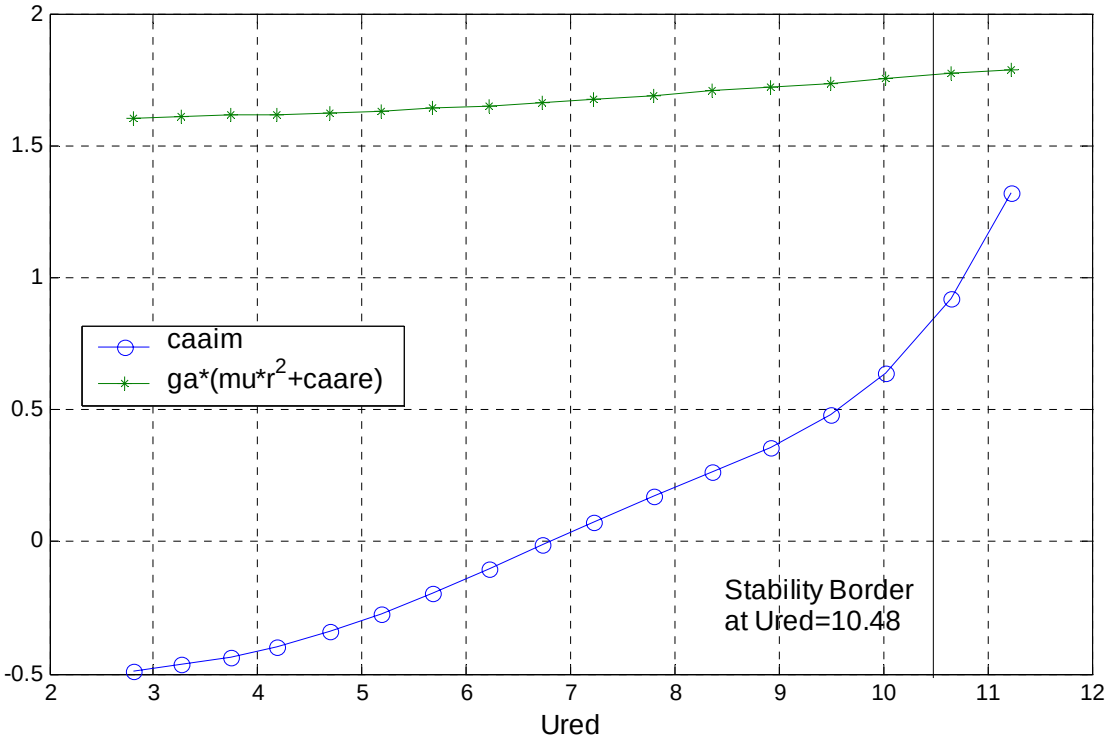

Figure 6.8: Simplified flutter prediction

7 CONCLUSION

Prediction of the aerodynamic stability of a bridge deck is based on the flutter derivatives, which can be extracted from the section model wind tunnel tests. In most of the previous works, the emphasis is usually given to the direct flutter derivatives A_2^* and A_3^* for the bluff cross sections, which exhibit pure torsional flutter, as in the case of Tacoma Narrows bridge. However, today's most of the long span bridges with streamlined sections exhibit coupled-mode flutter. Therefore, all eight-flutter derivatives associated with vertical and torsional motions should be calculated to predict the aerodynamic stability of the bridge deck under wind loading.

In the present work all eight flutter derivatives are identified simultaneously from the free vibration wind tunnel test results of a two-degree of freedom system under smooth wind flow with zero angle of attack. Different identification methods are investigated by comparing their advantages and disadvantages in the identifying of the system parameters. As an identification method, Modified Ibrahim Time Domain (MITD) is selected among the other methods because of its reliability in the identification of system parameters even from noise-corrupted displacement time histories obtained from the section model wind tunnel tests. Therefore MITD method also works well under turbulent flow conditions. Because the buffeting forces caused by the turbulence are treated as additional noise in the response of the motion.

Although the MITD method does not require any information for the initial displacement given to the section model, the identical initial displacement should be given to the model for each set of experiments in order to get consistent results of the identified parameters. Because the maximum amplitude of the oscillation plays a very important role in the identification of the flutter derivatives.

In order to evaluate aerodynamic behavior of a rectangular section with an aspect ratio of 1:8, its flutter derivatives are calculated by MITD method from the free vibration wind tunnel test results for three different initial condition cases. The results are compared with the results of the flutter derivatives that are already obtained from two different forced vibration tests. Most of the flutter derivatives calculated with different techniques exhibit reasonable agreement. For some flutter derivatives, such as A_2^*, the discrepancies not only exist between the different techniques, but also there exist discrepancies between the forced vibration test results. Therefore, free vibration test results provide the opportunity to compare forced vibration test results for A_2^*, which is the most important flutter derivative for the rectangular

section. The discrepancies in the flutter derivatives A_4^*, H_4^* are independent of the selected method or technique because of the general problems in the identification of these derivatives.

The comparison between the rectangular section and the flat plate confirms that the rectangular section behaves totally different with respect to the streamlined sections from the aerodynamic point of view. On the other hand, the results of the rectangular section model show that the coupled motion flutter is more critical than the pure torsional flutter, which is the case for bluff cross sections.

The measured critical wind speed at the wind tunnel is compared with the one calculated by the flutter derivatives and the system parameters that are identified from the free vibration and the forced vibration test results. The difference between the measured and calculated critical wind speeds for each technique is in acceptable limits. As it was expected, the minimum difference is calculated with respect to the free vibration test results. Because the flutter derivatives are identified exactly from this test results, which is not the case for the forced vibration test results.

The reliable results of the flutter derivatives obtained from the free vibration tests proves the applicability of the proposed approximate model, which is given in the Eqns. 5.4 and 5.5 to solve the uniqueness problem in the identification of flutter derivatives.

Finally, it is concluded that, the flutter derivatives obtained from the free vibration test results, can be used for the prediction of the aerodynamic stability of a section model, which provides an easy and effective way of stability prediction due to the simplicity of the free vibration tests.

References

[1] U. Starossek. *Brückendynamik – Winderregte Schwingungen von Seilbrücken.* Friedr. Vieweg & Sohn Verlagsgesellschaft mbH, Braunschweig/Wiesbaden, 1992.

[2] E. Simiu, R.H. Scanlan. *Wind Effects on Structures*: fundamentals and applications to design. 3rd Edition, John Wiley & Sons, Inc. Canada, 1996.

[3] Sarkar, P. P. *"New identification methods applied to the response of flexible bridges to wind."* PhD thesis, The John Hopkins University, Baltimore, Md, 1992.

[4] B. Wienand. *Experimentelle und rechnerische Untersuchung der aerodynamischen Stabilität weitgespannter Brücken unter Berücksichtigung nichtlinearer Windkräfte.* Diss., Fachbereich Bauingenieurwesen der Universität Kassel, 1994.

[5] H. G. Natke. *Application of System Identification in Engineering.* Springer Verlag, Germany, 1988.

[6] S. C. Chapra, R. P. Canale. *Numerical Methods for Engineers: with software and programming applications.* 4th Edition. McGraw-Hill, Inc. 2002.

[7] K. Badenhausen. Idetifikation der Modellparameter elastomechanischer Systeme aus Schwingungsversuchen. Diss., Universität Kassel, 1986.

[8] R. W. Clough, J. Penzien. *Dynamics of Structures.* 2nd Edition, McGraw-Hill, Inc. 1993.

[9] M. Iwamoto, Y. Fujino. Identification of flutter derivatives of bridge deck from free vibration data. *Journal of Wind Engineering and Industrial Aerodynamic,* 54/55, pp. 55-63, 1995.

[10] R. H. Scanlan, J. J. Tomko. Airfoil and bridge deck flutter derivatives. *Journal of the Engineering Mechanics Division,* 97(EM 6), pp. 1717-1737, 1971.

[11] P. P. Sarkar, N. P. Jones, R. H. Scanlan. System identification for estimation of flutter derivatives. *Journal of Wind Engineering and Industrial Aerodynamic,* 41/44, pp. 1243-1254, 1992.

[12] P. P. Sarkar, N. P. Jones, R. H. Scanlan. Identification of aeroelastic parameters of flexible bridges. *Journal of the Engineering Mechanics,* Vol.120, No.8, pp. 1718-1742, 1994.

[13] A. Chen, X. He, H. Xiang. Identification of 18 flutter derivatives of bridge decks. *Journal of Wind Engineering and Industrial Aerodynamic,* 90, pp. 2007-2022, 2002.

[14] T. Theodorsen. *General theory of aerodynamic instability and the mechanism of flutter.* National Advisory Committee for Aeronautics (NACA), Washington, D. C., 1934, Technical Report No. 496, pp. 413-433, 1935.

[15] R. H. Scanlan and N. P. Jones. Aeroelastic analysis of cable-stayed bridges. *Journal of Structural Engineering.*, ASCE 116, pp. 279-297, 1990.

[16] G. Welch, G. Bishop. An introduction to the kalman filter. *Technical Report,* Department of Computer Science, University of North Carolina at Chapel Hill, March 2002.

[17] M. Shinozuka, C. B. Yun and H. Imai. Identification of linear structural dynamic systems. *Journal of the Engineering Mechanics,* ASCE, Vol. 108, No.6, pp. 1371-1390, 1982.

[18] H. Yamada, T. Miyata, H. Ichikawa. Measurement of aerodynamic coefficients by system identification methods. *Journal of the Engineering Mechanics,* ASCE, 41-44, pp. 1255-1263, 1992.

[19] Y. Li, H. Liao, S. Qiang. Weighting ensemble least-squares method for flutter derivatives of bridge decks. *Journal of Wind Engineering and Industrial Aerodynamic,* 91, pp. 713-721, 2003.

[20] A. Zasso, A. Cigada, S. Negri. Flutter derivatives identification through full bridge aeroelastic model transfer function analysis. *Journal of Wind Engineering and Industrial Aerodynamic,* 60, pp. 17-33, 1996.

[21] L. Thiesemann, D. Bergmann, U. Starossek. Numerical and experimental evaluation of flutter derivatives by means of the forced vibration method. *Technical Report,* Structural Mechanics and Steel Structures Section, Technical University Hamburg-Harburg, Germany, 2003.

[22] D. Bergmann, U. Kaiser, S. Wagner. *Experimentelle Ermittlung der instationären aerodynamischen Beiwerte von Brückenprfilen im Wasserkanal*. Institut für Aerodynamik und Gasdynamik (IAG), Universität Stuttgart, 2002.

[23] M. Hortmanns, *Zur Identification und Berücksichtigung nichtlinearer aeroelastischer Effekte.* Dissertation, Shaker Verlag, 1997.

Appendix A: Flutter Derivatives

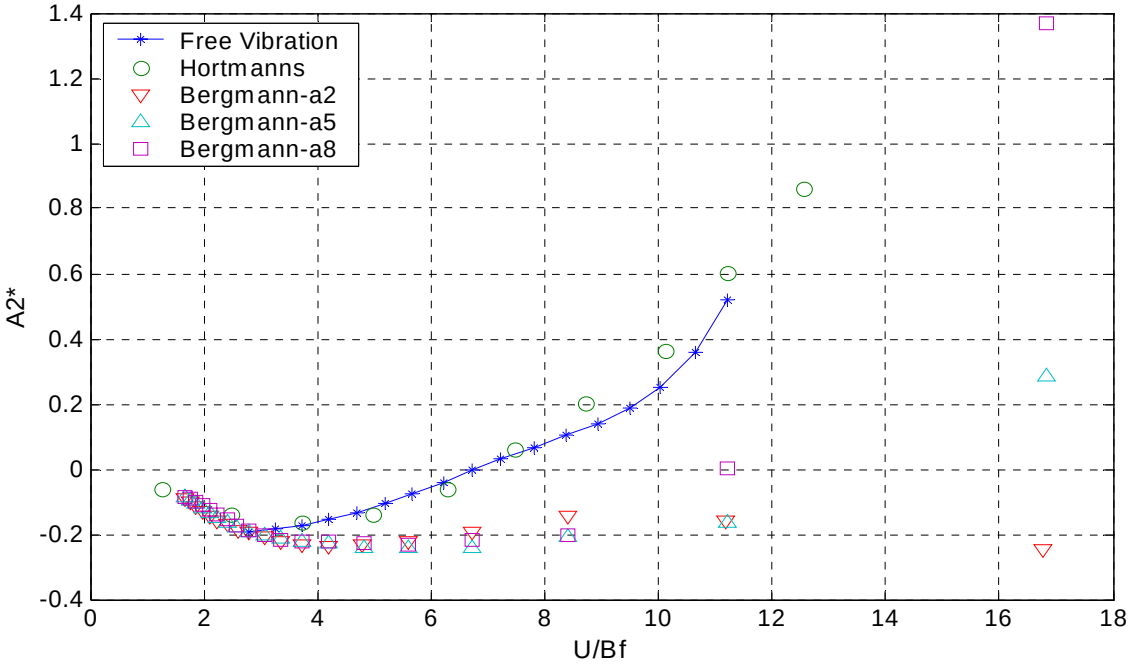

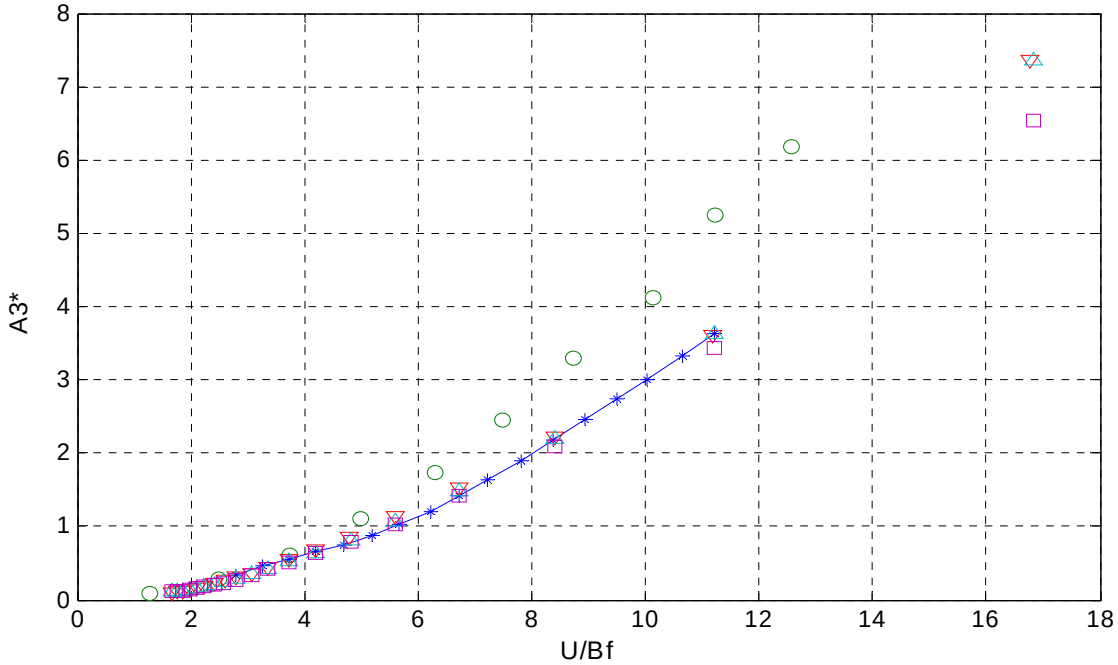

Figure A.1: Comparison of A_2^* and A_3^* of the initial condition case bs_10

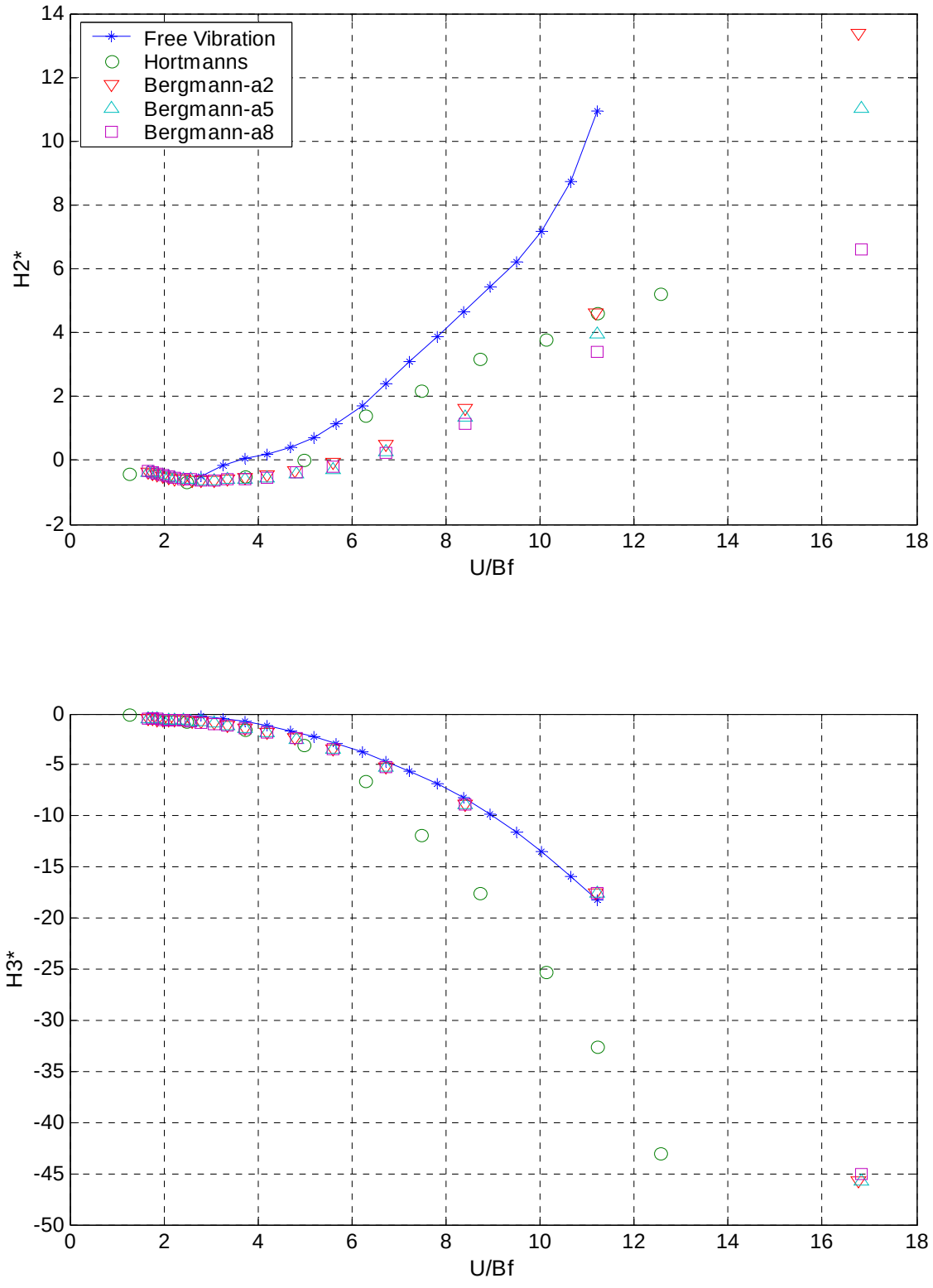

Figure A.2: Comparison of H_2^* and H_3^* of the initial condition case bs_10

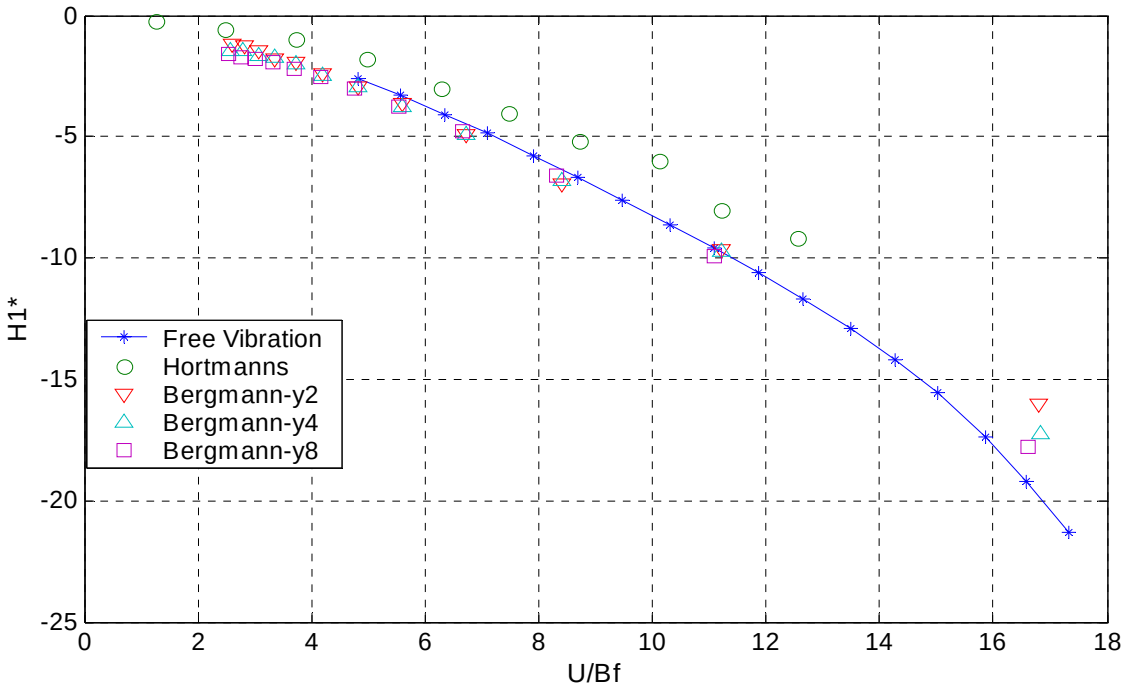

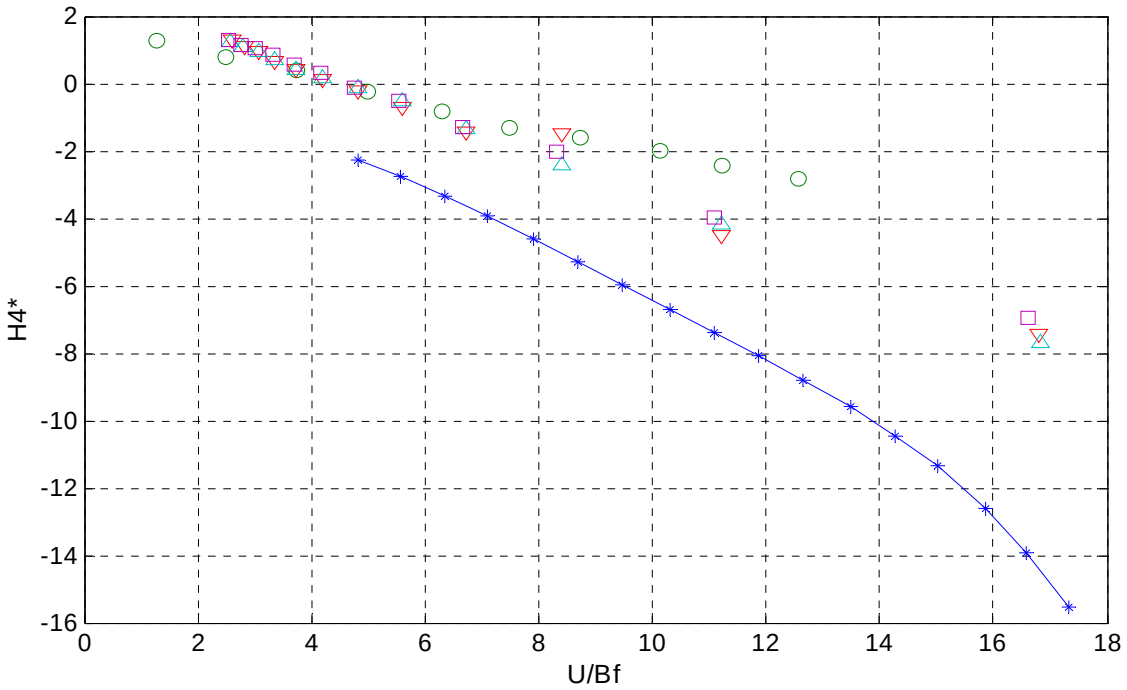

Figure A.3: Comparison of H_1^* and H_4^* of the initial condition case bs_10

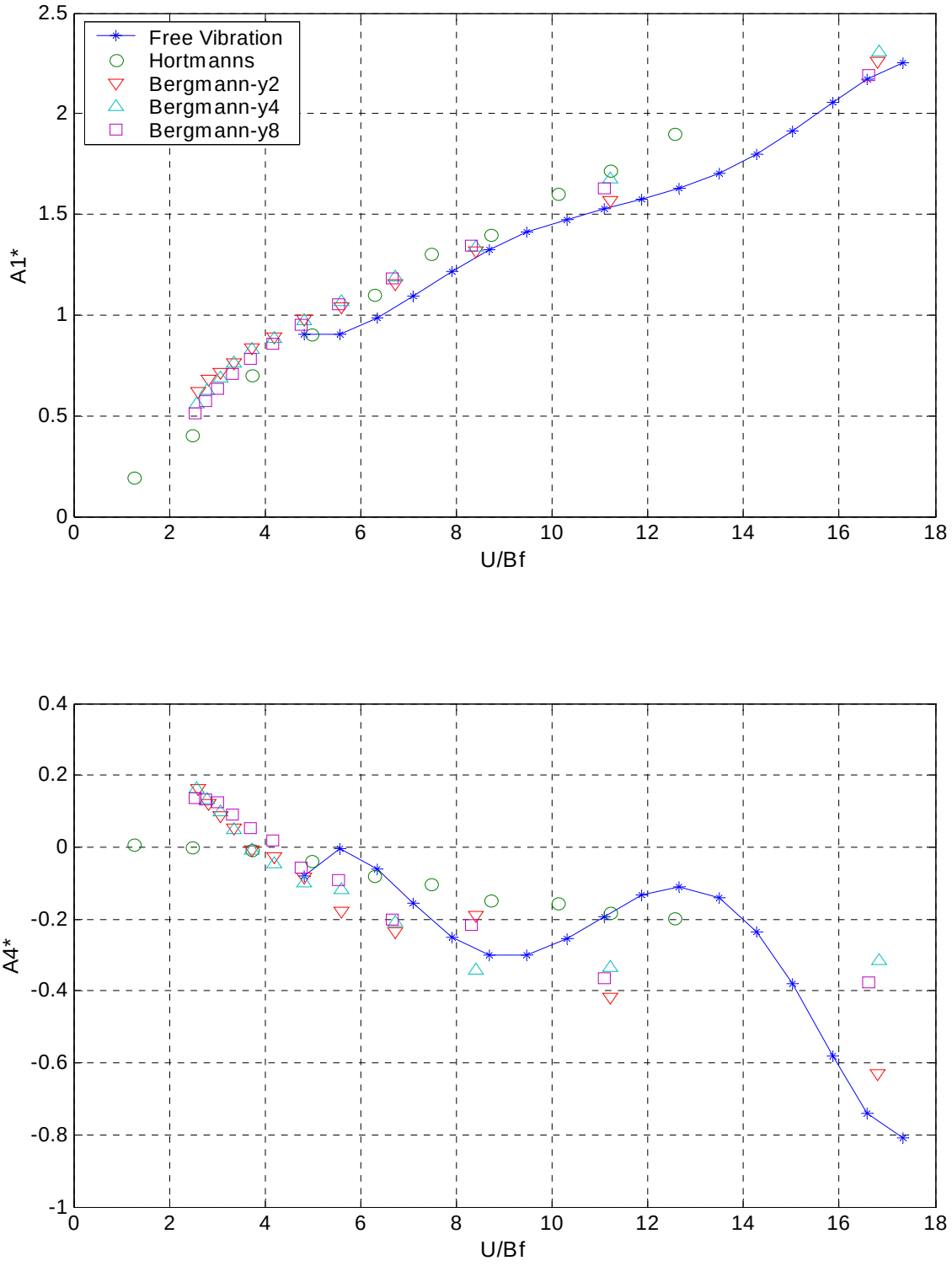

Figure A.4: Comparison of A_1^* and A_4^* of the initial condition case bs_10

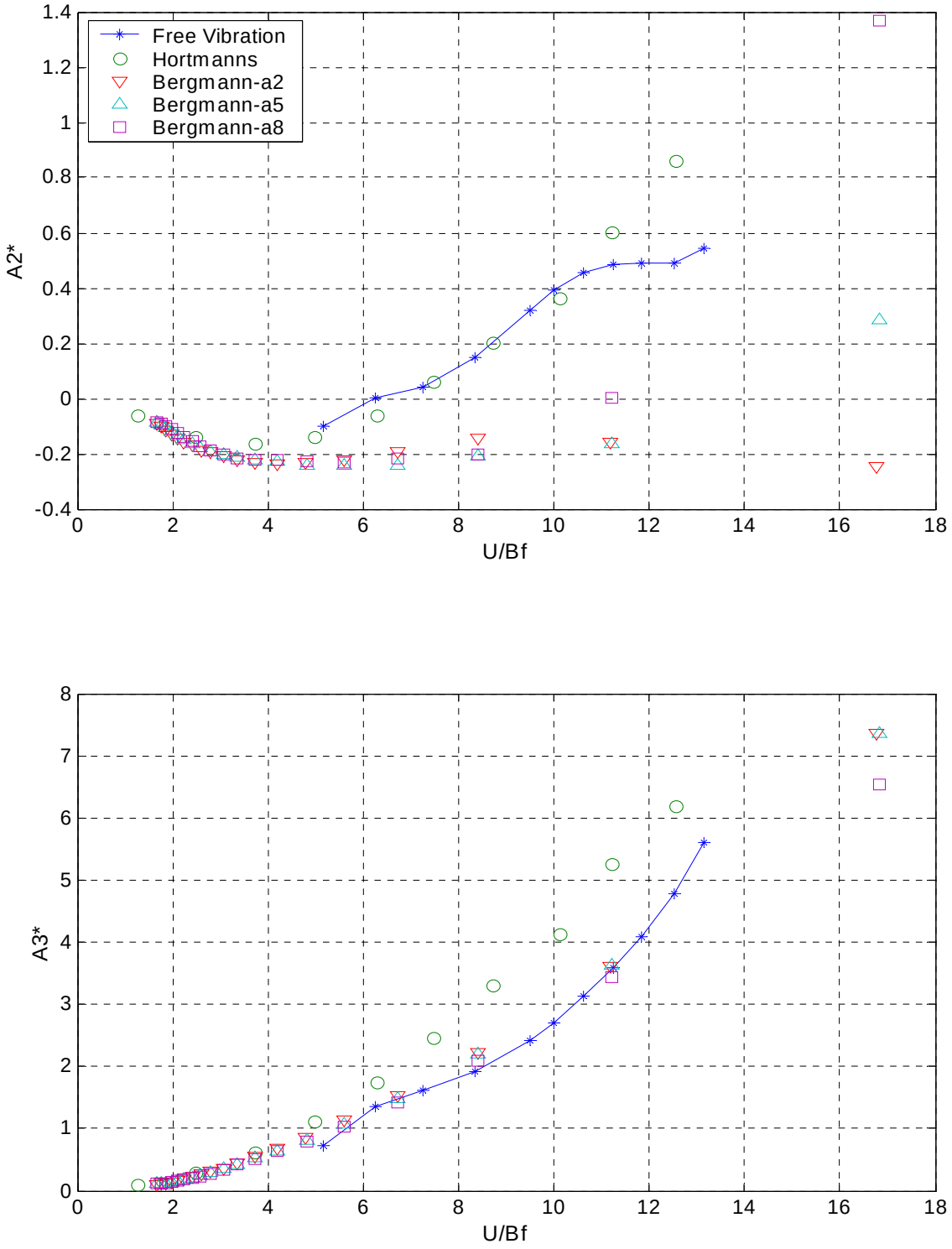

Figure A.5: Comparison of A_2^* and A_3^* of the initial condition case bs_20

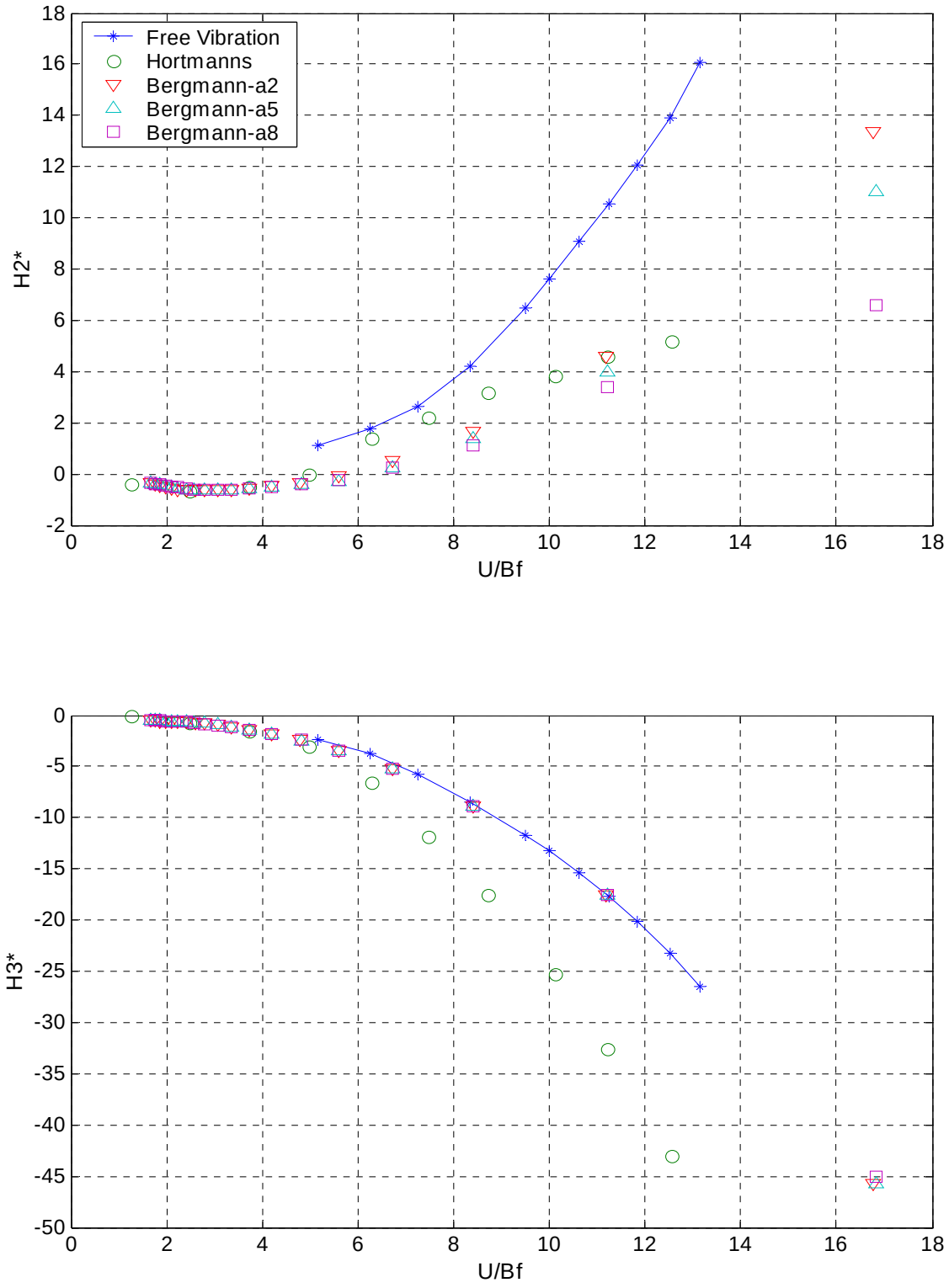

Figure A.6: Comparison of H_2^* and H_3^* of the initial condition case bs_20

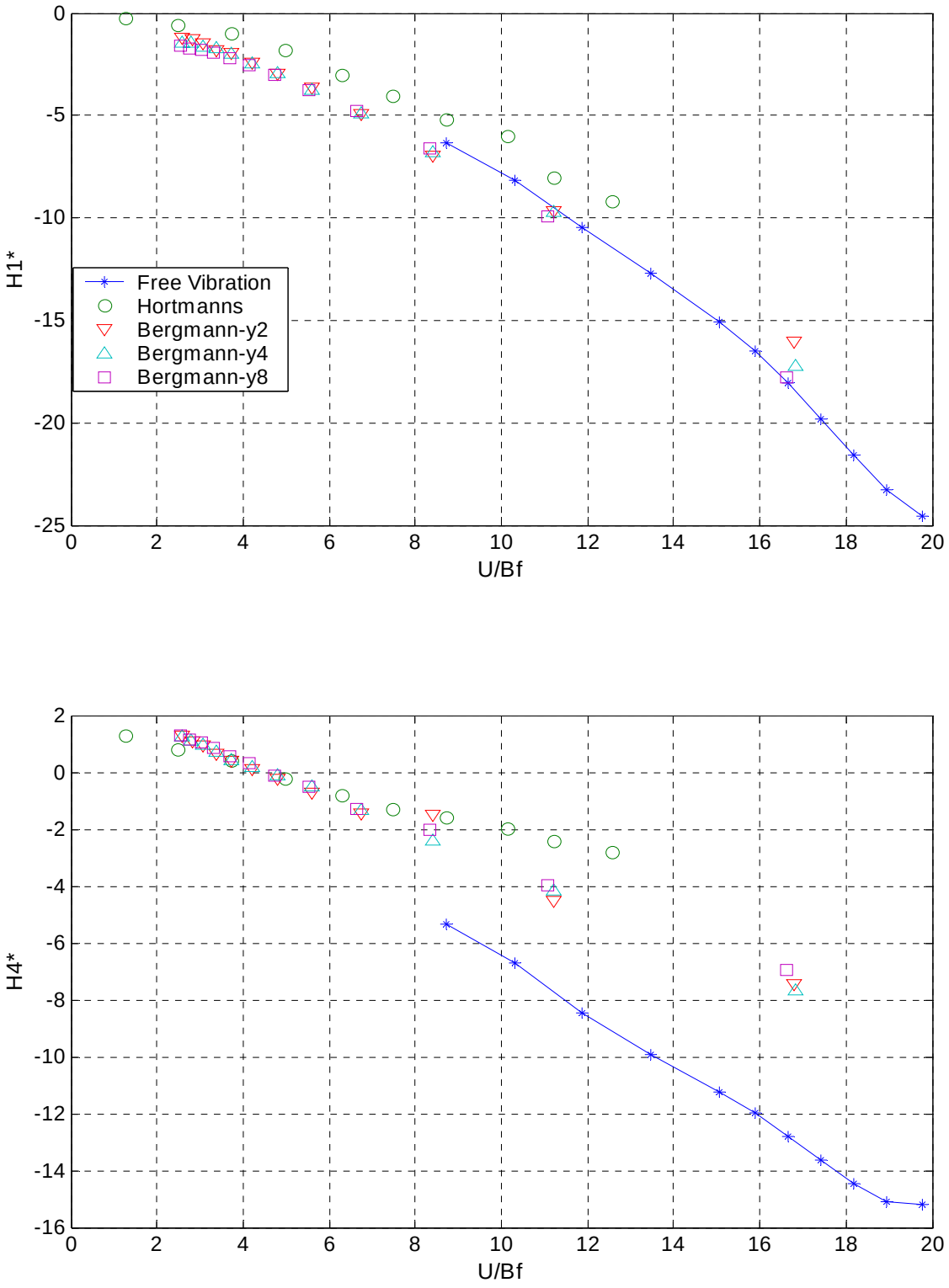

Figure A.7: Comparison of H_1^* and H_4^* of the initial condition case bs_20

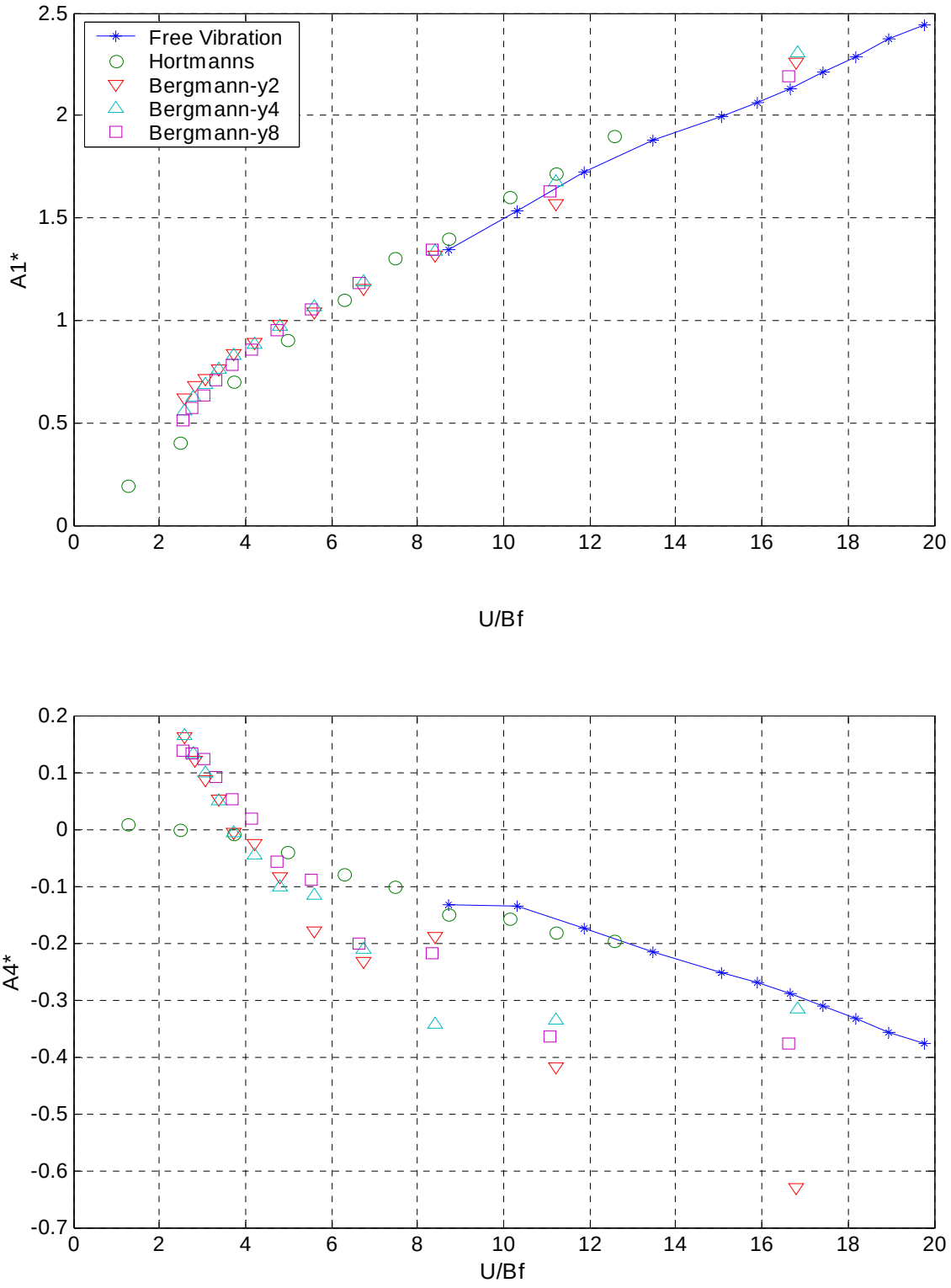

Figure A.8: Comparison of A_1^* and A_4^* of the initial condition case bs_20

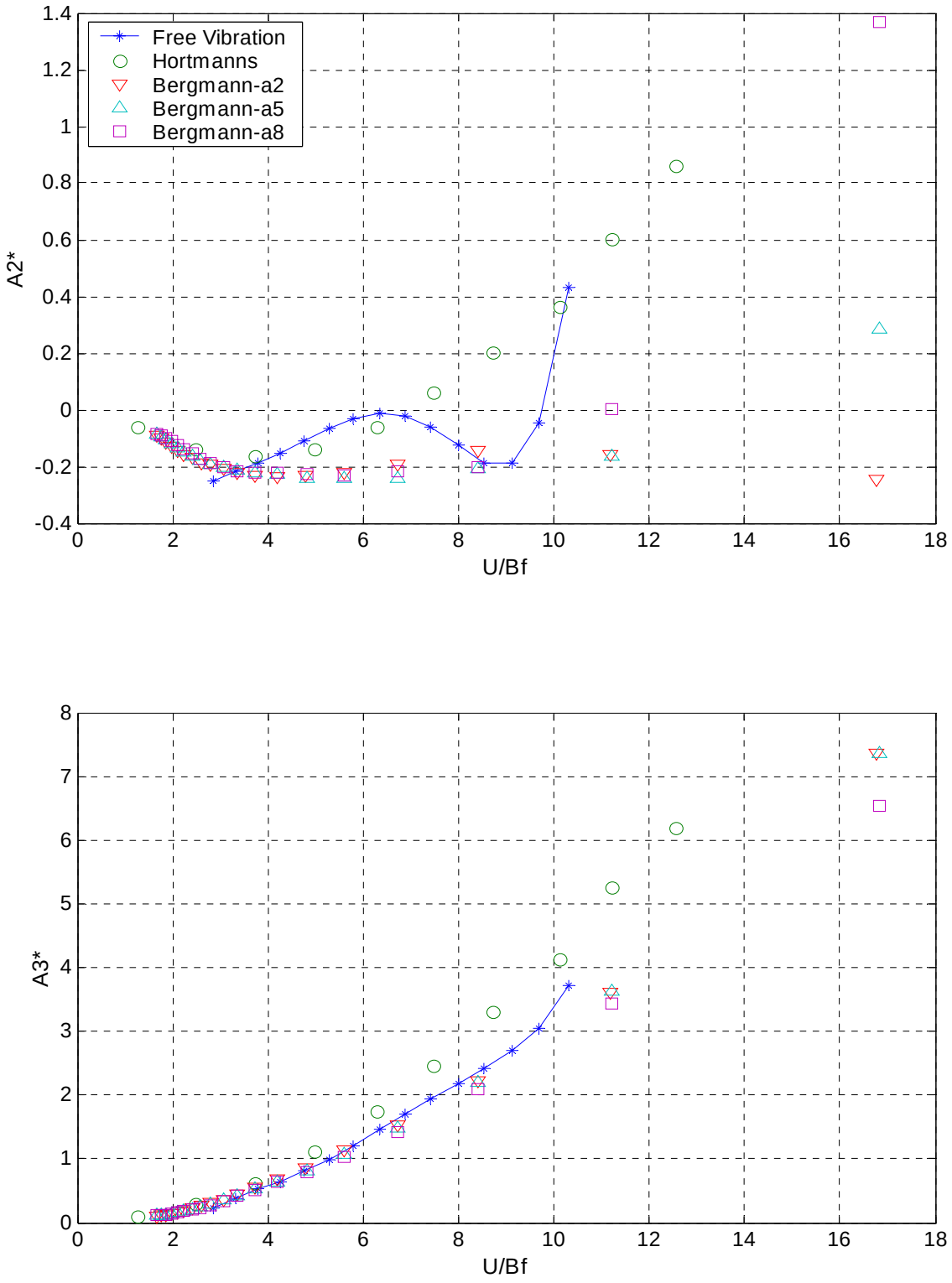

Figure A.9: Comparison of A_2^* and A_3^* of the initial condition case os_10

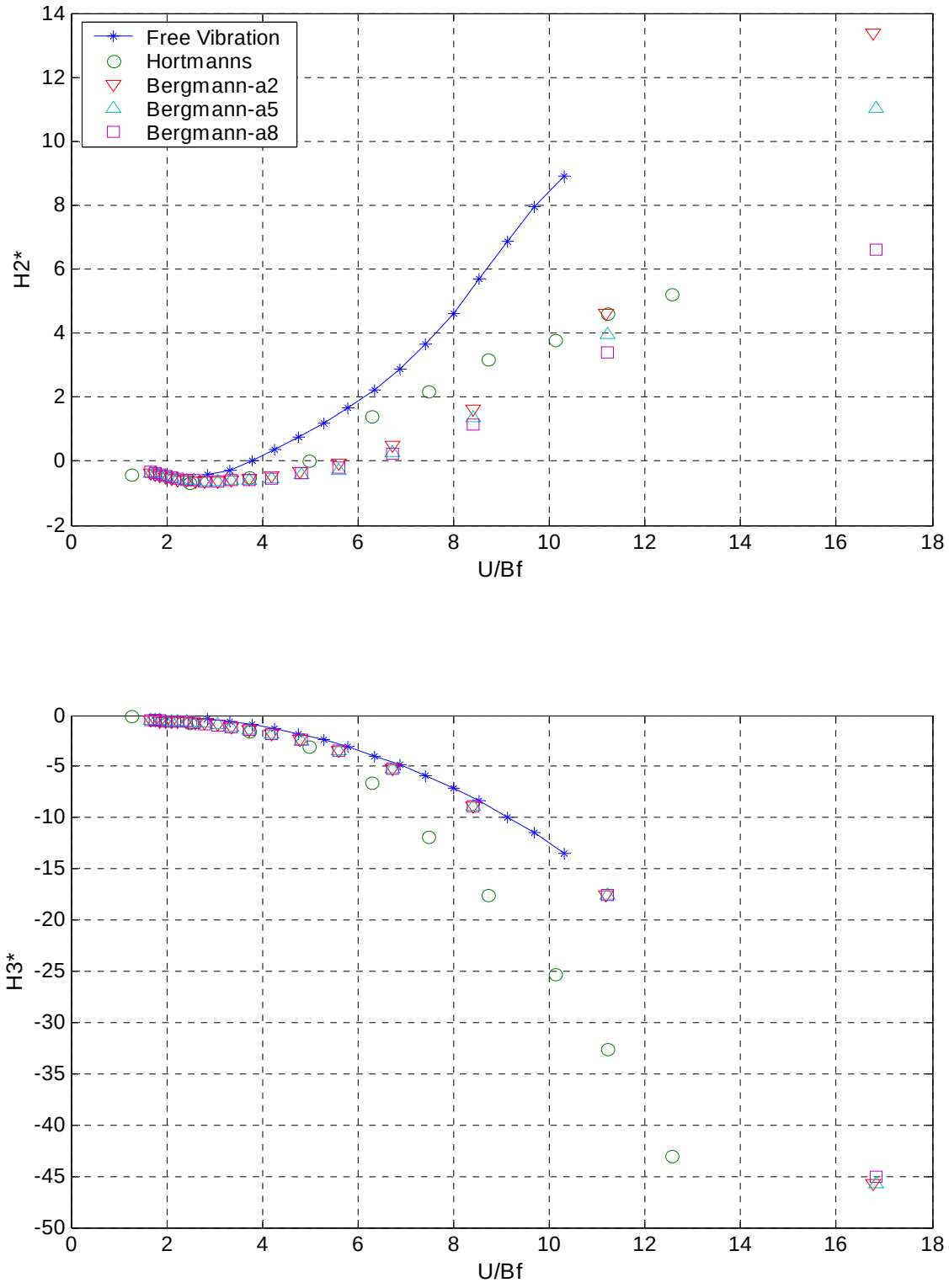

Figure A.10: Comparison of H_2^* and H_3^* of the initial condition case os_10

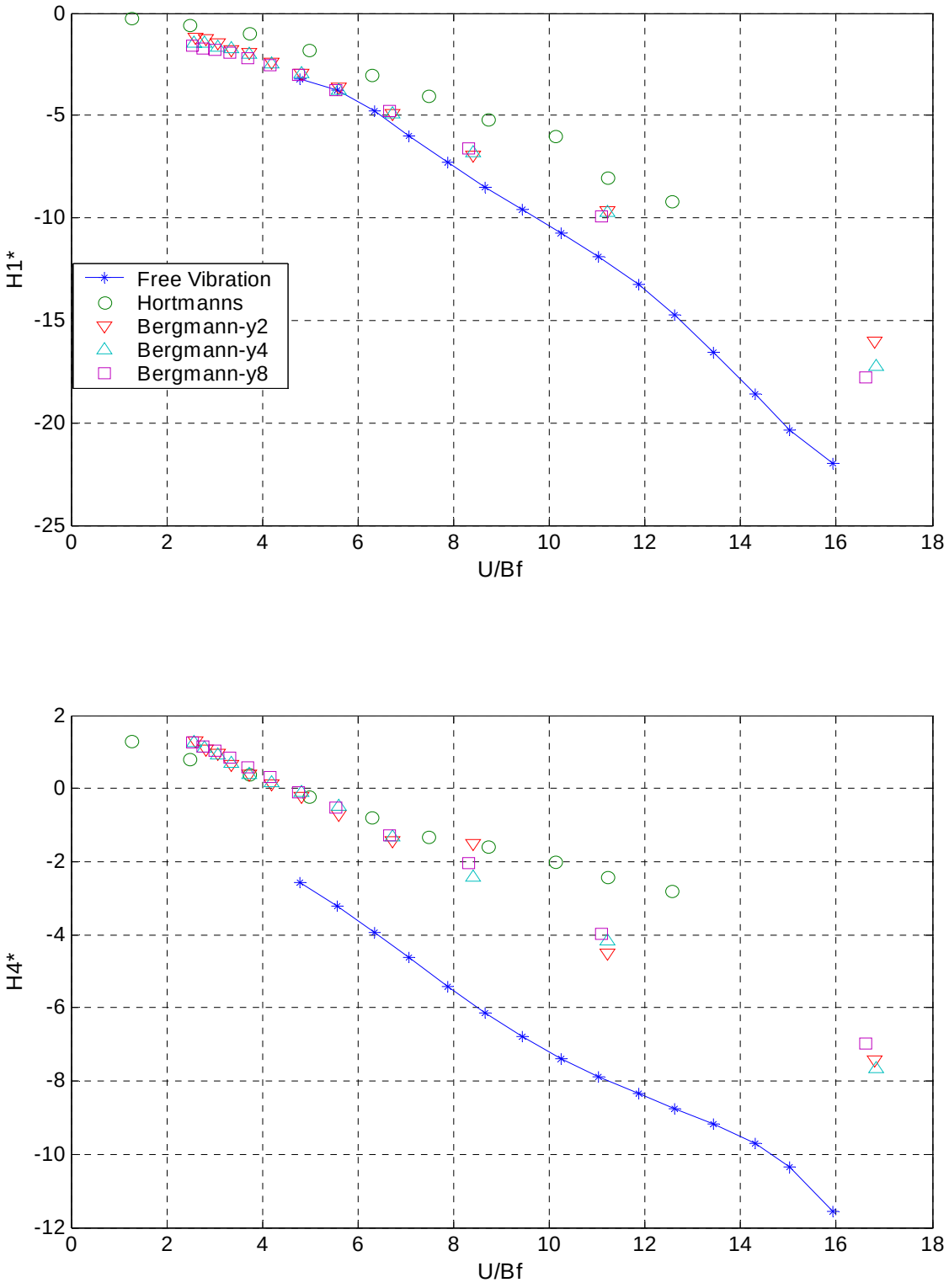

Figure A.11: Comparison of H_1^* and H_4^* of the initial condition case os_10

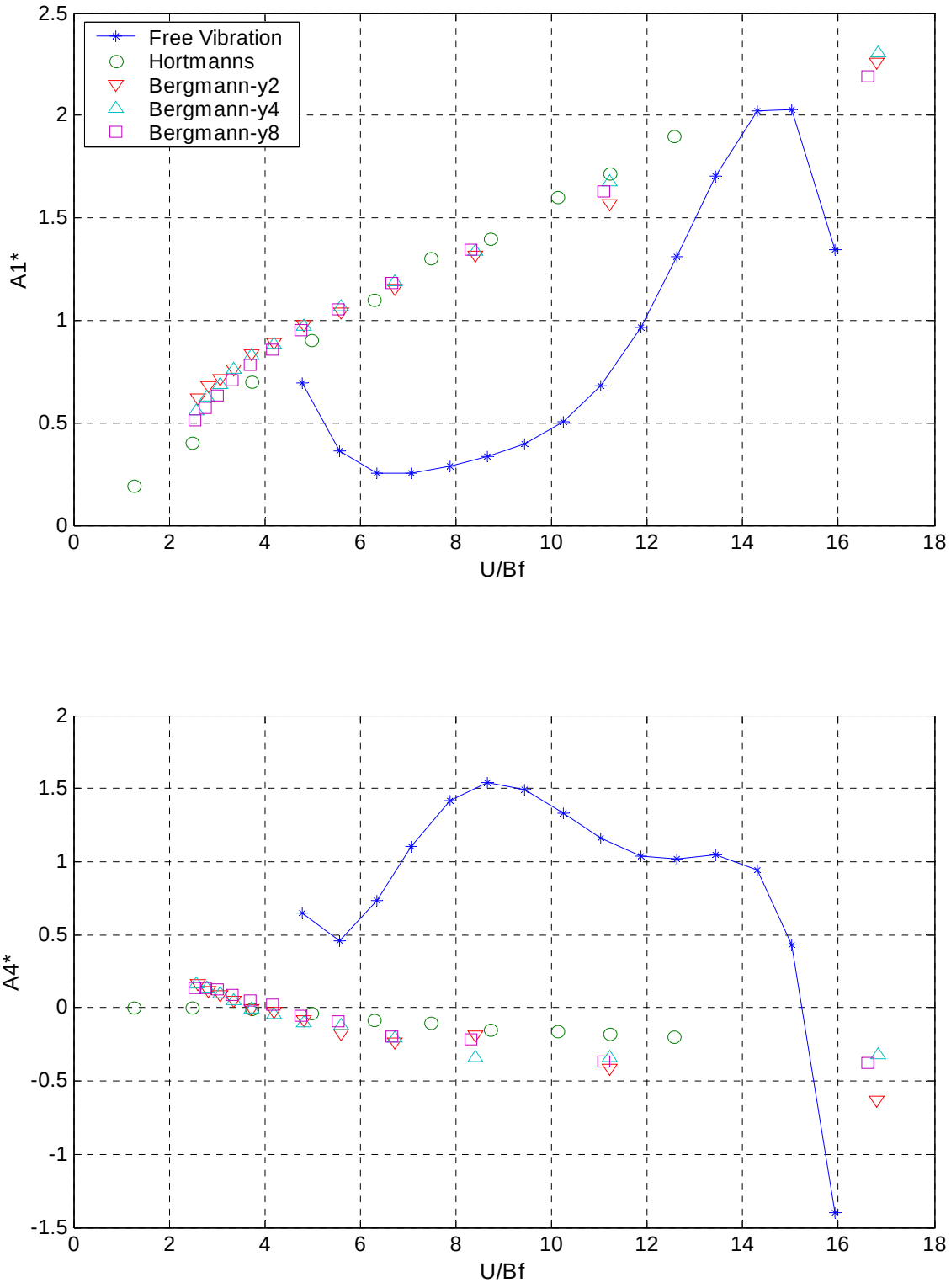

Figure A.12: Comparison of A_1^* and A_4^* of the initial condition case os_10